การจำลองการซึมผ่านของคลอไรด์ในโครงสร้างคอนกรีต ภายใต้การรับแรงดันแบบวัฏจักรและสภาพแวดล้อมแบบน้ำขึ้นน้ำลง

นายเมียนวัน เจิ่น

วิทยานิพนธ์นี้เป็นส่วนหนึ่งของการศึกษาตามหลักสูตรปริญญาวิศวกรรมศาสตรดุษฎีบัณฑิต
สาขาวิชาวิศวกรรมโยธา ภาควิชาวิศวกรรมโยธา
คณะวิศวกรรมศาสตร์ จุฬาลงกรณ์มหาวิทยาลัย
ปีการศึกษา 2551

MODELING OF CHLORIDE PENETRATION INTO CONCRETE STRUCTURES UNDER FLEXURAL CYCLIC LOAD AND TIDAL ENVIRONMENT

Mr. MIEN VAN TRAN

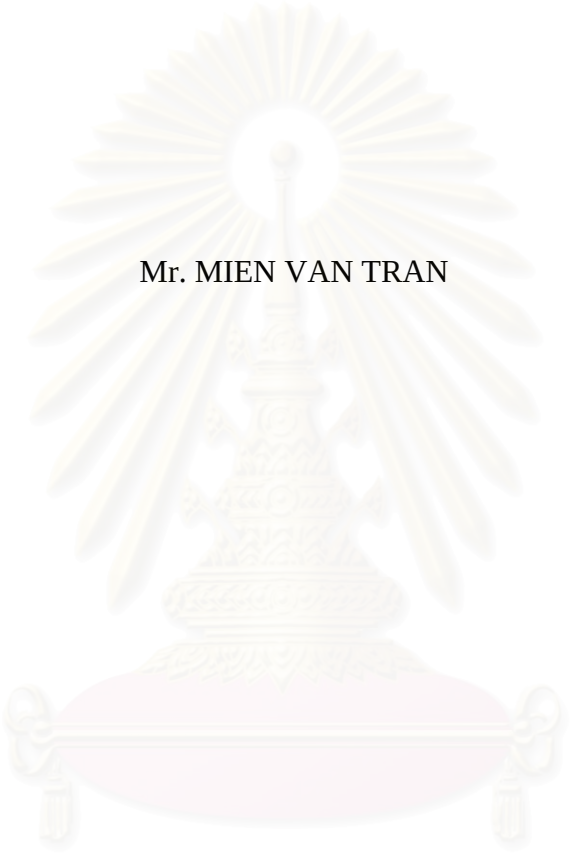

A Dissertation Submitted in Partial Fulfillment of the Requirements
for the Degree of Doctor of Philosophy Program in Civil Engineering
Department of Civil Engineering
Faculty of Engineering
Chulalongkorn University
Academic Year 2008

Thesis Title	Modeling of chloride penetration into concrete structures under flexural cyclic load and tidal environment
By	Mr. Mien Van Tran
Field of study	Civil Engineering
Thesis Principal Advisor	Associate Professor Boonchai Stitmannaithum, D.Eng.
Thesis Co-Advisor	Professor Toyoharu NAWA, D.Eng.

Accepted by the Faculty of Engineering, Chulalongkorn University in Partial Fulfillment of Requirements for the Doctoral Degree

.....Dean of the Faculty of Engineering
(Associate Professor Boonsom Lerdhirunwong, Dr.Ing)

THESIS COMMITTEE

..... Chairman
(Professor Ekasit Limsuwan, Ph.D)

..... Thesis Principal Advisor
(Associate Professor Boonchai Stitmannaithum, D.Eng.)

..... Thesis Co-Advisor
(Professor Toyoharu NAWA, D.Eng.)

..... Member
(Associate Professor Phoonsak Pheinsusom, D.Eng)

..... Member
(Associate Professor Teerapong Senjuntichai, Ph.D)

..... Member
(Associate Professor Suvimol Sujjavanich, Ph.D)

เมียนวัน เจิ่น : การจำลองการซึมผ่านของคลอไรด์ในโครงสร้างคอนกรีตภายใต้การรับแรงดัดแบบวัฏจักรและสภาพแวดล้อมแบบน้ำขึ้นน้ำลง (MODELING OF CHLORIDE PENETRATION INTO CONCRETE STRUCTURES UNDER FLEXURAL CYCLIC LOAD AND TIDAL ENVIRONMENT). อ. ที่ปรึกษาวิทยานิพนธ์หลัก : รศ.ดร. บุญไชย สถิตมั่นในธรรม, อ. ที่ปรึกษาวิทยานิพนธ์ร่วม: ศ.ดร. โทโยฮารุ นาวา, 157 หน้า.

ในสภาพแวดล้อมทางทะเลความเสียหายของโครงสร้างคอนกรีตเสริมเหล็กโดยมากเกิดจากคลอไรด์ ซึ่งทำให้เกิดการสึกกร่อนของเหล็กเสริมโครงสร้าง โดยสภาพความเสียหายของโครงสร้างคอนกรีตนั้นจะขึ้นอยู่กับทั้งน้ำหนักบรรทุกและสภาพแวดล้อมกระทำร่วมกัน เมื่อโครงสร้างคอนกรีตรับน้ำหนักบรรทุกจนเกิดการแตกร้าวในโครงสร้างคอนกรีต อันเป็นผลให้การซึมผ่านของคลอไรด์เข้าไปยังโครงสร้างคอนกรีตมีอัตราเพิ่มสูงขึ้นอย่างรวดเร็วจะทำให้อายุการใช้งานของโครงสร้างคอนกรีตเสริมเหล็กลดลงอย่างมีนัยสำคัญ ในอดีตมีการศึกษาด้านพฤติกรรมเชิงกลของโครงสร้างคอนกรีตและการเสื่อมสภาพของโครงสร้างคอนกรีตแล้วเป็นจำนวนมาก อย่างไรก็ตามแบบจำลองที่เสนอขึ้นเหล่านั้นมิได้พิจารณาผลจากการกระทำของน้ำหนักบรรทุกทางกลและสภาพแวดล้อมร่วมกันแต่อย่างใด

วัตถุประสงค์ของงานวิจัยนี้คือการพัฒนาแบบจำลองการซึมผ่านของคลอไรด์เข้าสู่เนื้อคอนกรีตภายใต้การรับแรงดัดแบบวัฏจักรและสภาพแวดล้อมแบบน้ำขึ้นน้ำลง แบบจำลองนี้ตั้งอยู่บนพื้นฐานทางทฤษฎีและผลการทดสอบการซึมผ่านของคลอไรด์ ปริมาณคลอไรด์และการรับแรงดัดแบบวัฏจักร โดยแรงดัดแบบวัฏจักรในการทดสอบใช้แรงดัดจากระดับร้อยละ50 ถึงร้อยละ80 ของกำลังดัด แบบจำลองการแตกร้าวเสมือนได้รับการปรับปรุงเพื่อทำนายการเสียรูปจากการล้าของคานคอนกรีตภายใต้แรงดัด การทดสอบใช้ซีเมนต์สี่ชนิดในการตรวจสอบความสามารถในการจับยึดคลอไรด์อิออน (Chloride Binding Isotherms) สภาพแวดล้อมแบบน้ำขึ้นน้ำลงจำลองโดยการทดสอบในสภาพเปียก 12 ชั่วโมง และ แห้ง 12 ชั่วโมง ผลการทดสอบความสามารถในการจับยึดคลอไรด์อิออนแสดงให้เห็นถึงความสัมพันธ์แบบเชิงเส้นระหว่างผลการทดสอบระยะสั้นและระยะยาว ทั้งนี้ซีเมนต์ปอตแลนด์ชนิดธรรมดา (OPC) มีความสามารถในการจับยึดคลอไรด์อิออน (Bind Chloride Ions) สูงสุด ขณะที่ซีเมนต์ประเภทความร้อนต่ำมีการจับยึดคลอไรด์อิออนน้อยที่สุด แบบจำลองที่เสนอขึ้นใหม่นี้แสดงให้เห็นว่าการรับแรงดัดแบบทำซ้ำทำให้คลอไรด์ซึมผ่านคอนกรีตมากขึ้น ระดับการรับแรงดัดที่สูงขึ้นยิ่งทำให้การซึมผ่านของคลอไรด์เร็วขึ้น การทำนายโดยแบบจำลองสอดคล้องเป็นอย่างดีกับผลการทดสอบเมื่อใช้พารามิเตอร์ความหนาแน่นการแตกร้าว (μ) และพารามิเตอร์ด้านการบิดงอ (τ)

ภาควิชา วิศวกรรมโยธา ..... ลายมือชื่อนิสิต .....

สาขาวิชา วิศวกรรมโยธา ..... ลายมือชื่อ อ. ที่ปรึกษาวิทยานิพนธ์หลัก .....

ปีการศึกษา 2551 ..... ลายมือชื่อ อ. ที่ปรึกษาวิทยานิพนธ์ร่วม Tetsuharu Nawa

4871874721 MAJOR CIVIL ENGINEERING
KEYWORDS: MODEL / CHLORIDE PENETRATION / CONCRETE / FLEXURAL CYCLIC LOAD / TIDAL ENVIRONMENT

MIEN VAN TRAN: MODELING OF CHLORIDE PENETRATION INTO CONCRETE STRUCTURES UNDER FLEXURAL CYCLIC LOAD AND TIDAL ENVIRONMENT. ADVISOR: ASSOC.PROF. BOONCHAI STITMANNAITHUM, D.ENG. CO-ADVISOR: PROF. TOYOHARU NAWA, D.ENG., 157 pp.

In marine environment, the deterioration of concrete structures is mainly due to chloride induced corrosion. With real concrete structures, the deterioration is controlled by the combination of mechanical load and climatic load. The mechanical load results cracks in concrete structures. The cracks accelerate the chloride penetration into concrete structures. As a result, the service life of concrete structures will be reduced considerably. There were many models proposed to predict the deterioration of concrete structures. However, these models are not reliable due to not having simultaneous combination of mechanical and climatic loads.

In this research, a model, which simulates the chloride ingress into plain concrete, using different cement types, under flexural cyclic load and tidal environment, was proposed. This model is based on theoretical analysis and experiments of chloride diffusion test, chloride content test and flexural cyclic loading test. Flexural cyclic load is applied from 50% to 80% of to ultimate bending load. Fictitious crack model is adopted to predict fatigue crack growth of plain concrete beam under flexural fatigue. Experimental results show the linear relation between results of short-term and long-term test of chloride diffusion coefficient. Of the four common cement types, Ordinary Portland cement is the best cement type using for concretes in term of the chloride induced corrosion resistance because of the highest capacity to bind chloride ions. The proposed model shows that the flexural cyclic load accelerates chloride penetration into concrete. The higher the flexural load level, *SR*, the faster chloride penetration occurred. The model predictions fit well with experimental results when the crack density parameter, μ, and the tortuosity parameter, τ, are introduced.

Department: CIVIL ENGINEERING.....
Field of study: CIVIL ENGINEERING.....
Academic year: 2008.....

Student's signature: .....
Advisor's signature: .....
Co-advisor's signature: ...Toyoharu Nawa

ACKNOWLEDEMENTS

JICA is most sincerely thanked for funding this Ph.D project through AUN/SEED-Net program. Without the financial support given to me by JICA, this project would never have become about.

I wish to express my honest gratitude to my advisor, Assoc.Prof. Boonchai Stitmannaithum, to the staff and my colleagues at Department of Civil Engineering (CU) for their guidance, encouragement and support during my research.

I also wish to express my gratitude to Prof. Toyoharu NAWA for interesting discussions, as well as for helping me improve my model, and for his support of a useful year of doing research in his Laboratory at Hokkaido University, Japan.

Furthermore, I would like to express my gratitude to Assoc.Prof. Kiyofumi KURUMISAWA and to my friends at Resources and Eco Materials Engineering Laboratory, Hokkaido University, Japan, for their help and friendliness.

Finally, I would like to thank my sending institution – HoChiMinh City University (HCMUT) and host institution - Chulalongkorn University (CU) for giving me the opportunity to study Ph.D degree under AUN/SEED-Net program.

TABLE OF CONTENTS

LIST OF TABLES

LIST OF FIGURES

CHAPTER I

INTRODUCTION

1.1 Introduction

Oceans make up 80 percent of the surface of the earth. Up to now, many concrete structures have been built in marine environment such as piers, foundations, retaining walls, etc. Concrete is not only the most economic structural material for construction of large structures but also is the most durable when compared to other construction materials. There is a tendency of increasing the number and hugeness of concrete structures, which are exposed to deeper and rougher seawater, this demands on the safety and long-term durability. As a result, it is necessary to consider seriously the durability of concrete in marine environment.

The serviceability and durability of concrete structures in marine environment are governed by many mechanisms of deterioration such as chloride penetration and sulfate attack. However, in marine environment, the deterioration of concrete structures is mainly due to chloride induced corrosion. Chloride corrosion can be divided into three periods: initiation corrosion, corrosion propagation until concrete crack, and concrete crack up to degradation of structural performance. Marine environment includes atmospheric zone, tidal zone, splash zone and submerged zone. Of these four zones, tidal zone and splash zone are the most severe ones to corrosion of concrete structures.

In durability design of concrete structure in marine environment, with the viewpoint of durability of concrete, the first period of corrosion is chosen in design procedure of concrete structures. In the initial corrosion period, corrosion of reinforcement will start when critical chloride content is reached, pH of concrete surrounding reinforcement is below 11 to breakdown the passive film on surface of reinforcement, and there is the appearance of oxygen on the surface of the reinforcement. In the viewpoint of safety, the initial corrosion period is assumed to appear when the critical chloride concentration reaches. According to many researches, the critical chloride concentration is about 0.4% by cement content (Luca Bertolini, 2003).

In real concrete structures, damage is controlled by combination of mechanical actions and environmental actions. The cracks in concrete structures may be formed when concrete structures are subjected to mechanical action. As the results, in marine environment, chloride penetration into concrete structures is accelerated, and the service life of concrete structures will be reduced considerably.

There are numerous studies and proposed models on mechanical behaviour of concrete structures as well as material degradation in concrete (Xing Feng, 2005). But, these models of chloride penetration into concrete structures are proposed without simultaneous combination the actions of mechanical and environmental loads. As the results, these studies conducted separately by structure/ mechanics oriented people and material oriented people have not been integrated. Most of real concrete structures are under the influence of combined mechanical and climatic loads. Although, the consideration of multi-factorial deterioration will be more complex and will consume more time, but received results will be more representative for real structures and predictive models developed from these results will be more reliable.

The purpose of this research is to develop a model which combines chloride ingress and loading action to predict the chloride penetration and the initial corrosion time of concrete structures in the marine environment. This model will be based on theories and experiments of chloride diffusion test, chloride content tests and flexural cyclic loading test.

1.2. The objective of study

In this study, main objectives are considered as following:

1. Develop a model to predict the chloride penetration and the initial corrosion time of concrete structures which are subjected to the combination of flexural cyclic loading and marine environment.
2. Experimental study of chloride penetration into concrete with the simultaneous combination of flexural cyclic loading and marine environment.

With viewpoint of safety, the initial corrosion time is assumed to be the time when the critical chloride concentration reaches. This model will be developed basing on experimental data and mathematical analysis.

1.3. The scopes of study

To get these objectives, the scopes of this study are included as following:

1. Propose model to predict the initial corrosion period of concrete structures under combination of cyclic loading and tidal environment.
2. Do the experimental flexural cyclic loading of concrete structures in the simulated marine environment – tidal environment.
3. Experiments of chloride diffusion are made for concrete structures subjected to cyclic loading and non-loading.
4. Experiments of chloride diffusion by short-term and long-term test.
5. Experiments of chloride contents are made to set up chloride binding capacity.
6. Experiments of X-ray diffraction Rietveld (XRD Rietveld) analysis for Friedel's salt and of EPMA (Electron probe micro analysis) for chloride ion distribution before and after washing.
7. Verify model of predicting the chloride penetration and the initial corrosion period of concrete structures under combination actions of cyclic loading and tidal environment.

1.4. Literature review

Up to now, transport properties and models of transport of aggressive ions coupling with humid-thermal transport into concrete structures have been concerned by many researchers. Much effort concerns chloride permeability and diffusion mechanism. Also, models of permeability of seawater and chloride diffusion are made. These models based on microstructure and numerical solution to form mathematical formulations.

Because of the importance of chloride ingress to deterioration, mathematical models of chloride ingress are really necessary. Chloride ingress, from the external environment, occurs by diffusion and by capillary suction. In the early stages of exposure, chlorides are transported into concrete by absorption. The absorption effect may reduce with time unless the concrete is subject to wetting and drying. Mathematical models of chloride ingress currently being developed are primarily based on chloride diffusion although attempts have been made to take absorption into account. The following review illustrates the variety of approaches to model chloride ingress that could be used as starting points in the development of service life prediction tools and performance-based

specification. These approaches are models of chloride penetration in a saturated condition and models of chloride penetration in an unsaturated condition.

1.4.1 Models of chloride penetration in a saturated condition

The models, which describe the chloride penetration into concrete in a saturated condition, based on consideration of diffusion alone is constructed around Fick's second law of diffusion and the error function solution by Crank's solution, see Figure 1.1.

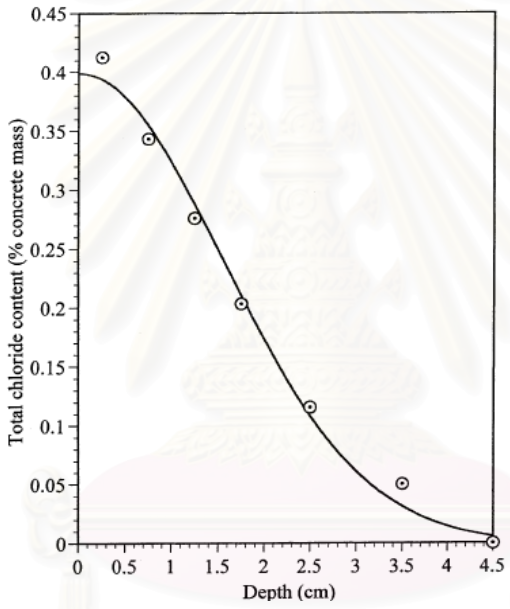

Figure 1.1 Application of Crank's solution to predict total chloride content (Yang, 2004)

Fick's second law of diffusion concerns the rate of change of concentration with respect to time. It may be stated as follows for diffusion in a semi-infinite, homogenous medium, where the apparent diffusion coefficient D_a is independent of the dependent and independent variables:

$$\frac{\partial C}{\partial t} = D_a \frac{\partial^2 C}{\partial x^2} \tag{1.1}$$

with C as the total chloride content, surface chloride concentration C_s, time t and the apparent diffusion coefficient D_a. On the following conditions:

(a) a single spatial dimension x, ranging from 0 to ∞

(b) $C = 0$ at $t = 0$ and $0 < x < \infty$ (initial condition)

(c) $C = C_s$ at $x = 0$ and $0 < t < \infty$ (boundary condition)

There are many researches applying Crank's solution to predict the chloride content by time at a specific depth as:

$$C = C_s\left[1 - erf\left(\frac{x}{2\sqrt{D_a t}}\right)\right] \tag{1.2}$$

or alternative as:

$$C = C_s erfc\left(\frac{x}{2\sqrt{D_a t}}\right) \tag{1.3}$$

where C_s is constant and with the error-function *erf()* and the error function complement *erfc()* as:

$$erf(p) = \frac{2}{\sqrt{\pi}}\int_0^p e^{-q^2}dq, \quad erfc(p) = \frac{2}{\sqrt{\pi}}\int_p^\infty e^{-q^2}dq, \quad erfc(p) = 1 - erf(p) \tag{1.4}$$

The error-function ranges from 0 (p=0) to 1 (p=∞). Equation (1.2) also can be written as:

$$x = 2erf^{-1}\left(\frac{C_s - C}{C_s}\right)\sqrt{D_a t} \tag{1.5}$$

where erf^{-1} is the inverse of the error-function.

1.4.1.1 Surface chloride content C_s

In conjunction with the above analytical solution, the surface chloride content is different in different structures, but may also vary in time. For structures exposed to a marine environment it was observed that the value of C_s reached in a few months' time tends to

remain constant. In marine environments, several transport processes may interact like capillary absorption and diffusion, depending on relative position with respect to the mean water level, wave height, tidal cycle. Moreover, cyclic wetting and drying (with different cycle lengths for tidal and splash zones) may cause accumulation of chloride, exposure to prevailing wind and precipitation may wash out previously absorbed chloride, and carbonation will release bound chloride. The high values of C_s were found in the tidal and splash zone, where evaporation of water leads to an increase in the chloride content at the concrete surface.

With regards to the change of surface chloride content by time, Kimitaka Uji et al 1990 proposed equation of calculation the surface chloride content by time as:

$$C_s = S.\sqrt{t} \tag{1.6}$$

where S is the surface coefficient and t is the time (s)

The results of this research showed that the value of S changed from 2 to 5×10^{-6} and 18 to 23×10^{-6} in the atmospheric zone and the tidal zone respectively.

1.4.1.2 Variability of chloride diffusion coefficient with w/c

With regard to *w/c*, JSCE proposed the equations of relationships between chloride diffusion coefficient and w/c as follow:

(a) Concrete without blast furnace slag of silica fume:

$$\log D = 4.5(w/c)^2 + 0.14(w/c) - 4.47 \tag{1.7}$$

(b) Concrete with blast furnace slag of silica fume:

$$\log D = 19.5(w/c)^2 - 13.8(w/c) - 1.7 \tag{1.8}$$

Also, Mohamed Boulfiza et al 2003 proposed model as following:

(c) Concrete without blast furnace slag of silica fume:

$$\log D = -3.9(w/c)^2 + 7.2(w/c) - 14.0 \quad (1.9)$$

(d) Concrete with blast furnace slag of silica fume:

$$\log D = -3.0(w/c)^2 + 5.4(w/c) - 13.7 \quad (1.10)$$

From these equations, it can be seen that the chloride diffusion coefficient increases as w/c increases and vice versa. With a given w/c, the chloride diffusion coefficients of concretes, which use additives, are smaller than those of concretes without additives.

1.4.1.3 Variability of D_a with relative humidity, time and temperature

Saetta et al 1990 proposed model to take into account the influences of all the variables as temperature; relative humidity and hydration degree. She considered a reference value of the intrinsic diffusion coefficient $D_{i,ref}$. The value of $D_{i,ref}$ is calculated in standard conditions : temperature (T_0 = 23^{0}C), relative humidity (h = 100%) and cement hydration degree after 28 days of maturation in standard conditions. With taking into account the influences of variables mentioned above, the value of intrinsic diffusion coefficient is evaluated as follow:

$$D_a = D_i/\phi \quad (1.11)$$

With ϕ is the binding capacity of material

$$D_i = D_{i,ref}.f_1(T).f_2(t).f_3(h) \quad (1.12)$$

where $f_1(T)$ is a function that takes into account the dependence of D_i on temperature T, $f_2(t_e)$ is a function that takes into account the effect of hydration degree on D_i, and $f_3(h)$ considers the effect of relative humidity on D_i.

$$f_1(T) = \exp\left[\frac{U}{R}.(\frac{1}{T_o} - \frac{1}{T})\right] \quad (1.13)$$

with T and T_o are expressed in deg K (T_o = 296K), R is the gas constant [KJ/(mol.K)] and U is the activation energy of the diffusion process (KJ/mol).

$$f_2(t) = \left(\frac{28}{t}\right)^m \tag{1.14}$$

with t is time (days), m is constant that depends on property of mix.

$$f_3(h) = \left[1 + \frac{(1-h)^4}{(1-h_c)^4}\right]^{-1} \tag{1.15}$$

with h is the relative humidity in concrete, h_c is the humidity at which the coefficient D_i drops halfway between its maximum and minimum values.

The value of $D_{i,ref}$ can be evaluated by the equation as (Sang-Hun Han 2007):

$$D_{i,ref} = D_{H2O}.0.15.\frac{1+\rho_c.\frac{w}{c}}{1+\rho_c.\frac{w}{c}+\frac{\rho_c}{\rho_a}.\frac{a}{c}}\left(\frac{\rho_c.\frac{w}{c}-0.85}{1+\rho_c.\frac{w}{c}}\right) \tag{1.16}$$

where D_{H2O} is the diffusion coefficient of chloride ion in infinite solution (equal to 1.6×10^{-9}m^2/s for NaCl and to 1.3×10^{-9}m^2/s for $CaCl_2$), ρ_c and ρ_a is the density of cement and aggregate respectively, a and c is the content of aggregate and of cement respectively.

1.4.2 Models of chloride penetration in an unsaturated condition

If the porous media is subjected to drying and wetting cycles, a certain amount of chlorides in solution will be dragged by water flux and this will cause a further term to be added to the diffusion process.

Grace et al 1987 modeled chloride ingress in concrete with using a convection-diffusion equation as:

$$\frac{\partial C}{\partial t} = (D_c + kv)\frac{\partial^2 C}{\partial x^2} - v\frac{\partial C}{\partial x} \tag{1.17}$$

with t is time, C is the free chloride concentration, D_c is the chloride diffusion coefficient, x is the concrete depth, k is the dispersion distance and v is the velocity of water.

Due to capillarity:

$$v = \frac{S}{2\varepsilon\sqrt{t}} \tag{1.18}$$

where S is the sorption coefficient as:

$$S = s_0\sqrt{1 - 1.08\frac{m(x)}{\varepsilon}} \tag{1.19}$$

with s_0 is constant, $S=s_0$ as $m=0$.

And due to moisture diffusion:

$$v = D_w\frac{\partial m(x,t)}{\partial x}\frac{1}{m(x,t)} \tag{1.20}$$

where ε is the porosity, D_w is the moisture diffusion coefficient and m is the moisture concentration.

Boddy et al 1999 described a model of convection-diffusion of chloride ions as follow:

$$\frac{\partial C}{\partial t} = D\frac{\partial^2 C}{\partial x^2} - v\frac{\partial C}{\partial x} + \frac{\rho}{n}\frac{\partial S}{\partial t} \tag{1.21}$$

with t is time, x is depth of concrete, C is the free chloride in solution, D is the diffusion coefficient, ρ is concrete density, n is the porosity, S is the bound chloride content and v is the average linear flow velocity defined as:

$$v = -\frac{k}{n}\frac{\partial h}{\partial x} \tag{1.22}$$

where k is the permeability coefficient and h is hydraulic head. Eq.(1.21) can be rearranged as:

$$n\frac{\partial C}{\partial t} - \rho\frac{\partial S}{\partial t} = nD\frac{\partial^2 C}{\partial x^2} - nv\frac{\partial C}{\partial x} \tag{1.22}$$

The righthand-side of Eq.(1.22) equals the global net influx of free chlorides. The lefthand-side, therefore, have to be equal to the change of total chlorides C_{tot} as:

$$\frac{\partial C_{tot}}{\partial t} = n\frac{\partial C}{\partial t} - \rho\frac{\partial S}{\partial t} \tag{1.23}$$

Eq.(1.23) implies that C_{tot} is the difference between free chloride and bound chloride, this is obviously not correct. The chloride diffusion coefficient described in Eq.(1.22) is dependent on time and temperature as bellow:

$$D(t,T) = D_{ref}\left(\frac{t_{ref}}{t}\right)^m e^{\frac{U}{R}\left(\frac{1}{T_{ref}} - \frac{1}{T}\right)} \tag{1.24}$$

where D_{ref} is the chloride diffusion coefficient at reference time t_{ref} and reference temperature T_{ref}, m is constant, U is activation energy of the diffusion process and R is the gas constant.

Relationship between bound chloride, C_b, and free chloride, C_f, follows Langmuir isotherm as:

$$C_b = \frac{\alpha C_f}{1 + \beta C_f} \tag{1.25}$$

with α and β are constants

Martín-Pérez et al 2001 modeled four coupled balances in two spatial dimensions *x* and *y*, which includes chloride transport, moisture diffusion, heat transfer and oxygen transport. Their potentials are free chloride concentration C_f, pore relative humidity *h*, temperature *T* and amount of oxygen dissolved in the pore solution of concrete C_o. The system of balance is defined as:

$$\begin{bmatrix} 1 & 0 & 0 & 0 \\ 0 & \dfrac{\partial w_e}{\partial h} & 0 & 0 \\ 0 & 0 & \rho_c c_q & 0 \\ 0 & 0 & 0 & 1 \end{bmatrix} \begin{Bmatrix} \dfrac{\partial C_f}{\partial t} \\ \dfrac{\partial h}{\partial t} \\ \dfrac{\partial T}{\partial t} \\ \dfrac{\partial C_o}{\partial t} \end{Bmatrix} = \nabla . \left(\begin{bmatrix} D_c^* & C_f D_h & 0 & 0 \\ 0 & D_h & 0 & 0 \\ 0 & 0 & \lambda & 0 \\ 0 & C_o D_h & 0 & D_o \end{bmatrix} \begin{Bmatrix} \nabla C_f \\ \nabla h \\ \nabla T \\ \nabla C_o \end{Bmatrix} \right) \tag{1.26}$$

with *t* is time, $\dfrac{\partial w_e}{\partial h}$ is moisture capacity, ρ_c is concrete density, c_q is specific heat capacity of concrete, D_c^* is apparent chloride diffusion coefficient, D_h is humidity diffusion coefficient, λ is thermal conductivity of concrete and D_o is oxygen diffusion coefficient. $C_f D_h$ and $C_o D_h$ account for convective terms in the chloride and oxygen balance. D_c^* is formulated as:

$$D_c^* = \frac{D_c}{1 + \dfrac{1}{w_e}\dfrac{\partial C_b}{\partial C_f}} \tag{1.27}$$

where w_e is the evaporable water content and $\dfrac{\partial C_b}{\partial C_f}$ is the chloride binding capacity. Chloride diffusivity D_c is specified as:

$$D_c = D_{c,ref} F_1(T) F_2(t) F_3(h) \tag{1.28}$$

in which, $D_{c,ref}$ is the chloride diffusivity reference value at time t_{ref} and temperature T_{ref}.

$$F_1(T) = e^{\frac{U}{R}\left(\frac{1}{T_{ref}} - \frac{1}{T}\right)} \tag{1.29}$$

$$F_2(t) = \left(\frac{t_{ref}}{t}\right)^m \tag{1.30}$$

$$F_3(h) = \frac{1}{1 + \left(\frac{1-h}{1-h_c}\right)^4} \tag{1.31}$$

with h_c is a constant (0.75)

However, Meijers et al 2003 commended that Eq.(1.27) seems to be inconsistent with the chloride balance, and this balance has probably been derived from:

$$\frac{\partial C_t}{\partial t} = \nabla.\left(w_e D_c \nabla C_f + C_f D_h \nabla h\right) \tag{1.32}$$

$$C_t = w_e C_f + C_b \tag{1.33}$$

$$C_f \frac{\partial w_e}{\partial t} + \left(w_e + \frac{\partial C_b}{\partial C_f}\right)\frac{\partial C_f}{\partial t} = \nabla.(w_e D_c \nabla C_f + C_f D_h \nabla h) \tag{1.34}$$

The humidity diffusion coefficient, D_h is further described as:

$$D_h = D_{h,ref} G_1(T) G_2(t_e) G_3(h) \tag{1.35}$$

in which, $D_{h,ref}$ is the humidity diffusivity reference.

$$G_1(T) = e^{\frac{U_m}{R}\left(\frac{1}{T_{ref}} - \frac{1}{T}\right)} \tag{1.36}$$

$$G_2(t_e) = 0.3 + \sqrt{\frac{13}{t_e}} \tag{1.37}$$

$$G_3(h) = 0.05 + \frac{0.95}{1 + \left(\frac{1-h}{1-h_c}\right)^n} \tag{1.38}$$

where n is a constant (from 6 to 16), U_m is the activation energy of the moisture diffusion process and t_e is the equivalent hydration period of concrete (s).

A model was proposed couple convection-diffusion of chloride ions from the following set of partial differential equations as (Roelfstra, 1996):

$$\begin{bmatrix} C_{\theta\theta} & C_{\theta h} & -Q \\ C_{h\theta} & C_{hh} & C_{h\alpha} + P \\ 0 & 0 & 1 \end{bmatrix} \begin{Bmatrix} \frac{\partial \theta}{\partial t} \\ \frac{\partial h}{\partial t} \\ \frac{\partial \alpha}{\partial t} \end{Bmatrix} = \begin{Bmatrix} \nabla.(\lambda_{\theta\theta}\nabla\theta + \lambda_{\theta h}\nabla h \\ \nabla.(\lambda_{h\theta}\nabla\theta + \lambda_{hh}\nabla h \\ F_1(\alpha, w/c)F_2(\theta)F_3(h) \end{Bmatrix} \tag{1.39}$$

with t is time, θ is temperature, α is degree of hydration, Q is total heat of hydration, P is total amount of water consumed in the hydration process, C_{ij} are capacitances, λ_{ij} and F_i are permeabilities and functions respectively.

The free chloride ion concentrations, e, are obtained from the following convection-diffusion equation:

$$\frac{\partial b}{\partial t} we + (b-1)\frac{\partial w}{\partial t} e + bw\frac{\partial e}{\partial t} - D_c w \nabla^2 e + v\nabla e = 0 \tag{1.40}$$

where:

$$b = \frac{C_t}{C_f} = 1 + (1-p)\gamma \tag{1.41}$$

with C_t and C_f are total chloride and free chloride content, respectively, p is porosity, w is the evaporable moisture content, D_c is the chloride diffusion coefficient, v is moisture flux, γ is the ration between C_p and C_f, C_p is physically bound chloride content.

The free chloride content, C_f and free chloride concentration, e, is related through the moisture content, w, as:

$$C_f = we \tag{1.42}$$

$$C_t = bwe \tag{1.43}$$

The flux of free chloride ions, J_c, is defined as:

$$J_c = -D_c w \nabla e - D_w e \nabla w \tag{1.44}$$

The net flux of free chloride ions balances the increases of the total chloride content in time:

$$\frac{\partial C_t}{\partial t} = -\nabla . J_c \tag{1.45}$$

That results in:

$$\frac{\partial C_t}{\partial t} = D_c w \nabla^2 e + (D_c + D_w) \nabla e \nabla w + D_w e \nabla^2 w \tag{1.46}$$

With:

$$\frac{\partial C_t}{\partial t} = \frac{\partial b}{\partial t} we + b \frac{\partial w}{\partial t} e + bw \frac{\partial e}{\partial t} \tag{1.47}$$

$$\frac{\partial w}{\partial t} = D_w \nabla^2 w \tag{1.48}$$

And the moisture flux, v, as:

$$v = -(D_c + D_w)\nabla w \tag{1.49}$$

Saetta et al 1993 modeled chloride transport in concrete accounted for moisture migration and heat flow. Saetta considered an element of infinitesimal dimension *dx*, *dy* and *dz* of porous body subjected to a moisture flux $J_w = (J_{w,x}; J_{w,y}; J_{w,z})$. The total chloride content variation is equal to the difference between the entering chloride flux and the exiting flux as following:

$$\begin{aligned}\frac{dQ_{C,t}}{dt} &= \frac{dC_t}{dt}dx.dy.dz \\ &= [J_{C,x}(x) - J_{C,x}(x+dx)]dy.dz \\ &+ [J_{C,y}(y) - J_{C,y}(y+dy)]dx.dz \\ &+ [J_{C,z}(z) - J_{C,z}(z+dz)dxdy\end{aligned} \tag{1.50}$$

The chloride flux J_C due to water flux can be expressed as an equation of the moisture flux and the free chloride concentration C_f in solution as follow:

$$J_C = C_f.J_w \tag{1.51}$$

In a small area of material and with assumption of constant free chloride concentration, J_w can be expressed by Fourier's series as follow:

$$J_w(x+dx) \approx J_w(x) + \frac{\partial J_w(x)}{\partial x}.dx \tag{1.52}$$

From equations (1.50), (1.51) and (1.52) we have:

$$\frac{\partial C_t}{\partial t} = -C_f.div(J_w) = \frac{C_t}{\phi}.\frac{\partial w}{\partial t} \tag{1.53}$$

where ϕ is the chloride binding capacity of the concrete (ratio between C_t and C_f), and w is free water content in concrete.

Therefore, in the cycle drying-wetting media, the equation used to express the total chloride movement is as follow:

$$\frac{\partial C_t}{\partial t} = D_a . \frac{\partial^2 C_t}{\partial x^2} + \frac{C_t}{\phi} . \frac{\partial w}{\partial t} \tag{1.54}$$

Moisture and heat transport in concrete are described by:

$$\begin{bmatrix} \rho c & 0 \\ -K & 1 \end{bmatrix} \begin{Bmatrix} \frac{\partial T}{\partial t} \\ \frac{\partial h}{\partial t} \end{Bmatrix} = \nabla . \left(\begin{bmatrix} \lambda & 0 \\ 0 & D_h(h,T,t_e) \end{bmatrix} \begin{Bmatrix} \nabla T \\ \nabla h \end{Bmatrix} \right) + \begin{Bmatrix} 0 \\ \frac{dh_s}{dt} \end{Bmatrix} \tag{1.55}$$

with temperature T, relative humidity in concrete h, concrete specific mass ρ, specific heat capacity c, coupling factor moisture-heat K, thermal conductivity λ, humidity diffusion coefficient D_h, equivalent maturation time t_e and dh_s/dt as the relative humidity variation due to self-desiccation. The free water content w is determined by the relative humidity in concrete, h, as bellow:

$$w = \begin{cases} w_{sat} h & , h \downarrow \quad desorption \\ w_{sat} h(1.16h^3 - 1.05h^2 - 0.11h + 1) & , h \uparrow \quad sorption \end{cases} \tag{1.56}$$

The total chloride content is a sum of free chloride and bound chloride content as:

$$C_t = wC_f + (1 - w_{sat})C_b \tag{1.57}$$

where w_{sat} is the saturated water content.

Assumption of linear chloride binding yields:

$$C_b = \gamma C_f \tag{1.58}$$

Substitute Eq.(1.58) in to (1.57), we have:

$$C_t = \phi C_f \tag{1.59}$$

with,

$$\phi = w + (1 - w_{sat})\gamma \tag{1.60}$$

The total chloride balance is:

$$\frac{\partial C_t}{\partial t} = \nabla.(D_a \nabla C_t) \tag{1.61}$$

$$D_a = \frac{D_i}{\phi} \tag{1.62}$$

where D_i is intrinsic diffusion coefficient and associated with the free chloride concentration. D_i is further defined as:

$$D_i = D_{i,ref}\, f_1(T)\, f_2(t_e)\, f_3(h) \tag{1.63}$$

with:

$$f_1(T) = e^{\frac{U}{R}(\frac{1}{T_o} - \frac{1}{T})} \tag{1.64}$$

$$f_2(t_e) = \zeta + (1 - \zeta)\sqrt{\frac{28}{t_e}} \tag{1.65}$$

$$f_3(h) = \frac{1}{1 + \left(\frac{1-h}{1-h_c}\right)^4} \tag{1.66}$$

with T_o is the reference temperature (296 K), and ζ is the ratio between the diffusion coefficient at $t_e \to \infty$ and the one at t_e=28 days.

The convective part of Eq.(1.54) is obtained by first balancing the convective chloride ion flux J_c with the total chloride content as:

$$\frac{\partial C_t}{\partial t} = -\nabla . J_c \tag{1.67}$$

And,

$$J_c = C_f J_w \tag{1.68}$$

In which J_w is the moisture flux. Substitute Eq.(1.68) into (1.67), we have:

$$\frac{\partial C_t}{\partial t} = -C_f \nabla . J_w - J_w \nabla C_f \tag{1.69}$$

One can see that the last term of Eq.(1.69) has been neglected in Saetta's model. The moisture balance presents as:

$$\frac{\partial w}{\partial t} = -\nabla . J_w \tag{1.70}$$

Substitution of Eq.(1.70) into Eq.(1.69) results in:

$$\frac{\partial C_t}{\partial t} = \frac{C_t}{\phi}\frac{\partial w}{\partial t} \tag{1.71}$$

The total chloride content calculated by Eq.(1.71) is the total chloride content due to the convective chloride ion in drying period.

1.4.3 Chloride binding in concrete structures

Chlorides in concrete are present in various forms that are internal chlorides and external chlorides. The internal chlorides are included in mix ingredients and in the principal constituent of most accelerating admixtures. The external chlorides are present in marine environment or in deicing salts.

Chloride-induced corrosion of reinforcement of concrete structures in marine environments is a major concern in marine construction. The chloride involved in this corrosion is present in concrete both in free or uncombined form as well as bound to cement hydration products through adsorption of C-S-H or in the chemical composition in the form of Friedel's salt ($C_3A.CaCl_2.10H_2O$). Generally, free chloride is considered to be responsible for the initiation of corrosion, and also that only free chloride can penetrate deeper inside the concrete cover through solution to reach the steel surface. Therefore, the binding of chloride retards the penetration process which delays the time when corrosion starts. As a result, it is necessary to consider chloride binding capacity of cement in the models to predict chloride penetration into concrete structures. Many models have been proposed to evaluate the contents of free and bound chloride, these models were based on experimental analysis of free and bound chloride and showed linear, Langmuir, or Freundlich isotherms. However, the models are still limited when applied to all commonly used cement types, and also, they do not specify clearly the various contributions of the physically bound chloride absorbed by C-S-H gel, or the chemically bound chloride which is present in the solid phase of Friedel's salt due to the reaction of AFm with chloride ions, to the complete chloride binding isotherms of cement types.

Hirao et al 2005 stated that the major hydrates of cement paste are C-S-H gel, $Ca(OH)_2$, Aft ($C_3A.3CaSO_4.32H_2O$), and AFm ($C_3A.3CaSO_4.10H_2O$). Of these hydrates, Aft and $Ca(OH)_2$ has little capacity to bind chloride; C-S-H has a very large surface and is able to bind various kinds of ions (Rayment, 1983) including chloride ions. Further, the chloride binding capacity of C-S-H depends on the chemical composition and surface area as well as the kind of chloride solution and experimental conditions (Delagrave, 1997). Tang et al 1993 confirmed that the chloride binding capacity of AFm is higher than that of the C-S-H gel, however, C-S-H gel comprises most of concrete, maybe up to 70% of the mass of cement paste. Hence, overall, the physically bound chloride amount due to the absorption of chloride ions on C-S-H is much higher than that of the chemically bound chloride. Various cement

types have different contents of compounds that make the cement paste formed with different amounts of hydrates. Consequently, the chloride binding isotherms of various cement types may have been different.

Regarding to chloride binding capacity of Ordinary Portland cement (OPC) added with mineral admixture, Rui Luo et al 2001 found that ground granulated blastfurnace slag (GGBS) can improve the pore structure of OPC and decrease the chloride diffusion coefficient greatly, and that sulfates do not do good for the pore structure and chloride diffusion for GGBS. GGBS increases the chloride-binding capability greatly without reference to the internal or external chloride and sulfates decrease the chloride-binding capability of GGBS greatly. The fact that GGBS can form more Friedel's salt is the reason why GGBS can increase the chloride-binding capability, as shown in Figure 1.2, and the reason why sulfate and alkalinity influence the chloride binding is the competition among sulphate ions, hydroxyl ions and chloride ions during the formation of Fridel's salt.

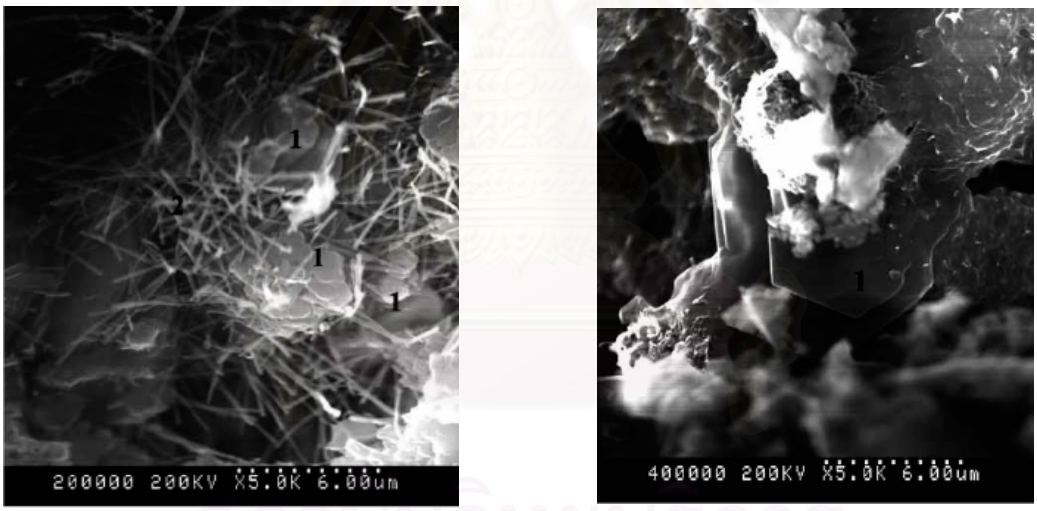

Figure 1.2 Friedel's salt "1" and Ettringite "2"(Rui Luo, 2001)

Nielsen et al 2004 studied binding of chloride and alkalis in Portland cement system. In this study, the effect of the chloride and alkalis has been quantified by experiments on cement pastes prepared from white Portland cements containing 4% and 12% C_3A, and a grey Portland cement containing 7% C_3A. One weight percent calcite was added to all cements. The pastes prepared at w/s ratio of 0.70 were stored in solutions of different Cl ($CaCl_2$) and Na (NaOH) concentrations. When equilibrium was reached, the mineralogy of the pastes was investigated by Energy dispersive X-ray analysis (EDS analysis) on the Scanning electron microscopy (SEM). A well-defined distribution of chloride was found

between the pore solution, the C-S-H phase, and an AFm solid solution phase consisting of Friedel's salt and monocarbonate. Partition coefficients varied as a function of iron and alkali contents. The lower content of alkalis in white Portland cement results in higher chloride contents in the C-S-H phase, see Figure 1.3. High alkali contents result in higher chloride concentrations in the pore solution.

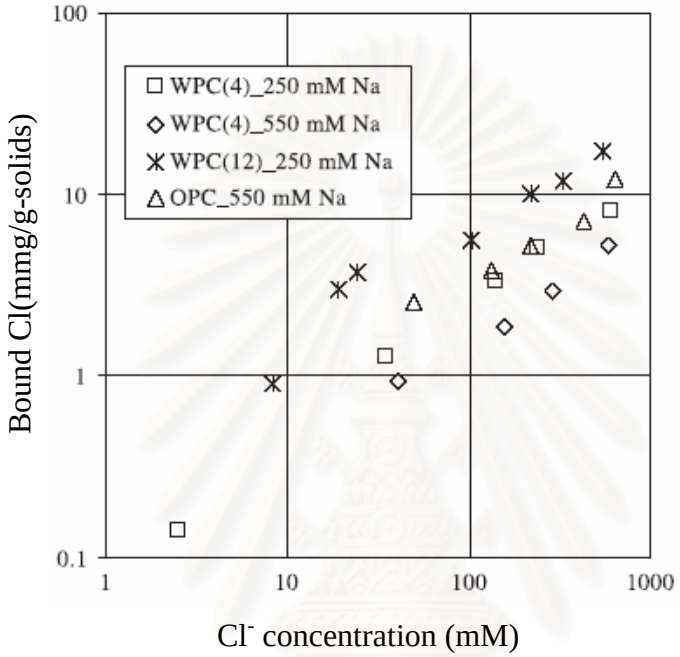

Figure 1.3 Chloride binding isotherms determined for cement pastes,
OPC: Ordinary Portland cement ; WPC: white Portland cement (Nielsen, 2004)

Paul Sandberg et al 1998 investigated chloride binding in concrete exposed in marine environment. In this research, the concentrations of "free" chloride and hydroxide ions in extracted pore solution from concrete exposed and submerged in a marine field station were studied by the pore solution expression method. In addition, the corresponding concentrations of total acid soluble chloride in the concrete were analyzed. The relationship between total and free chlorides was analyzed and compared with similar data from laboratory-exposed cement paste and concrete. Hydroxide ions were found to be transported away from the concrete at a rate similar to the penetration rate of chloride ions into the concrete. The amount of bound chlorides was found to increase as the concentration of hydroxide ions in the pore solution decreases. As a consequence, the relationship between free and total chlorides in concrete with a chloride and hydroxide ion gradient was found to be almost linear. It was suggested that the nonlinear chloride binding relationship observed in laboratory equilibrium tests is not relevant for submerged concrete with diffusion gradients of

chloride and hydroxide. However, only limited information exists on the long-term chloride binding relationship reflecting the long-term situation when all alkali hydroxides have been leached to the sea. It was speculated that the chloride binding and the transport rate depend on the available amount of mobile alkali hydroxide and thus on the thickness of the concrete member.

1.4.4 Chloride ingress into concrete structures under combined mechanical and climatic loads

In real concrete structures, cracks may occur in the concrete cover due to mechanical load, and the corrosion of reinforcement will be accelerated with passing aggressive agents through the crack. Ema Kato et al 2005 studied the influence of crack formation on chloride penetration. Reinforced beams as shown in Figure 1.4, which have different concrete covers and different water/cement ratio, were subjected to 4 point load to generate a flexural crack after being cured in water for 28 days. Then, specimens were subjected to accelerated penetration of chloride ions through a wet test and cyclic drying – wetting test. The solution used in the accelerated test was sodium chloride solution (3% NaCl). In each test, the environmental temperature was kept constant. After the chloride penetration accelerated test, concrete samples were drilled to measure the chloride content at different thickness. In this study, cracked zone was considered as exposed surface. Results of this study showed that chloride content at the cracked zone were higher than other places because of chloride penetration through cracks, and chloride contents in cyclic drying – wetting condition were higher than those of wet condition. And the deeper from the crack face the sampling points were, the smaller the chloride content. Chloride concentration varied in the cracked zone and influenced the chloride profile in the cracked zone.

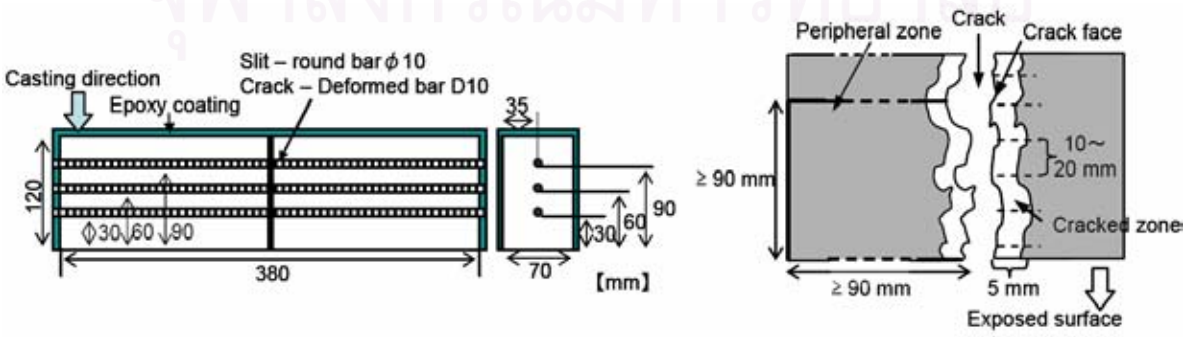

Figure 1.4 Specimen and sample for measurement (Ema Kato, 2005)

A.Nakhi et al 2000 studied the chloride penetration by the simultaneous action of mechanical loading and saltine environment. In this study, compression cyclic loading was used and three loading levels were used: 50%, 60% and 70% of the ultimate compression strength. The chloride penetration test was modified standard of the long-term chloride penetration test using AASHTO T259. This test used concrete specimen with a hollow square cross section. On each loading cycle, load was held for 20 minutes, and totally, 13 loading cycles were applied. Results of this study showed that a significant increase in concrete permeability occurs when the concrete is loaded above 60% of its compressive strength. With increasing load level from zero up to 70% of compressive strength, both chloride concentration and penetration depth increases. The most drastic increase occurred in the loading range from 60% to 70% of compressive strength. And, the higher level of mechanical loading on concrete is, the higher degree of internal damage appears, cyclic loading accelerates chloride penetration through concrete. However, the effect of acceleration is not significant when the applied loading is below 60% of the concrete strength.

Also, Gontar et al 2000 studied the chloride penetration in to plain concrete beam subjected to flexural cyclic load with different load level. Results of this research stated that chloride penetration, in the tension zone, increases with increasing load level, especially with load level 0.7 and 0.8.

Xing Feng et al 2005 studied the influence of long-term load on the chloride permeability in reinforced concrete. Result of this research confirmed that the chloride penetration in to tension zone of reinforced concrete beam, in term of chloride diffusion coefficient, is accelerated as load level increases. However, in the compression zone, the chloride diffusion coefficient is decreased with increasing load level. And, experimental equations were established to determined chloride diffusion coefficients in compression zone and tension zone as:

(a) In the tension zone

$$\frac{D_L}{D} = 1 + aL^3 \tag{1.72}$$

(b) In the compression zone

$$\frac{D_L}{D} = a + b_1 L + b_2 L^2 \tag{1.73}$$

where L is flexural load level (%) compared to ultimate flexural load, a, b_1 and b_2 are regression constants. D_L and D are chloride diffusion coefficient with and without loading, respectively.

1.5. Methodology

Methodology used in this study includes experimental and theoretical approaches.

1. Experimental study includes mix concrete design, flexural strength, flexural cyclic loading, chloride diffusion, chloride content, XRD, EPMA tests and microscopy. Some of these tests follow standard tests and the others are modified standard tests.
2. Theoretical study includes numerical solution (finite difference method) and mathematical analysis.

Mix concrete design follows the ACI 211 guideline. The materials such as coarse aggregate and fine aggregate satisfy ASTM standard. The flexural test is designed to follow ASTM C78 – Standard test method for flexural strength of concrete using simple beam with third – point loading. The result of flexural test – flexural strength is not the parameter of chloride predicting model. However, the result of this test will help to determine a frame of flexural cyclic loading, which is the ratio of applied flexural cyclic loading to flexural strength (SR).

Regarding to flexural cyclic loading test in simulated tidal environment, this test is not standard test. Firstly, flexural cyclic loading is conducted to determine the loading speed for each cycle and the number of cyclic loading N at which cracks do not appear and it is enough to create the internal cracks in concrete structures. The internal cracks of concrete structures are assumed to form when the flattening of the loop is visual. Secondly, after determining the loading speed and the number of cycle as mentioned above, the flexural cyclic loading test will be conducted in simulated tidal environment. In this test, the simulated tidal environment is wetting – drying cycle environment. To simulate the real tidal environment, the cycle regime of 12 hour wetting in sodium chloride and then 12 hour drying is reasonable. With this simulated tidal environment, concrete beams are immerged in sodium chloride solution (NaCl 10%) for 12 hours and then they are dried for 12 hours, the temperature is kept constant during the test. Simultaneously, the flexural cyclic load applies to concrete beams.

The chloride diffusion tests, which include long-term and short-term tests, are made for both concrete beams with cyclic loading and concrete beams without cyclic loading. The

result of this test is the chloride diffusion coefficient. The chloride diffusion coefficient will be used as one of the parameters of model to predict chloride content. In this model, the chloride diffusion coefficient will be a function of the flexural cyclic loading frame. After finishing flexural cyclic loading test, chloride content tests are made at different depth.

In order to quantitative the kinds of chloride ions in concrete structure, XRD Rietveld analyse is used to determine contents of compounds as C-S-H, AFm and Friedel's salt.

In this study, numerical solution used to propose model of chloride ingress into concrete structure is finite difference method. To solve the equation of Fick's second law, Finite difference methods (FDM) can be applied to evaluate total chloride concentration by time and space. In FDM, we need to pay attention to choosing the time and space increments so that the numerical analysis can have fast convergence as well as good accuracy. Besides, mathematical analysis is used either to analyse experimental data or to solve approximately problems of fatigue deformations of concrete. FDM includes several methods with different accuracy. Therefore, in order to determine which method of FDM is the best, some initial comparisons of numerical analysis using different methods of FDM are needed to perform. The global steps of research are shown clearly in Figure 1.5.

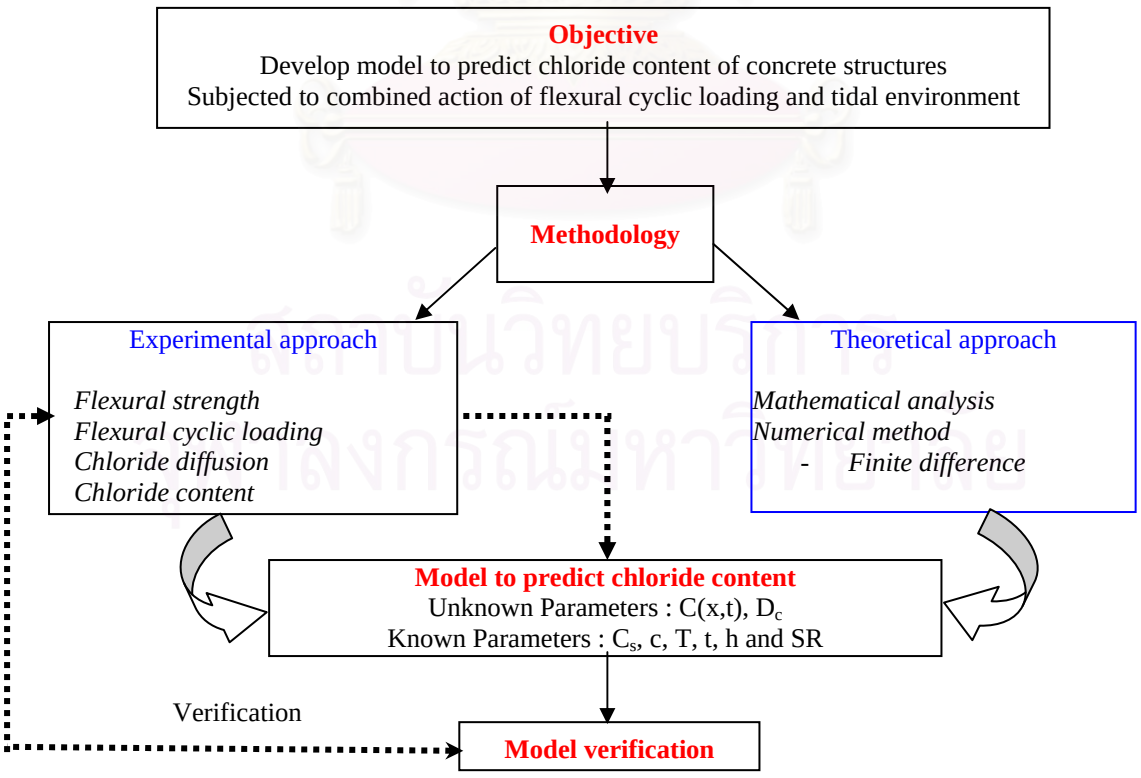

Figure 1.5 The global steps of research

1.6. Originality and expected results of research

So far, many models of chloride penetration into concrete structures have been proposed. However, these models only account for chloride penetration under environmental load. Recently, a new tendency of modelling chloride penetration into concretes, in which concrete structures are under mechanical load and climatic load, has been being issued. The researches regarding to this new tendency are still a few. In addition, of common cement types used for construction, we do not know what type of cement is the best used for concrete structures in marine environment.

The originality of this research includes as:

1. Model of chloride penetration into concrete structure under flexural cyclic load and tidal environment. Results archived from this model show crack growth of plain concrete beam under fatigue, effect of cyclic on chloride diffusion coefficient, and chloride profiles of concrete under different load level of cyclic load and different exposed time. This model can also apply for a prediction of chloride profile of reinforced concrete as long as we know crack characteristics in term of crack width and crack length.
2. Propose clearly chloride binding capacities of four common cement types. Thereby, results help designer know how to choose the suitable cement type to increase durability of concrete structures used in marine environment.

Following methodology and originality mentioned above, this research expects to archive results as:

1. Model of crack growth of plain concrete beam under fatigue.
2. Model of chloride diffusion coefficient of plain concrete under fatigue.
3. Model of chloride penetration into concrete under flexural cyclic load and tide.
4. Propose chloride binding capacities of four common cement types and method to estimate bound chloride content in different cement pastes.

1.7. Concluding remarks

This chapter presents the objective, literature review and methodology of research. Major concluding remarks are drawn from this chapter as following:

1. Most of research concentrated on effects of materials and environment on the chloride penetration into concrete. There are a few researches integrating mechanical load and climatic load on the chloride penetration into the real concrete structures.
2. Regarding to modelling of chloride penetration into the real concrete structures, the chloride diffusion coefficient, D, the chloride binding capacity, ϕ and loading effect are major parameters needed to consider.
3. Cements have different chemical and physical compositions, which result in the differences in the chloride binding capacity of the cements.
4. With point of view of safety, the initial corrosion starts as the chloride content, at the surface of reinforcement, reaches the critical chloride content of 0.4% by mass of cement.
5. The objective of this research is to propose a model to predict the chloride penetration into concrete structures under flexural cyclic load and tidal effect, in which effects of the flexural cyclic load, in terms of number of cycles and load level, on the chloride diffusion coefficient and the chloride binding capacities of different cement are investigated.
6. The proposed model of this research bases on the experimental and theoretical studies. Then, the validity of the proposed model is verified by experimental data.

CHAPTER II

DEVELOPMENT OF MODEL

2.1 Prediction of mechanical and physical properties of concrete

Mechanical and physical properties of concrete depend on components and mixture proportions of concretes such as cement type, maximum size of coarse aggregate, content of cement and water to cement ratio. However, at a given cement type, cement content and aggregate properties, mechanical and physical properties of concrete are governed by water to cement ratio, *w/c*.

Normally, in the procedure of mix design of concrete proportions, compression strength of concrete can be estimated using chart built from experimental data, as shown in Figure 2.1.

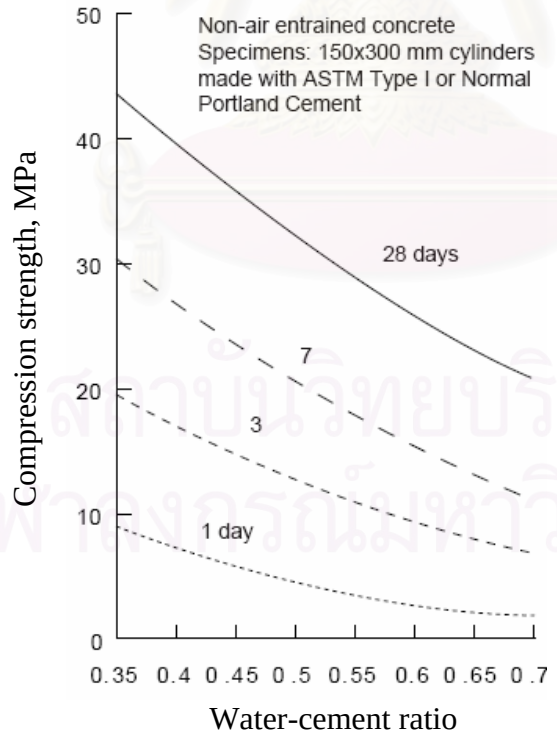

Figure 2.1 Influence of water-cement ratio on the compression strength of concrete (Mehta, 1993)

Obviously, at a give water-cement ratio, the longer the moist curing period the higher the strength. The estimation of the compression strength of moist cured concrete with time is proposed by ACI 209 as following:

$$\sigma_c(t) = \sigma_{c28}\left(\frac{t}{4 + 0.85t}\right) \tag{2.1}$$

where $\sigma_c(t)$ is the compression strength at time t, days. σ_{c28} is the compression strength measured at 28 days of moist curing.

It has been pointed out that the compression strength and tensile strength are closely related. The tensile strength increases as the compression strength increases. The tension-compression strength ratio depends on the general level of the compression strength, the higher the compression strength, the lower the ratio. Tensile strength to compression strength ratio decrease from 9.2% to 7.2% as the compression strength increases from 21 to 55 MPa (Mehta, 1993). The tension strength can be determined indirectly via the compression strength by recommendations of ACI as bellow:

$$\sigma_t = 0.3\sigma_c^{2/3} \tag{2.2}$$

where σ_t and $\sigma_{c,}$ MPa, are the tensile strength and the compression strength, respectively.

Commonly, the tensile strength of concrete is estimated by ASTM C496 splitting tension test and the ASTM C78 four-point bending test. In the four-point bending test, flexural strength is expressed as:

$$R = \frac{P_{ult}l}{bh^2} \tag{2.3}$$

where R is the flexural strength, P_{ult} is the ultimate bending load, l is the span length, b is width of specimen and h is depth of specimen.

With normal strength concrete, ratio of tensile strength to flexural strength changes from 0.59 to 0.75 depending on the compression strength of concrete (Mehta, 1993).

Therefore, the ultimate bending load, P_{ult}, can be estimated through the tensile strength, σ_t, as:

$$P_{ult} = (0.59 \div 0.75)\frac{\sigma_t bh^2}{l} \tag{2.4}$$

When the ultimate bending load is reached, concrete beam is fractured. At this stage, the deflection at the middle bottom position of beam can be estimated as (Ulfkjær, 1995):

$$\delta_c = \frac{Ml^2}{12EI}\beta(\lambda) \tag{2.5}$$

With:

$$M = \frac{bh^2}{6}R \tag{2.6}$$

$$\beta(\lambda) = 1 + \frac{2.85}{\lambda^2} - \frac{0.84}{\lambda^3} \tag{2.7}$$

where M is moment corresponding to flexural strength, EI is bending stiffness of the beam, $\lambda = l/b$ is slenderness ratio.

Corresponding to the deflection of concrete beam at the fracture stage, critical fictitious crack width, w_c, is estimated about 50-120μm depending on tensile strength of the concrete (Reinhardt, 1984 and Wittmann, 1987).

Another mechanical property of concrete needed to consider is Young's modulus, E. Young's modulus can be determined either by direct method through relationship between bending load and deflection of concrete beam or by indirect method depending on the compression strength of concrete as below:

$$E = 4.7\sqrt{\sigma_c} \tag{2.8}$$

where E is the Young's modulus of concrete, GPa. σ_c is the compression strength, MPa.

Regarding to model of chloride penetration into concrete structures, the chloride diffusion coefficient, as mentioned in Chapter I, is one of the major parameters to govern the chloride ingress. So far, the chloride diffusion coefficient has been modelled as a function mainly depending on water-cement ratio and types of binders.

Also, Mohamed Boulfiza et al 2003 proposed model as following:

(a) Concrete without blast furnace slag of silica fume:

$$\log D = -3.9(w/c)^2 + 7.2(w/c) - 14.0 \tag{2.9}$$

(b) Concrete with blast furnace slag of silica fume:

$$\log D = -3.0(w/c)^2 + 5.4(w/c) - 13.7 \tag{2.10}$$

Webster et al 1999 proposed the following equation for chloride contamination in marine environment, based on data collected around the world, but normalized to an average United Kingdom ambient temperature using the Arrhenius function:

$$D = 0.004(1166^{w/b})10^{-12} \tag{2.11}$$

where D is the chloride diffusion coefficient and w/b is the water-binder ratio.

By the time, as concrete matures, the mass transfer of concrete will decrease since the capillary pore system becomes denser as hydration products continue to form. This reduces the diffusion paths for the penetration of ions, including chloride ions, through concrete cover. As a result, chloride diffusion coefficient of concrete is time dependent, it is decreased by time. Time dependent diffusion of concrete is modeled as (Michelle Nokken, 2006 and Kyle Stanish, 2003):

$$D(t) = D_{28}\left(\frac{t_{28}}{t}\right)^m \tag{2.12}$$

where $D(t)$ is diffusion coefficient at time t; D_{28} is diffusion coefficient at reference time 28 days; m is constant which depends on mixture proportions.

2.2 Fatigue and fatigue deformation of plain concrete beam under flexural cyclic load

2.2.1 Fatigue of concrete

Fatigue is the process of cumulative damage that is caused by repeated fluctuating loads. Fatigue loading types are generally distinctly divided between high-cycle low amplitude and low-cycle high amplitude. Hsu classified the fatigue loads into three ranges: the low-cycle fatigue loading occurs with less than 1000 cycles, the high-cycle fatigue loading is defined in the range of 10^3 to 10^7 cycles which normally occurs in bridges, highways, airport runways and machine foundations, the super high-cycle fatigue loading is characterized by even higher cycles of fatigue loads.

Fatigue damage occurs at non-linear deformation regions under applied fluctuating load. However, fatigue damage for members that are subjected to elastic fluctuating stress can occur at regions of stress concentrations where localized stresses exceed the linear limit of the material. After a certain number of load fluctuation, the accumulated damage causes the initiation or propagation of cracks in the concrete matrix, this results in an increase in deflection and crack width and in many cases can cause the fracture of concrete. The total fatigue life *N*, is the number of cycles required to cause failure of a concrete structure. There are many parameters affecting the fatigue strength of concrete structures. These parameters are related to state of stress, stress range, stress ratio, frequency, maximum strength, geometry of the element, concrete properties and external environment. Concrete structures are subjected to a variety of stress histories. The simplest form of these stress histories is the constant-amplitude cyclic-stress fluctuation. This type of loading can be represented by a constant stress range, Δf; a mean stress f_{mean} and stress ratio R as shown in Figure 2.2. One can see that a complete reversal of load from a minimum stress to an equal maximum stress corresponds to an R=-1 and a mean stress of zero (Figure 2.2a). Acyclic stress from zero to a peak value corresponds to an R=0 and a mean stress equal to half the peak stress value as shown in Figure 2.2b. R=1 represents a case of constant applied stress with no intensity fluctuation. Normally, range of fatigue load for concrete structures is between R=0 and R=1.

$$\Delta f = f_{\max} - f_{\min} \tag{2.13}$$

$$f_{mean} = \frac{f_{\max} - f_{\min}}{2} \tag{2.14}$$

$$R = \frac{f_{\min}}{f_{\max}} \tag{2.15}$$

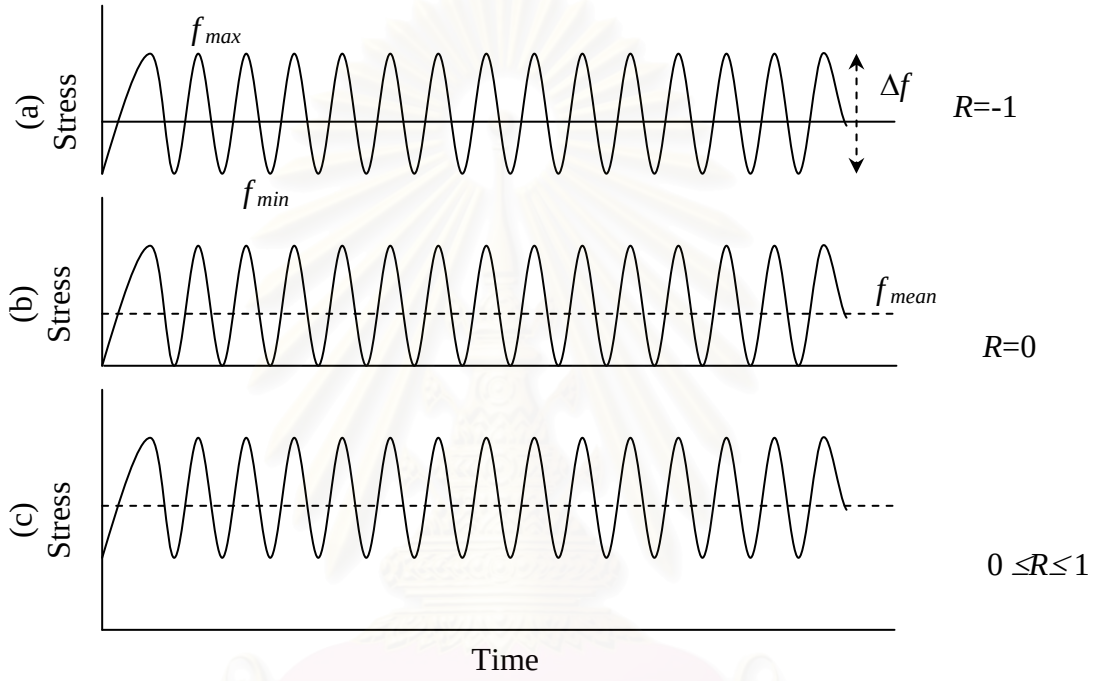

Figure 2.2 Constant amplitude fatigue loading

Concern with fatigue damage of concrete, cementitious composites possessed the properties of progressive failure, which becomes total under the repetition of load well below the ultimate strength of the material. The stress-strain curve of concrete varies with the number of cycles, changing from concave towards the strain axis to a straight line, which shifts at a decreasing rate (plastic permanent deformation) and finally to concave toward the stress axis, see Figure 2.3. The degree of this later concavity is an indication of how near the concrete is to failure.

2.2.2 Nonlinear fracture mechanics of concrete

So far, linear elastic fracture mechanics (LEFM) had been proposed and applied to concrete as concrete was considered as brittle material. With LEFM, the stress-strain relationship was used, it showed that the stress and strain in the vicinity of a crack tip are very large, and that during the fracture process the entire body remained elastic and energy was only dissipated at the crack tip. However, it demonstrates conclusively that the fracture behaviour of concrete deviates significantly from the predictions of LEFM. The primary reason for the observed deviation of the behaviour of concrete from the LEFM prediction is the formation of an extensive fracture process zone, where softening of material occurs as concrete is a quasi-brittle material, ahead of a crack tip. The material in this zone progressively softens due to microcracking as shown in Figure 2.4. Since linear elastic fracture mechanics (LEFM) can not adequately characterize the cracking and failure of concrete, several nonlinear facture mechanics have been proposed including fictitious crack model which is the first of the nonlinear fracture mechanics.

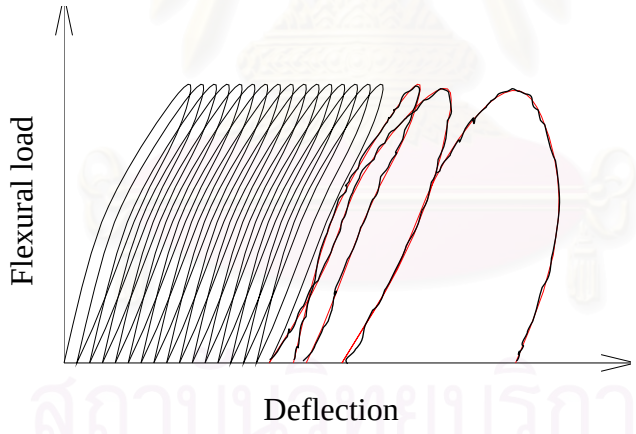

Figure 2.3 Deflection of concrete beam by number of cycles

Fictitious crack model (FCM) has been proposed as a discrete crack approach to analyze the fracture of concrete, in which there is a zone in the vicinity of the crack-tip with varying closing stress. In FCM, a crack is initiated when the tensile stress reaches the tensile strength of concrete, f_t, and it propagates in a direction normal to the stress. As the crack-opening (w) increases, the closing stresses, $\sigma(w)$, in the fracture process zone behind the crack-tip gradually decrease from f_t at the tip of the fictitious crack to zero at the tip of the

pre-existing traction-free macrocrack, see Figure 2.5. In other words, the distribution of the closing stresses, $\sigma(w)$, along the fracture process zone depends on the opening of the fictitious crack faces, w.

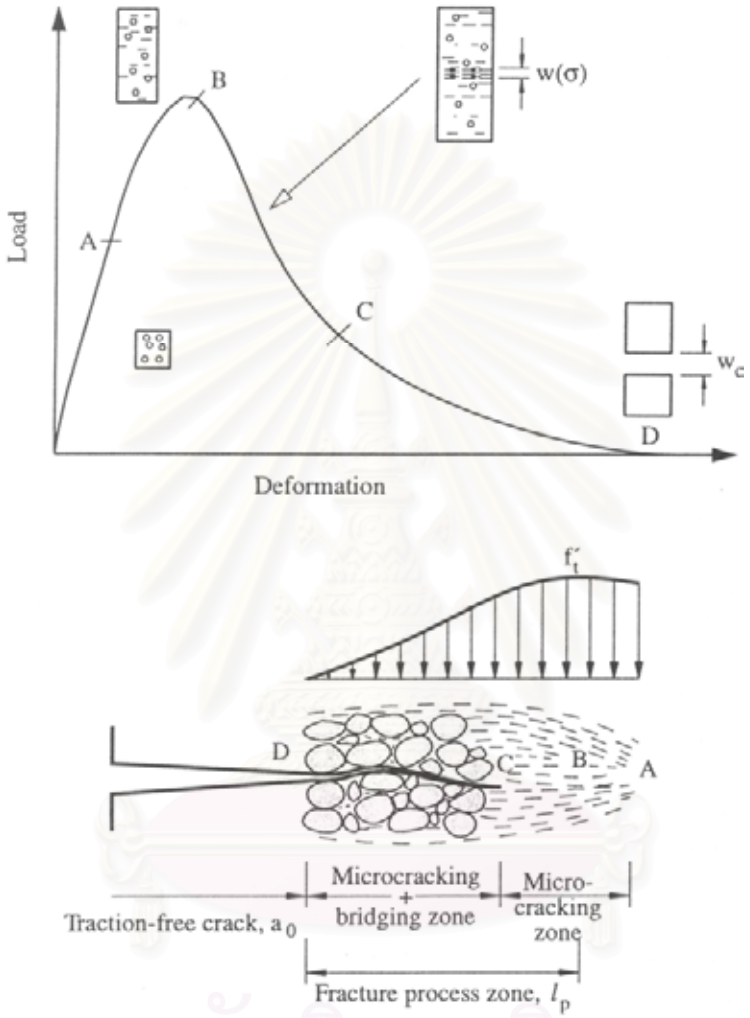

Figure 2.4 Typical fracture process of a pre-cracked concrete specimen. Fracture process extends over the softening region (BCD) and surrounded by a nonlinear region (BA)

The stress-crack opening relation is assumed to be a property of concrete. The fracture criteria of the FCM can be summarized as:

$$w = 0, \quad \sigma = f_t \tag{2.16}$$

$$w = w_c , \quad \sigma = 0 \tag{2.17}$$

$$\int_0^{w_c} \sigma(w)dw = G_f \tag{2.18}$$

where w_c is the critical crack opening. The conditions in Eq.(2.15) and (2.16) occur at the tips of the fictitious crack (l_p) and the traction-free crack (a_o), respectively. Several different shapes have been proposed for the $\sigma(w)$ relation including linear, bilinear and smoothly varying functions.

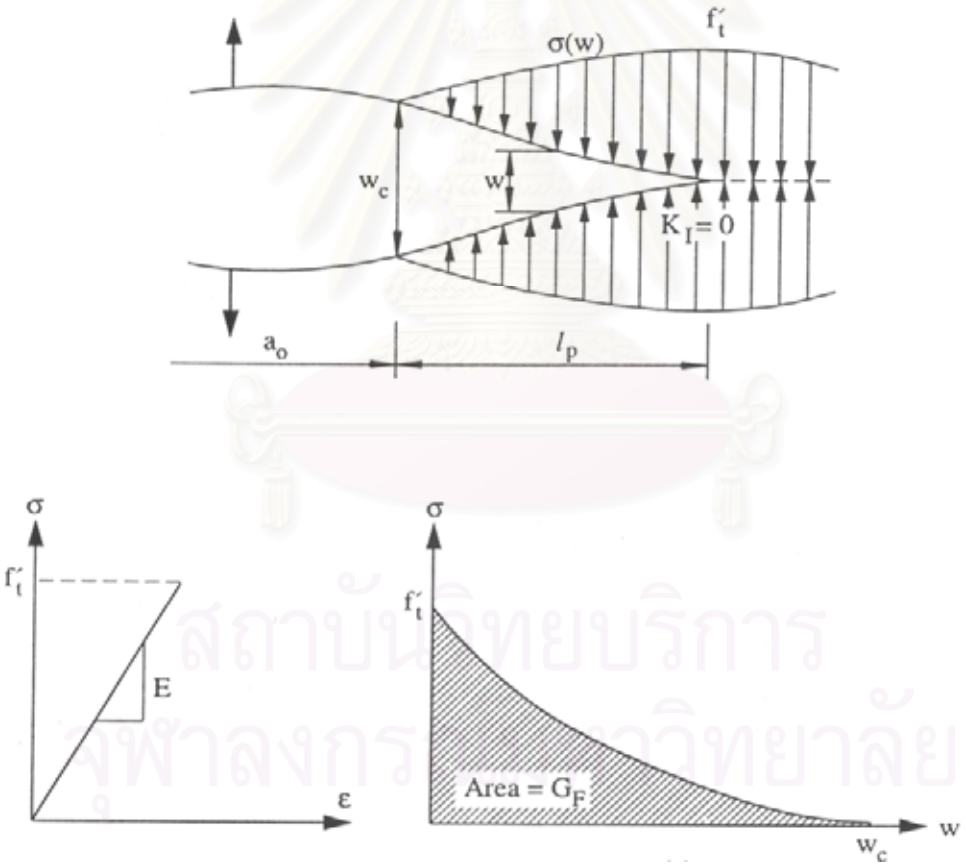

Figure 2.5 The distribution of closing stresses in the fictitious crack model

2.2.3 Prediction of fatigue deformation of concrete under flexural cyclic load

The crack growth process of plain concrete beam with depth *h*, width *b* and span *l* under flexural cyclic load can be generally divided into two stages: the fictitious crack initiation stage and the fictitious crack developing stage. The former will occur when bending load reaches the first crack load. In the later, as shown in Figure 2.6, stress distribution is nonlinear and linear in the cracked zone and uncracked zone, respectively.

In the cracked zone, a linear crack opening profile can be expressed (Jun Zhang, 1999):

$$w = \delta\left(1 - \frac{x}{ah}\right) \tag{2.19}$$

where w is the crack width at a specific location x, and δ is crack mouth opening.

The stress distribution in the cracked zone, $\sigma_I(x)$, can be expressed as a function of crack length ah, $0 \le a \le 1$, and δ, combining stress-crack relationship and Eq. (2.19) as below:

$$\sigma_I(x) = \sigma(w) = \sigma\left(\delta\left(1 - \frac{x}{ah}\right)\right) \tag{2.20}$$

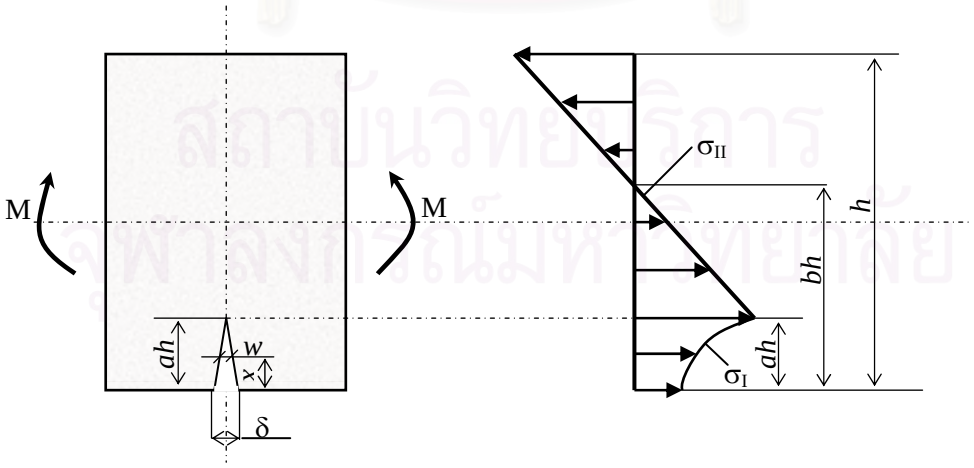

Figure 2.6 Distribution of stress in the second stage

For flexural cyclic load, in the cracked zone, $\sigma_I(x)$ can be contributed by stress degradation law. With plain concrete beam, the stress degradation law can be expressed as a function of logarithm of the number of cycles:

$$\frac{\sigma_N}{\sigma_1} = 1 - \varphi k \log(N) \tag{2.21}$$

where σ_N and σ_1 are the stresses in the cracked zone at the at maximum applied load, $P_{app,\,max}$, after N cycles and the first cycle, respectively. φ presents the influence of minimum crack width formed at the minimum applied load, $P_{app,\,min}$, on the stress degradation. When $P_{app,\,min}$ equals to zero, the maximum degradation, φ =1, will occur. On the contrary, the minimum degradation, φ =0, will appear when the crack width formed by $P_{app,\,min}$ equals to that formed by $P_{app,\,max}$. In this research, plain concrete was used, and $P_{app,\,min}$ was equal to zero as shown in Figure 2.7. Hence, the maximum degradation will occur, φ =1.

For plain concrete, k is expressed depending on $w_{1,N}$ and φ as:

$$k = \varphi(0.08 + 4w_{1,N}) \tag{2.22}$$

where $w_{1,N}$ is the crack width, in the cracked zone, formed by $P_{app,\,max}$ at the cycle N. From Eq. (2.21) and (2.22), we see that when the number of cycles increases, $w_{1,N}$ increases and consequently the stress in the cracked zone reduces until σ_N equals to zero, at which fracture of concrete beam occurs.

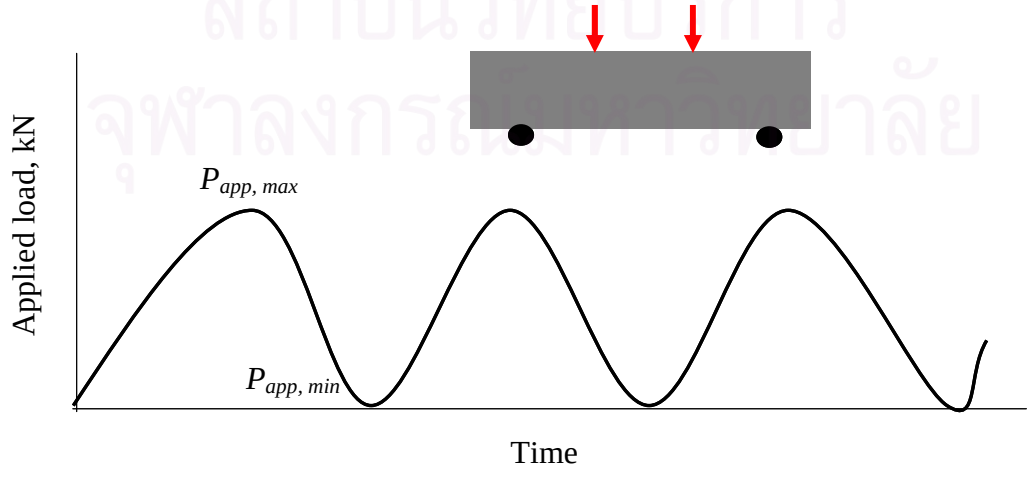

Figure 2.7 Loading procedure in flexural cyclic test

Based on the experimental data, Zhang et al 1999 proposed that σ_1 can be related to tensile strength of concrete, σ_t, and initially ramped up crack width w_i where the bending load is ramped up to $P_{app,\,max}$, as below:

$$\frac{\sigma_1}{\sigma_t} = c + dw_i \tag{2.23}$$

where c and d are parameters depending on w_i as shown in Table 2.1.

Table 2.1 Parameters of plain concrete (Jun Zhang, 1999)

Material	w_i (mm)	c (1/mm)	d (1/mm)
Plain concrete	0-0.04	1	-33.48
	0.04-0.18	0.569	-8.12
	0.18-0.75	0.321	-2.49
	0.75-2	0.187	-0.84

Assumed that the stress distribution in the uncraked zone, $\sigma_{II}(x)$, is linear, $\sigma_{II}(x)$ can be related to ah, bh and δ as:

$$\sigma_{II}(x) = \sigma_t\left(1 - \frac{x - ah}{bh - ah}\right) \tag{2.24}$$

where bh is the depth of tension zone, $0 \le b \le 1$.

At the equilibrium conditions of force and moment, following equations is satisfied:

$$\int_0^{ah} \sigma_I(x)dx + \int_{ah}^{h} \sigma_{II}(x)dx = 0 \tag{2.25}$$

$$\int_0^{ah} \sigma_I(x)(h-x)Bdx + \int_{ah}^{h} \sigma_{II}(x)(h-x)Bdx = M \tag{2.26}$$

where M is the bending moment.

Eqs. (2.25) and (2.26) involve there unknown parameters *a*, *b* and δ. For a determination of these unknown parameters, it is assumed that the crack mouth opening, δ, can be expressed as (Jun Zhang, 1999):

$$\delta = \frac{24a}{BhE}\left(MV_1(a) - M'V_2(a)\right) - \frac{4\sigma' ah}{E}V_3(a) \tag{2.27}$$

where, *E* is the Young's modulus of plain concrete.

$$M' = \int_0^{ah} B\sigma_I(x)\left(\frac{h}{2} - x\right)dx \tag{2.28}$$

$$\sigma' = \frac{1}{h}\int_0^{ah} \sigma_I(x)dx \tag{2.29}$$

$$V_1(a) = 0.33 - 1.42a + 3.87a^2 - 2.04a^3 + \frac{0.66}{(1-a)^2} \tag{2.30}$$

$$V_2(a) = 0.8 - 1.7a + 2.4a^2 + \frac{0.66}{(1-a)^2} \tag{2.31}$$

$$V_3(a) = \frac{1.46 + 3.42\left(1 - \cos\frac{\pi a}{2}\right)}{\left(\cos\frac{\pi a}{2}\right)^2} \tag{2.32}$$

Numerical solution of the system of nonlinear Eqs. (2.25), (2.26) and (2.27) is applied to archive results of crack length, *ah*, and crack mouth opening, δ. In the first cycle, $\sigma_I(x)$ equals to σ_1 according to Eq. (2.21) at N=1. In the second cycle, the stress degradation will occur in the cracked zone due to a closing and opening procedure of fatigue crack. A new fictitious crack is needed so that the external load, *P*, can reach $P_{app,\,max}$ in the zone where fictitious crack has been formed already. Hence, the stress degradation law will be applied to

both the old cracked zone and the newly developed crack zone, with N = 2 and N = 1, respectively. This procedure will be continued until σ_N equals to zero.

2.3 Prediction of chloride diffusion coefficient under fatigue

Considering a simple case of chloride flow through cracked concrete, total flow of chloride can be expressed as the sum of the flow through crack and flow through uncracked part of homogeneous material, see Figure 2.8. Thus, total flux of chloride through the entire cracked concrete can be written as follow (Gérard, 2000):

$$J_{tot} = \frac{J_{ucr} A_{ucr} + J_{cr} A_{cr}}{A_{ucr} + A_{cr}} \tag{2.33}$$

where J_{tot} is the total flux of chloride through entire cracked concrete, mole/m^{2}s. J_{ucr} is the flux of chloride through uncracked concrete, mole/m^{2}s, and J_{cr} is the flux of chloride through cracks. A_{ucr} and A_{cr}, m^2, are the areas, which are perpendicular to the chloride flow, of cracks and uncracked concrete, respectively.

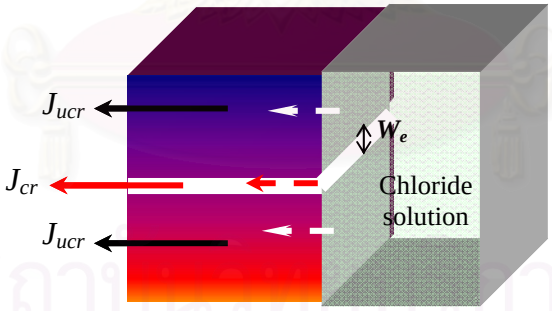

Figure 2.8 The flux of chloride in cracked concrete

The flux of chloride can be expressed as multiplying the transport coefficient with the driving force, F.

$$J_{ucr} = -D_{ucr} F \tag{2.34}$$

$$J_{cr} = -D_{cr} F \tag{2.35}$$

$$J_{tot} = -D_{tot} F \tag{2.36}$$

where D_{ucr} and D_{cr}, m^2/s, are the chloride diffusion coefficient of the uncracked concrete and through cracks, respectively. D_{tot}, m^2/s, is the apparent chloride diffusion coefficient of the cracked concrete.

Replacing Eqs. (2.34), (2.35) and (2.36) into Eq.(2.33) gives:

$$D_{tot} = \frac{A_{ucr} D_{ucr} + A_{cr} D_{cr}}{A_{ucr} + A_{cr}} \tag{2.37}$$

Kato et al 2005 proposed that D_{cr} increases with increasing the crack width and becomes almost constant when the crack width is 0.075mm or more. D_{cr} is approximately 2.51×10^{-7} m^2/s as the crack width is smaller than 0.075mm.

For crack due to flexural cyclic load, we adopt the simple assumption that a single-edge crack occurs; the crack shape is straight; the crack length at the edge side is equal to that at the bottom side of the beam (Figure 2.9). Hence, crack area, A_{cr}, can be expressed simply as:

$$A_{cr} = W_e a h \tag{2.38}$$

where W_e, m, is the effective crack width. However, the actual crack due to flexural cyclic load is not simply straight, it is tortuous. In order to account for tortuous effect in an actual crack, W_e can be related to crack mouth opening δ and the tortuosity parameter, τ $(1<\tau\leq5)$:

$$W_e = \frac{\delta}{\tau} \tag{2.39}$$

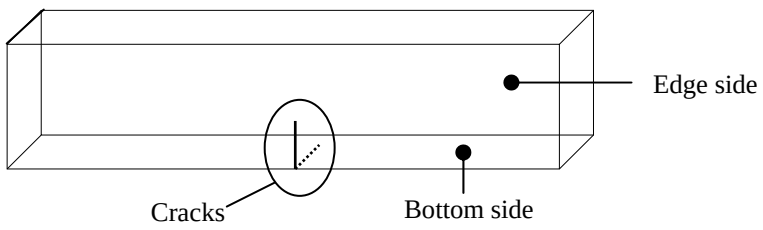

Figure 2.9 Assumption of crack growth in concrete beam under flexural cyclic load

2.4 Prediction of chloride penetration into concrete under flexural cyclic load and tidal environment

Considering chloride transport in concrete one-dimensionally, the mass balance can be expressed as (Byung Hwan Oh, 2007):

$$\frac{\partial C_t}{\partial t} + \frac{\partial J_c}{\partial x} = 0 \tag{2.40}$$

where C_t is the total chloride content by the mass of cement content (%), and J_c is the chloride flux (m/s). In drying-wetting conditions, with the assumption of a linear chloride binding isotherm, the chloride flux that expresses the chloride diffusion due to gradient concentration, J_{c1}, and chloride convection by moisture transport, J_{c2}, can be written as:

$$J_c = J_{c1} + J_{c2} \tag{2.41}$$

$$J_{c1} = -D_a \nabla C_t \tag{2.42}$$

$$J_{c2} = C_f J_w = \frac{C_t}{\phi} J_w \tag{2.43}$$

$$-\nabla J_w = \frac{\partial w}{\partial t} \tag{2.44}$$

with D_a the apparent chloride diffusion coefficient, w the free water content, and J_w the moisture flux (m/s) and ϕ is chloride binding capacity.

From Eq.(2.41), (2.42), (2.43) and (2.44), Eq.(2.40) is reformulated to:

$$\frac{\partial C_t}{\partial t} = D_a \frac{\partial^2 C_t}{\partial x^2} + \frac{C_t}{\phi} \frac{\partial w}{\partial t} \tag{2.45}$$

The correlation between the relative humidity and the free water content is assumed by desorption isotherms as (Saetta, 1993):

$$w = w_{sat} h \tag{2.46}$$

where, h is the relative humidity (%), and w_{sat} represents liquid content (%).

Substituting Eq.(2.45) into Eq.(2.44) gives:

$$\frac{\partial C_t}{\partial t} = D_a \frac{\partial^2 C_t}{\partial x^2} + \frac{C_t}{\phi} w_{sat} \frac{\partial h}{\partial t} \tag{2.47}$$

Under thermally constant conditions, the humidity, h, and the humidity diffusion coefficient, D_h, are related and expressed by the following equation:

$$\frac{\partial h}{\partial t} = D_h \frac{\partial^2 h}{\partial x^2} \tag{2.48}$$

Consequently, the governing equation describing the chloride penetration in the drying-wetting condition can be rewritten as:

$$\frac{\partial C_t}{\partial t} = D_a \frac{\partial^2 C_t}{\partial x^2} + \frac{C_t}{\phi} w_{sat} D_h \frac{\partial^2 h}{\partial x^2} \tag{2.49}$$

Under flexural cyclic load, the influence of fatigue on the chloride diffusion coefficient, D_a, is predicted through section 2.2 and 2.3, then the predicted chloride diffusion coefficients are used for the prediction of the chloride profiles of concrete as mentioned in Eq. (2.49).

The chloride profiles of concrete predicted through Eq. (2.49) depend on the predicted chloride diffusion coefficient, D_a, and chloride binding capacity, ϕ. The chloride binding capacity of various cements is different (Hirao, 2005).

2.4.1 Chloride binding in concrete structure

Chlorides in concrete are present in various forms that are internal chlorides and external chlorides. The internal chlorides are included in mix ingredients and in the principal constituent of most accelerating admixtures. The external chlorides are present in marine environment or in deicing salts. Usually, chlorides in concrete structures are classified into free and bound chloride as:

(a) The free chloride is dissolved in the concrete pore solution and movable according to the concentration gradient.

(b) And the remainder is bound chloride: physical bound chloride and chemical bound chloride.

Chemical bound chloride is present in the solid structure of concrete, as shown in Figure 2.10. Chemical bound chloride reacts chemically with the hydration compounds of cement, particularly with C_3A to form calcium chloroaluminate (Friedel salts). The physically bound chloride is attracted to the pore surface by weak Van der Waals forces. It is generally believed that free chloride content is proportional to the total chloride content, and the chemically bound chloride amount is supposed to be negligible, while physically bound chlorides are in dynamic balance with that dissolved in the porous solution.

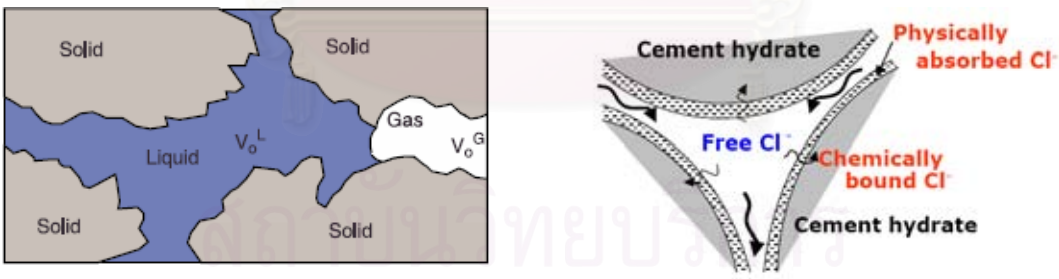

Figure 2.10 Types of chloride present in concrete structures (Delagrave, 1997)

The Friedel's salt formed by two separate mechanisms; an adsorption mechanism, and an anion-exchange mechanism (Suryavanshi, 1996). In the adsorption mechanism, Friedel's salt forms due to the adsorption of the bulk Cl^- ions present in the pore solution into the interlayers of the principal layers, $[Ca_2Al(OH^-)_6.2H_2O]^+$, of the AFm (Aluminate Ferrite mono) structure to balance the charge. In the anion-exchange mechanism, a fraction of the free-chloride ions bind with the AFm hydrates (C_4AH_{13} and its derivatives) to form Friedel's

salt by an anion-exchange with the OH^- ions present in the interlayers of the principal layer, $[Ca_2Al(OH^-)_6.nH_2O]^+$. As a result of Friedel's salt formation by the adsorption mechanism, an amount of Na^+ ions equivalent to the adsorbed chloride ions (in moles) are removed from the pore solution to maintain the ionic charge neutrality. The Na^+ ions thus removed from the pore solution, bind with the calcium silicate hydrate (C-S-H) gel lattice to balance the charge arising due to the replacement of Si^{4+} ions by Al^{3+} and Fe^{3+} ions. In contrast, the Friedel's salt formation by the anion-exchange mechanism involves the release of OH- ions from the AFm hydrates into the pore solution, thereby increasing the pH of the pore solution.

The total chloride concentration is the sum of free chloride and bound chloride. In a saturated concrete, the total chloride is (Saetta, 1993):

$$C_t = w_{sat}.C_f + (1\text{-}w_{sat}).C_b \tag{2.50}$$

where C_b is bound chloride, C_f and C_t is free and total chloride respectively, w_{sat} is the evaporable water content.

According to linear isotherm, if γ is considered as binding ratio then the relationship between free chloride in solution and bound chloride in solid structure can be expressed as:

$$C_b = \gamma C_f \tag{2.51}$$

The total chloride equation can be written:

$$C_t = w_{sat}.C_f + (1\text{-}w_{sat}).\gamma C_f = \phi.C_f \tag{2.52}$$

$$\text{with } \phi = w_{sat} + (1\text{-}w_{sat}).\gamma \tag{2.53}$$

Using Freundlich isotherm and with simplification that bound chloride is present in the product form of reaction between C_3A and chloride, the relationship between free chloride and bound chloride is expressed as follow (Sang-Hun Han, 2007):

$$C_b = gC_f^h \tag{2.54}$$

$$\text{with } g = 0.056 + 0.025C_3A \tag{2.55}$$

$$h = \frac{1}{0.076C_3A + 1.91} \tag{2.56}$$

The evaporable water content w_{sat} is the sum of the gel pore water content and capillary pore water content.

$$w_{sat} = w_g + w_c \tag{2.57}$$

with w_g and w_c is the gel pore water content and the capillary water content respectively.

$$w_g = w_{g,c}.c.\frac{1}{w_s} = 0.18\lambda.\frac{c}{1000} \tag{2.58}$$

$$w_c = (\frac{w}{c} - 0.36\lambda)\frac{c}{1000} \tag{2.59}$$

where $w_{g,c}$ and w_s is the gel pore water content and the density of water respectively, c is cement content and λ is degree of hydration of cement.

The chloride-binding capacity of a concrete, that is the amount of chlorides that are complex by the hydrated phases of the matrix, is modeled by the Langmuir isotherm, as shown in Figure 2.11, shown as:

$$C_b = \frac{\alpha.C_f}{1 + \beta.C_f} \tag{2.60}$$

where C_b is the amount of chloride bound, C_f is the free chloride in solution, and α and β are constants that are dependent on the concrete binder composition. The relationship between free and bound chlorides is unique for each cementitious system since its components, such as C_3A content, supplementary cementing materials, and pH of the pore solution influence its overall binding capacity. The effect of binding on the rate of chloride ingress has been dealt with in detail elsewhere.

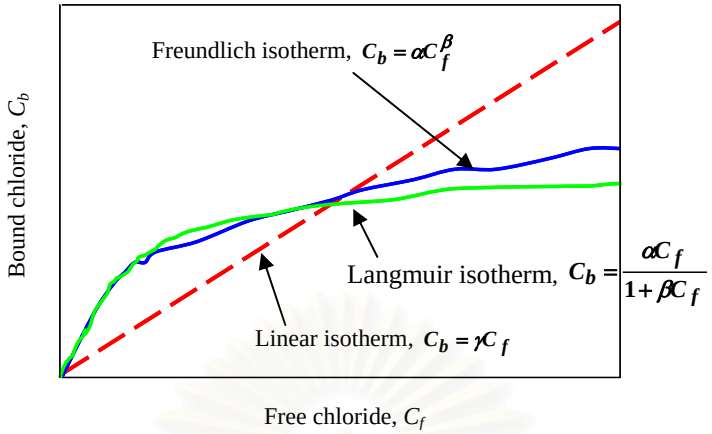

Figure 2.11 Proposed chloride binding isotherms

2.4.2 Methods of chloride diffusion coefficient testing

The penetration of chloride into concrete includes diffusion and adsorption. The chloride diffusion is characterized by chloride diffusion coefficient. Up to now, there have been many tests proposed for determination of the chloride diffusion coefficients that are divided into long-term test and short-term test.

The advantage of long-term test is that it characterizes the natural penetration in the real environment; however, its disadvantage is taking long time (90 days). The advantage of short-term test is testing acceleration so it takes short time (24 hours up to 4 days), however, its disadvantage is of not the natural penetration in the real environment. Also, there is a fact that results of chloride diffusion coefficient from short-term test are always higher than those from long-term test. This is assumed due to the acceleration testing. Generally, short-term chloride diffusion tests include ASTM C12O2 and Nordtest. Long-term chloride diffusion tests involve ASTM C1556.

2.4.2.1 Short-term diffusion test

With regarding to short-term diffusion test, the method requires cylindrical specimens with a diameter of 100 mm and a thickness of 50 mm, sliced from cast cylinders or drilled cores with a minimum length of 100 mm. The principle of this method is that the specimens are placed between two chambers: a chamber with 3% sodium chloride and the other chamber with 0.3N sodium hydroxide, and an external electrical potential of 30V or 60V is

applied axially across the specimen to force the chloride ions outside to migrate into the specimen, as shown in Figure 2.12. After 12 hours of test duration, the specimen is split axially and a silver nitrate solution sprayed onto one of the freshly split sections. The chloride penetration depth can then be measured from the visible white silver chloride precipitation, after which the chloride migration coefficient can be calculated from this penetration depth.

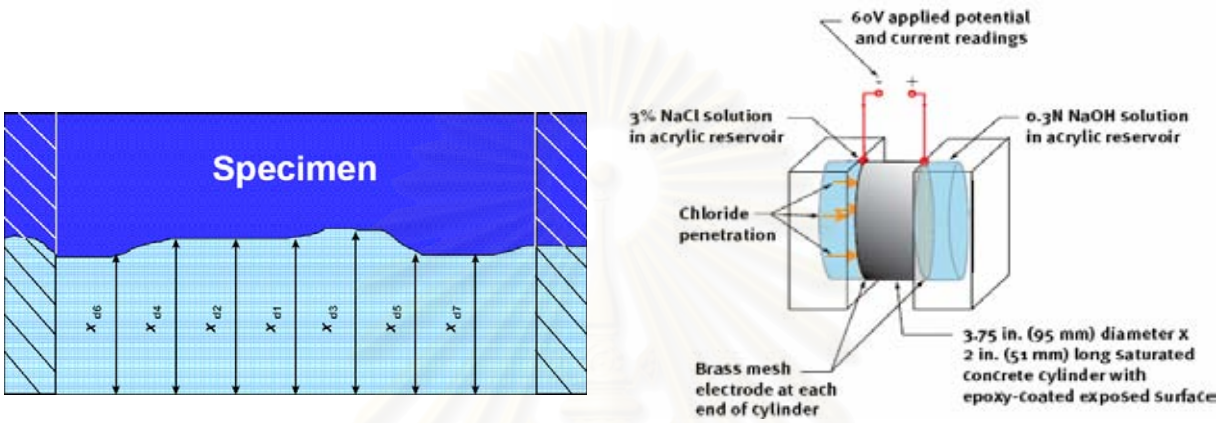

Figure 2.12 Set up of short-term diffusion test

The set up of short-term chloride diffusion method employed in this work is modified from ASTM C1202, but the principle approach is still based on Nordtest NT build 492 (Nordtest, 1991).

Based on Nordtest NT build 492, the chloride diffusion coefficient is determined as follows:

$$D=\frac{0.0239(273+T)\times L}{(U-2)\times t}\times\left(x_d-0.0238\sqrt{\frac{(273+T)\times L\times x_d}{U-2}}\right) \qquad (2.61)$$

where D is chloride diffusion coefficient (10^{-12} m^2/s), U is absolute value of the applied voltage (V), T is average value of the initial and final temperatures (^0C), L is thickness of the specimen (mm), x_d is average value of the penetration (mm), t is test duration (hour).

2.4.2.2 Long-term diffusion test

Long-term chloride diffusion follows ASTM C1556 in order to determine apparent chloride diffusion coefficient. In this test, cylindrical specimens with 100mm of diameter and 75mm of depth are used. All sides of the test specimen are sealed except the finished surface. Saturate the sealed specimen in a calcium hydroxide solution, rinse with tap water, and then place in a sodium chloride solution of 10% concentration, see Figure 2.13. After a specified exposure time (35 days), the test specimen is removed from the sodium chloride solution and thin layers are ground off parallel to the exposed face of the specimen. The acid-soluble chloride content of each layer is determined. The apparent chloride diffusion coefficient and the projected surface chloride-ion concentration are then calculated using the initial chloride-ion content, and at least six related values for chloride-ion content and depth below the exposed surface.

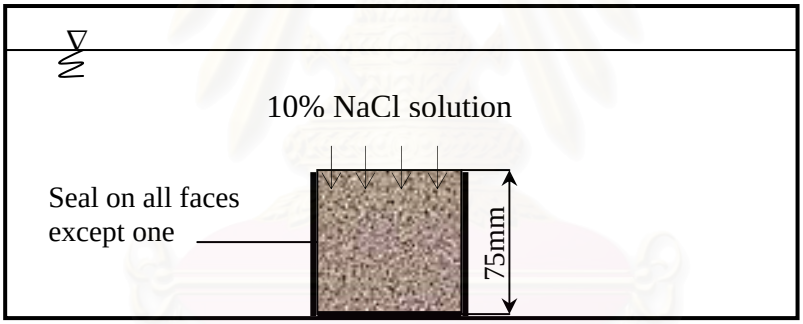

Figure 2.13 Immersion of concrete specimen in NaCl in long-term test of diffusion coefficient

The total chloride profile at different depth is got, then values of surface chloride content and apparent chloride diffusion coefficient is fitted by equation as:

$$C(x,t) = C_s - (C_s - C_i).erf\left(\frac{x}{\sqrt{4.D_a.t}}\right) \qquad (2.62)$$

where $C(x,t)$ is chloride content measured at depth x and exposed time t, %. C_s is surface chloride content determined by fitting, %. C_i is initial chloride content in concrete mixture prior to expose to solution, %. x is depth below exposed surface (the middle of a layer), m D_a is apparent diffusion coefficient, m^2/s. t is exposed time, s. erf is error function.

2.4.2.3 Relationship between Short-term and Long-term diffusion coefficient test

The advantage of long-term test is that it characterizes the natural penetration in the real environment, however, its disadvantage is taking long time (90 days). The advantage of short-term test is that it accelerates test so it takes short time (24 hours up to 4 days), however, its disadvantage is of not the natural penetration in the real environment. Also, there is a fact that results of chloride diffusion coefficient from short-term test are always higher than these from long-term test. This is assumed due to the acceleration testing. Yang et al 2004 proposed the linear relationship between long-term test and short-term test of chloride diffusion coefficient, in which values from short-term test are higher than those from long-term test, see Figure 2.14.

The experimental data from short-term and long-term tests will be used to set up the relationship between the short-term and the long-term diffusion test. Thereby, the following experimental data of short-term test can be converted to those of pounding test that is more reliable.

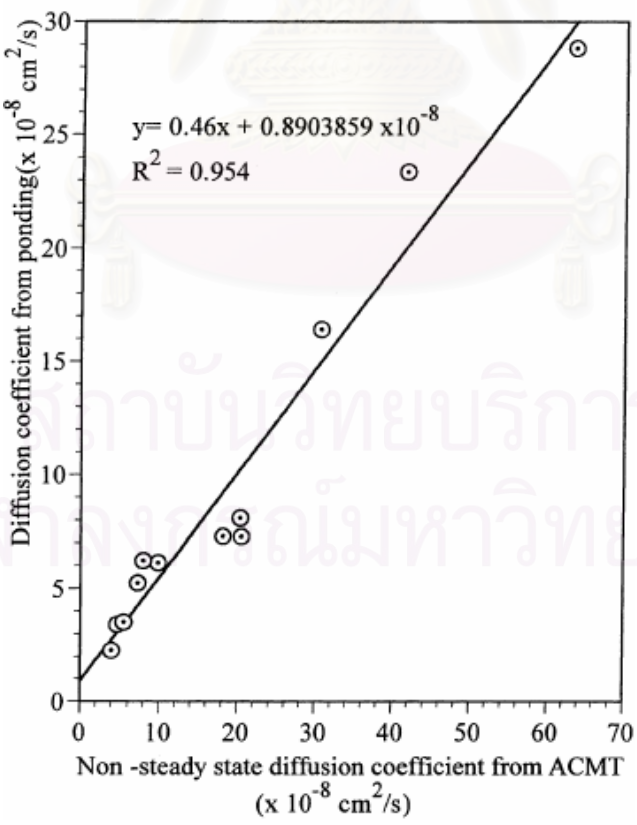

Figure 2.14 Relationship between long-term and short-term test of chloride diffusion (Yang, 2004)

2.4.3 Finite difference method

In order to predict chloride penetration into concrete structures through numerical solution of Eq. (2.49), Finite difference methods (FDM) and Finite element method (FEM) can be applied to evaluate total chloride concentration by time and space. However, FED is easier than FEM in developing algorithm of numerical solution. Commonly, there are three solutions of FDM used numerically to solve equation of Fick's second law as following:

a) Explicit method,
b) Implicit method,
c) Crank – Nicolson method.

Of those methods of FDM, at a given time and space increment, Crank-Nicolson method is supposed as the best because of the fast convergence and the high accuracy compared to other methods. Concerning with Crank-Nicolson method, the fast convergence and the high accuracy can be archived as the time increment and space increment are 12 hours and 5mm, respectively (Tralla, 2002 and Tran, 2006).

2.4.3.1 Explicit method

In this method, approximations are the second derivative in space and the first derivative in time. The approximations are conducted by a centered finite divided difference and finite divided difference, see Figure 2.15.

$$\frac{\partial^2 C}{\partial x^2} = \frac{C_{i+1}^l - 2C_i^l + C_{i-1}^l}{(\Delta x)^2} \tag{2.63}$$

This approximation has an error of $O[(\Delta x)^2]$

$$\frac{\partial C}{\partial t} = \frac{C_i^{l+1} - C_i^l}{\Delta t} \tag{2.64}$$

This approximation has an error of $O(\Delta t)$

Substitute equation (2.63) and (2.64) in to (2.49), we have

$$D_a.\frac{C_{i+1}^{l}-2C_i^{l}+C_{i-1}^{l}}{(\Delta x)^2}=\frac{C_i^{l+1}-C_i^{l}}{\Delta t} \tag{2.65}$$

$$C_i^{l+1} = C_i^{l} + \lambda(C_{i+1}{}^{l} - 2C_i^{l} + C_{i-1}{}^{l}) \tag{2.66}$$

where $\lambda = D_a.\Delta t/(\Delta x)^2$

× Grid point involved in time difference

O Grid point involved in space difference

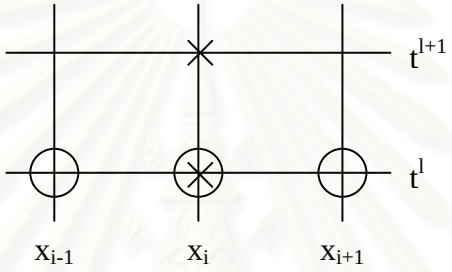

Figure 2.15 The grid of time and space in explicit method

2.4.3.2 Implicit method

In the implicit method, the spatial derivative is approximated at an advanced time level l + 1, see Figure 2.16.

$$\frac{\partial^2 C}{\partial x^2}=\frac{C_{i+1}^{l+1}-2C_i^{l+1}+C_{i-1}^{l+1}}{(\Delta x)^2} \tag{2.67}$$

Substitute (2.67) and (2.64) into (2.49) we have

$$D_a.\frac{C_{i+1}^{l+1}-2C_i^{l+1}+C_{i-1}^{l+1}}{(\Delta x)^2}=\frac{C_i^{l+1}-C_i^{l}}{\Delta t} \tag{2.68}$$

For the first interior node ($i=1$) :

$$(1+2\lambda)C_1{}^{l+1} - \lambda C_2{}^{l+1} = C_1{}^{l} + \lambda f_o(t^{l+1}) \tag{2.69}$$

where $C_o^{l+1} = f_o(t^{l+1})$

For the last interior node ($i=m$) :

$$(1+2\lambda)C_m^{l+1} - \lambda C_{m-1}^{l+1} = C_m^{l} + \lambda f_{m+1}(t^{l+1}) \tag{2.70}$$

× Grid point involved in time difference

O Grid point involved in space difference

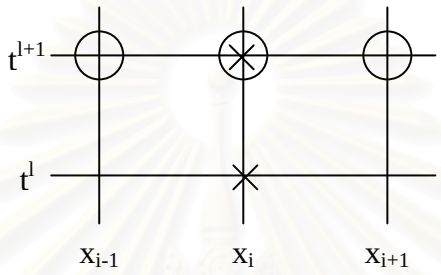

Figure 2.16 The grid of time and space in implicit method

2.4.3.3 The Crank - Nicolson method

The Crank – Nicolson method provides an alternative implicit scheme that is second-order accurate in both space and time. In this method, difference approximations are developed at the midpoint of the time increment, see Figure 2.17. With this point, the derivative can be approximated at $t^{l+1/2}$ by : $\frac{\partial C}{\partial t} = \frac{C_i^{l+1} - C_i^{l}}{\Delta t}$

The second derivative in space can be determined at midpoint by averaging the difference approximations at the beginning (t^l) and at the end (t^{l+1}) of the time increment.

$$\frac{\partial^2 C}{\partial x^2} = \frac{1}{2}\left[\frac{C_{i+1}^{l+1} - 2C_i^{l+1} + C_{i-1}^{l+1}}{(\Delta x)^2} + \frac{C_{i+1}^{l} - 2C_i^{l} + C_{i-1}^{l}}{(\Delta x)^2}\right] \tag{2.71}$$

Substitute (2.71) and (2.64) into (2.49), we have:

$$-\lambda C_{i-1}^{l+1} + 2.(1+\lambda)C_i^{l+1} - \lambda C_{i+1}^{l+1} = \lambda C_{i-l}^{l} + 2.(1-\lambda)C_i^{l} + \lambda C_{i+1}^{l} \tag{2.72}$$

with $C_o^{l+1} = f_o(t^{l+1})$ and $C_{m+1}^{l+1} = f_{m+1}(t^{l+1})$

For the first and the last interior nodes:

(a) The first node : $2.(1+\lambda)C_i^{l+1} - \lambda C_2^{l+1} = \lambda f_o(t^l) + 2.(1-\lambda)C_i^l + \lambda C_2^l + \lambda f_o(t^{l+1})$

(b) The first node : $2.(1+\lambda)C_m^{l+1} - \lambda C_{m-1}^{l+1} = \lambda f_{m+1}(t^l) + 2.(1-\lambda)C_m^l + \lambda C_{m+1}^l + \lambda f_{m+1}(t^{l+1})$

× Grid point involved in time difference

O Grid point involved in space difference

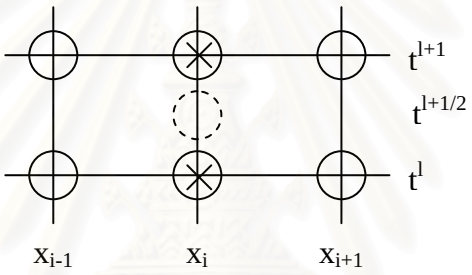

Figure 2.17 The grid of time and space in Crank-Nicolson method

Of the three solutions of FDM, the Crank - Nicolson method seems to be the best method due to fast convergence. Therefore, in this study, the Crank - Nicolson method will be used to predict the chloride penetration into concrete structures under cyclic load and tidal effect. In order to solve the govern equation of chloride penetration into concrete in tidal zone, Eq.(2.49), at first, the values of humidity at different time and depth will be found by numerical solution of Eq.(2.48), and then these values are applied to numerical solution of Eq.(2.49).

Numerical solution of Eq.(2.48)

$$\frac{h_i^{l+1} - h_i^l}{\Delta t} = D_a \frac{1}{2}\left[\frac{h_{i+1}^{l+1} - 2h_i^{l+1} + h_{i-1}^{l+1}}{(\Delta x)^2} + \frac{h_{i+1}^l - 2h_i^l + h_{i-1}^l}{(\Delta x)^2}\right]$$

$$\Leftrightarrow -\lambda h_{i-1}^{l+1} + 2.(1+\lambda)h_i^{l+1} - \lambda h_{i+1}^{l+1} = \lambda h_{i-l}^l + 2.(1-\lambda)h_i^l + \lambda h_{i+1}^l$$

with $\lambda = D_h.\Delta t/(\Delta x)^2$

$$\begin{bmatrix} 2(1+\lambda) & -\lambda & 0. & . & . & . & 0 \\ -\lambda & 2(1+\lambda) & -\lambda & 0 & . & . & 0 \\ \cdots\cdots\cdots & & & & & & \\ 0 & 0 & -\lambda & & 2(1+\lambda) & & 0 \\ & & & & & & \\ 0 & & 0 & & -\lambda & & 2(1+\lambda) \end{bmatrix} \begin{bmatrix} h_1^l \\ h_2^l \\ . \\ . \\ h_n^l \end{bmatrix} = \begin{bmatrix} a_1^l \\ a_2^l \\ . \\ . \\ a_n^l \end{bmatrix}$$

With

$$a_1^l = \lambda h_0^l + \lambda h_0^{l-1} + 2(1-\lambda)h_1^{l-1} + \lambda h_2^{l-1}$$
$$a_2^l = \lambda h_1^{l-1} + 2(1-\lambda)h_2^{l-1} + h_3^{l-1}$$
.
.
$$a_n^l = \lambda h_{n-1}^{l-1} + 2(1-\lambda)h_n^{l-1} + h_{n+1}^{l-1}$$

Numerical solution of Eq.(2.49)

$$\frac{C_i^{l+1} - C_i^l}{\Delta t} = D_a \frac{1}{2}\left[\frac{C_{i+1}^{l+1} - 2C_i^{l+1} + C_{i-1}^{l+1}}{(\Delta x)^2} + \frac{C_{i+1}^l - 2C_i^l + C_{i-1}^l}{(\Delta x)^2}\right] + \frac{w_{sat}}{\phi}.C_i^l\left(\frac{h_i^{l+1} - h_i^l}{\Delta t}\right)$$

Let

$$b = D_a.\Delta; \qquad c = (\Delta x)^2; \qquad d = \frac{w_{sat}}{\phi.\Delta t}$$

$$\begin{bmatrix} 2(b+c) & -b & 0. & . & . & . & 0 \\ -b & 2(b+c) & -b & & & & 0 \\ . & . & & . & . & . & 0 \\ . & . & & . & & & 0 \\ 0 & -b & & 2(b+c) & & & 0 \\ 0 & 0 & & -b & & & 2(b+c) \end{bmatrix} \begin{bmatrix} C_1^l \\ C_2^l \\ . \\ . \\ C_n^l \end{bmatrix} = \begin{bmatrix} e_1^l \\ e_2^l \\ . \\ . \\ e_n^l \end{bmatrix}$$

With

$$e_1^l = bC_0^l + bC_0^{l-1} + \left[-2b + 2c + d(h_1^l - h_1^{l-1})\right]C_1^{l-1} + bC_2^{l-1}$$
$$e_2^l = bC_1^{l-1} + \left[-2b + 2c + d(h_2^l - h_2^{l-1})\right]C_2^{l-1} + bC_3^{l-1}$$
.
.
$$e_n^l = bC_1^{l-1} + \left[-2b + 2c + d(h_2^l - h_2^{l-1})\right]C_2^{l-1} + bC_3^{l-1}$$

2.5 Concluding remarks

This chapter presents theories used as fundamental backgrounds. Some concluding remarks are drawn from these theories as following:

1. Mechanical and physical properties of the concrete can be predicted basing on water to cement ratio, *w/c*. These predicted properties are used as the input parameters for further prediction of chloride penetration into concretes under flexural cyclic load and tide.
2. Under flexural cyclic load, the crack growth of the plain concrete beam can be predicted using FCM together with stress degradation law.
3. The chloride diffusion coefficient of the cracked concrete is a function depending on the crack characteristics, in terms of crack width, crack length and crack tortousity. Therefore, the chloride diffusion coefficient of the cracked concrete can be predicted as the crack properties are known.
4. Concerning with the chloride penetration into concretes, at a given environmental condition, the predicted chloride content depends on the chloride diffusion coefficient and the chloride binding capacity of the cement. The chloride diffusion coefficient can be measured by long-term and short-term test. And, the chloride binding capacities of cements are different due to differences in the chemical and physical compositions of the cements.
5. The chloride profiles of concretes can be predicted well using FDM. Of methods of FDM, Crank-Nicolson method is supposed to be the best in terms of accuracy and fast convergence.

CHAPTER III

CHLORIDE BINDING ISOTHERMS OF CEMENTS

3.1 Procedures for determination of chloride binding isotherms of cements

In this study, the chloride binding isotherms were proposed for four common cement types as Ordinary Portland cement (OPC), modified cement (MC), rapid-hardening Portland cement (RHC) and low-heat Portland cement (LHC), according to ASTM, these cement types are classified into cement type I, II, III and IV, respectively. Main tests used for determination of chloride binding isotherms are free chloride content, ASTM 1218, total chloride content, ASTM 1152, and X-Ray diffraction Rietveld analysis (XRD). The flow chart describing the procedures of determination of the chloride binding isotherms is shown in Figure 3.1.

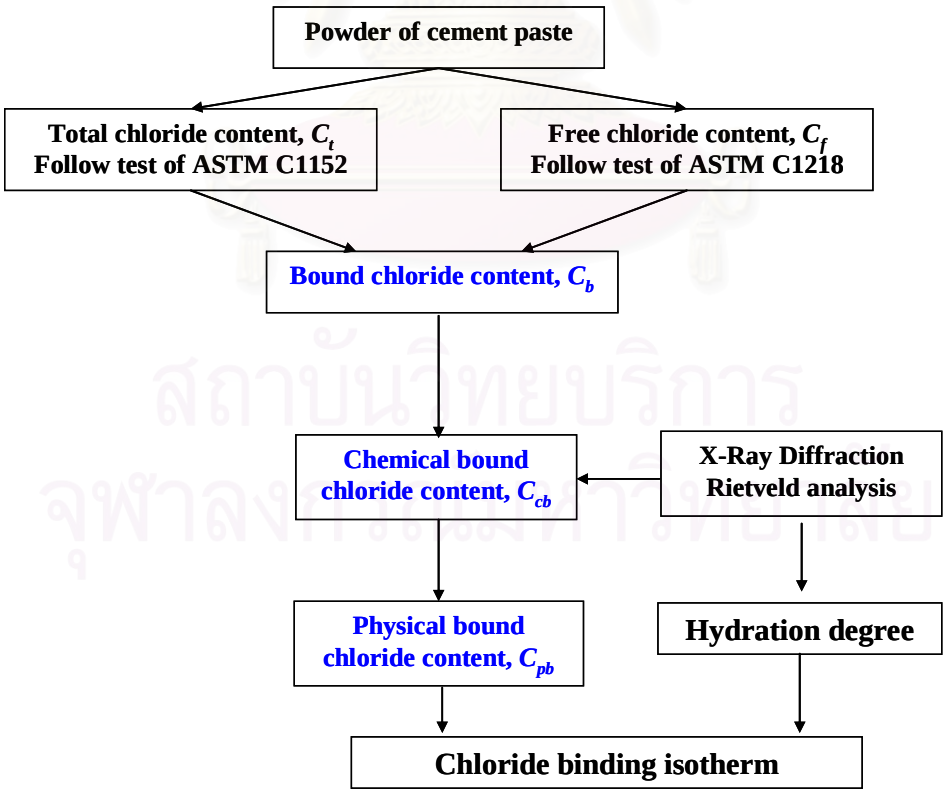

Figure 3.1 Procedures to determine the chloride binding isotherms of cements

Four common cement types are different in chemical and physical compositions, especially in the content of C_3A compound. The chemical and physical properties of four types of cement were quantified by XRD and XRF analysis and shown in Table 3.1. Cubic cement paste specimens were used for investigation of chloride binding isotherms with four common cement types and four ranges of water to cement ratios, *w/c*, of 0.3, 0.4, 0.5 and 0.6.

Table 3.1 Chemical and physical properties of various cement types

Chemical and physical properties	Cement type			
	OPC	MC	RHC	LHC
Chemical and mineral compositions (%)				
Lime	-	0.17	-	0.07
SiO_2	21.66	23.31	20.30	25.85
Al_2O_3	5.58	3.96	4.66	3.21
Fe_2O_3	2.79	4.32	2.63	3.70
CaO	63.92	63.59	64.70	63.09
MgO	2.55	0.26	1.91	0.10
SO_3	2.32	2.52	3.06	2.44
TiO_2	0.27	0.20	0.26	0.14
MnO	0.13	0.08	0.07	0.02
Na_2O	0.15	0.20	0.18	0.24
K_2O	0.34	0.39	0.35	0.51
P_2O_5	0.25	0.12	-	0.05
Cl	-	0.012	0.006	0.005
Ignition loss	0.72	0.77	0.54	0.81
C_3S	58.3	52.8	69.4	33.3
C_2S	22.6	28.5	16.1	53.0
C_3A	6.4	5.1	4.9	3.3
C_4AF	10.1	10.8	8.5	7.8
Physical properties				
Density (g/cm^3)	3.17	3.21	3.15	3.24
Blaine surface area (cm^2/g)	3500	3090	4660	3330

Regarding to preparation of cement paste specimens used for determination of chloride binding isotherms, a mixing regime is applied following ASTM C305-99 to avoid segregation due to the high *w/c*. After mixing, cement paste mix will be introduced into cubic moulds. All paste specimens are demolded at the following day and cured in water up to 28 days in controlled temperature room. After curing 28 days in the water, all specimens will be immersed in saturated exposed solution (sodium chloride 10%) for 1 month as *w/*c=0.5 and 0.6, and 2 months with *w/c*=0.3 and 0.4, respectively. The mixture design of cement paste is based on experimental method, and the mixtures of cement pastes are shown in Table 3.2.

Table 3.2 The estimated contents of types of cement used to cast cubic specimen

Series	Cement Type	w/c	Cement content, kg	Water, litre
I-1	Type I-OPC	0.3	2.5	0.75
I-2		0.4	2.2	0.88
I-3		0.5	1.9	0.95
I-4		0.6	1.7	1.02
II-1	Type II-MC	0.3	2.5	0.75
II-2		0.4	2.2	0.88
II-3		0.5	1.9	0.95
II-4		0.6	1.7	1.02
III-1	Type III-RHC	0.3	2.5	0.75
III-2		0.4	2.2	0.88
III-3		0.5	1.9	0.95
III-4		0.6	1.7	1.02
IV-1	Type IV-LHC	0.3	2.5	0.75
IV-2		0.4	2.2	0.88
IV-3		0.5	1.9	0.95
IV-4		0.6	1.7	1.02

3.1.1 Testing procedures of chloride content

For the tests of total chloride content – ASTM C1152, 10g of powder sample passing a 850μm sieve is dispersed in a 250ml beaker with 75ml of deionized water, 25ml of dilute (1+1) nitric acid added slowly, then 3ml of hydrogen peroxide (30% solution), and 20 drops

of acid nitric (1+1) added in excess, and heat the covered beaker rapidly to boiling. After removal of the beaker from the hot plate and filtering the solution, the chloride concentration in the filtrate will be analyzed by titration method or by ion chromatography.

Experimental procedures of tests of the free chloride content – ASTM C1218 are very similar to those of the total chloride content test. However, only 50ml of deionized water is used instead of 75ml, and boiling of the solution in the beaker is for 5 min. Then left to stand for 24 h for filtering by gravity or suction through a fine-texture. Adding 3 ml of (1:1) nitric acid and 3 ml of hydrogen peroxide (30% solution) to the filtrate, covering the beaker with a watch glass and allow it to stand for 1 to 2 min. Then heating the covered beaker rapidly to boiling, and the chloride concentration in the filtrate will be also analyzed by titration or by ion chromatography.

3.1.2 Testing procedures of XRD Rietveld and EPMA

After finishing exposure time in sodium chloride 10% as described above, cubic specimen of cement paste is sawn by diamond cutter in to slices with 10mm in depth, and 40mm in width, for measuring chloride profile by EPMA as shown in Figure 3.2, other parts of the cubic specimen is crushed in to small particles with size from 1-3mm for preparing samples of XRD Rietveld.

a *b*

Figure 3.2 XRD Rietveld and EPMA equipments used in this research
(a) XRD Rietveld equipment ; (b) EPMA equipment

For sample preparation of EPMA test, after sawing specimen with propanol, slices are cleaned by ultrasonic waves with propanol for 5min, dry them in vacuum dry for 1 day. After

vacuuming 1 day, slices are covered with acrylic solution and let them stable for 24 hours so that acrylic can harden. Then, again, coat one more layer of acrylic on the surface of sample, where the measurement will be, and let samples dry for 48 hours. Polish the surface of sample by alumina and sand paper. After polishing, wash sample again with propanol and ultrasonic machine for 5 min, vacuum sample in deciator for 48 hours, finally, coat sample with carbon for measurement.

Concerning with sample preparation for XRD Rietveld testing, particles, with size of 1-3mm, of cement paste are soaked into acetone for 1 day, dry sample at 20^0C for 1 day, dry at 40^0C for 1 day so that the hydration process can be delayed, place sample in vacuum deciator for 48 hours, then grind sample by ball mill with 300rpm for 4 min. After grinding, powder is mix with 10% of Al_2O_3 at 100rpm for 3 min. And, finally, sample is measured by XRD Rietveld. The XRD Rietveld apparatus used in this study is Rikaku, CuK_α operating at 40 kV and 20 mA. A range of 5^0 to 70^0 (2θ) is scanned at step intervals of 0.02^0 (2θ) using a step scan time of 1s and 2^0/s scan speeds. The divergence slit, scattering slit, and receiving slit were $1/2^0$, $1/2^0$, and 0.3 mm, respectively. To detect the amount of amorphous phase, the C-S-H compound, in the cement pastes, X-ray corundum (SRM 676) is added and used as an internal reference in the paste specimen with a content of 10% by mass of the cement paste. The XRD Rietveld data is analyzed by SIROQUANT version 3.0 software, which is one of the useful, the world's most efficient and widely used software tools for mineral analysis. SIROQUANT software uses data from XRD analysis to determine the mineral composition of every thing from cements. This software is one of the Australian technologies and developed at CSIRO Energy Technology, part of Australia's national science agency.

3.2 Propose chloride binding isotherms of cements

3.2.1 Chloride binding isotherms of various cements

The cements investigated in this study include Ordinary Portland cement (OPC), Modified cement (MC), Rapid-hardening Portland cement (RHC), and Low-heat Portland cement (LHC), with *w/c* ratios of 0.3; 0.4; 0.5, and 0.6. The experiments to determine total chloride were conducted using ASTM C1152 and the free chloride was determined with ASTM C1218. Additionally, X-ray diffraction Rietveld (XRD Rietveld) analysis was used to

determine the degrees of hydration and hydrate contents of cement pastes, especially of C-S-H and Friedel's salt.Deionized water was used to prepare all mixtures. Reagent grade sodium chloride and deionized water were used to prepare the sodium chloride solution. In total 16 different mixtures were investigated in this study.

Cubic specimens with 5 cm sides were cast in steel cubic molds. The molds were sealed and kept in a box, with a controlled temperature of 22^0C and a relative humidity of 60% for 24 hours. Then, specimens were demolded and cured in a saturated lime condition for 28 days. After this, specimens were immersed in a 10% sodium solution for 1 month and 2 months with the *w/c* = 0.5, 0.6 mixes and *w/c* = 0.3, 0.4 mixes, respectively. At the end of the immersion period, three 1cm in thick samples were sawn from the exposed surfaces, and determinations of the total chloride and free chloride were conducted with the procedures in ASTM. In addition, cement pastes, which were used in the tests of chloride contents, also were used to conduct XRD Rietveld tests to calculate the C-S-H contents, Friedel's salt contents and hydration degrees of cement pastes.

Following experimental procedures as mentioned above, results of the chloride binding isotherms of mixtures made of four cement types and four *w/c* ratios are shown in Figure 3.3 and 3.4.

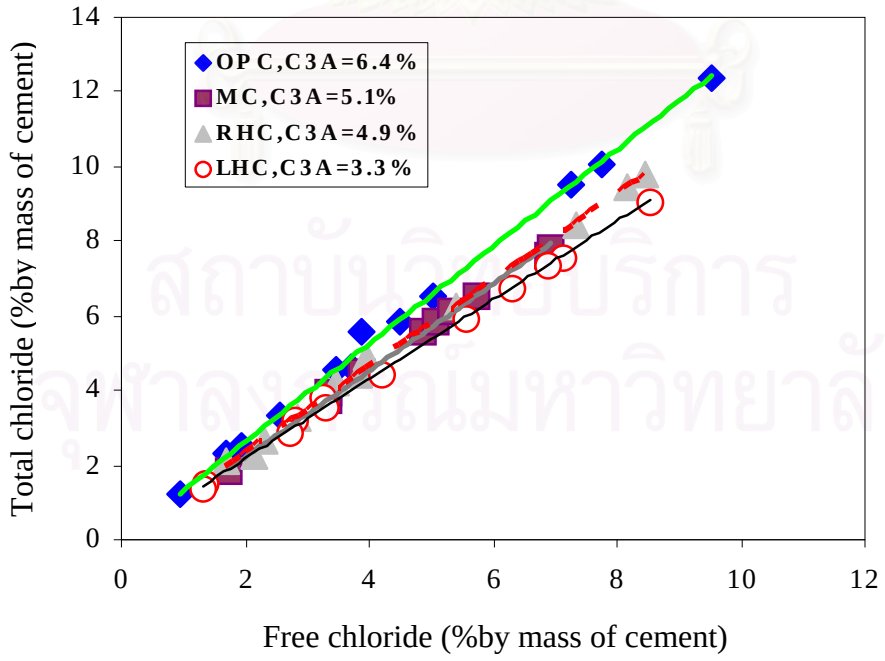

Figure 3.3 Relationship between free chloride and total chloride of various cement types

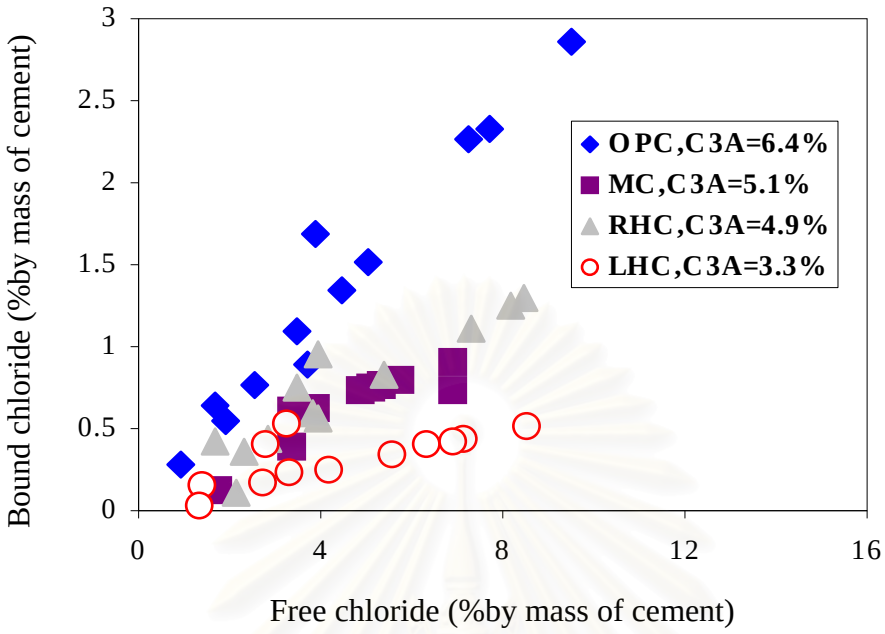

Figure 3.4 Chloride binding capacity of various cement types

Figure 3.3 shows the relationship between the free chloride contents and the total chloride contents of various cement pastes made from different cement types. As shown in the figure, under the same conditions of concentration and immersion period, the total chloride content is always higher than the free chloride content. There are differences in chloride binding capacity of various cement types. The relationship between the free chloride content and the total chloride content can be formulated by a power approximation of the test results obtained from paste specimens as follows:

OPC: $y = 1.3218x^{0.995}$ (3.1)

MC: $y = 1.0989x^{1.022}$ (3.2)

RHC: $y = 1.1695x^{0.9954}$ (3.3)

LHC: $y = 1.0987x^{0.9864}$ (3.4)

where, *x* is the free chloride (% by mass of cement) and *y* is the total chloride (% by mass of cement).

To be more specific, the bound chloride content, the physically bound chloride content which is adsorbed by C-S-H gel, and the chemically bound chloride content formed by reaction of AFm with chloride ions were analyzed detailed. The content of bound chloride ions is determined by deducting the content of free chloride ions from the total content of chloride ions. The chemically bound chloride content, which is present in the solid phase of Friedel's salt, is determined by XRD Rietveld analysis. Then, the content of physically bound chloride ions is determined by deducting the content of chemically bound chloride ions from the content of bound chloride ions.

Figure 3.4 shows the relationship between the bound chloride and the free chloride for paste series OPC, MC, RHC and LHC. It can be seen that the chloride binding isotherm is different only for different types of cement. The differences in chloride binding capacity of various cement types is assumed to be due to differences in the compositions of cement types as shown in Table 3.1. Differences in cement compounds and compositions result in differences in the hydration degree of the cement paste as well as differences in the kinds and contents of hydrates, especially, C-S-H and AFm compounds. However, all four cement types show similar trends, at which the amount of bound chloride increases consistently with increases in the free chloride content. With the point of view of the chloride binding capacity, the OPC paste everywhere has the highest ability to bind chloride ions, whereas LHC paste has the lowest capacity to bind chloride ions, and the chloride binding capacity of MC paste and RHC paste are very similar. Among of four cement types, OPC has the highest C_3A content which results in the highest content of Friedel's salt since the content of AFm hydrate in OPC paste is the highest of the four cement types, see Figure 3.5 and 3.6. Further, on average, the hydration degree of OPC paste is the second highest; this makes the content of C-S-H hydrate in OPC paste high enough to absorb more chloride ions. On the contrary, LHC has the lowest content of C_3A and this results in the lowest Friedel's salt content, in which, the chemically bound chloride is present. Additionally, LHC paste has the lowest C-S-H hydrate content since the hydration degree is the lowest, as shown in Figure 3.7, due to the high content of C_2S compounds. All explanations described here answer the question why OPC paste has the highest capacity to bind chloride ion, while LHC paste has the lowest.

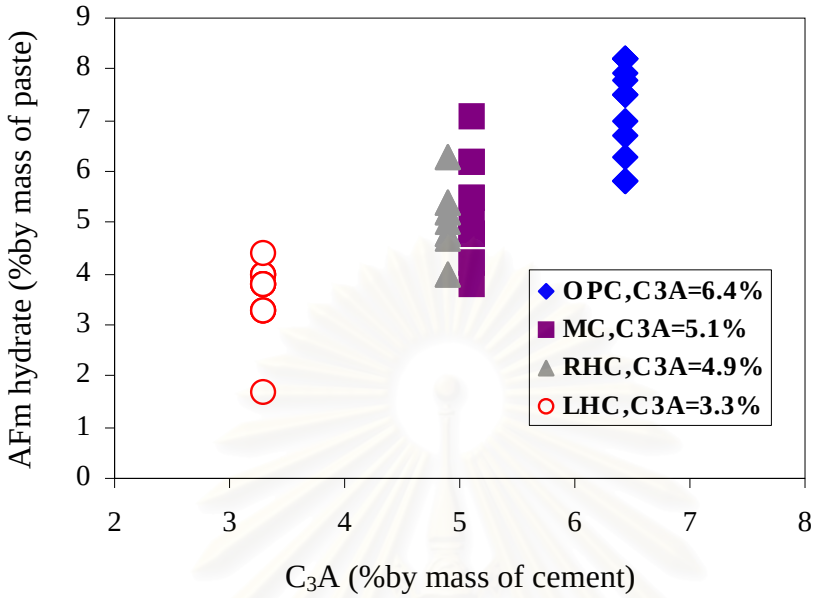

Figure 3.5 AFm hydrate content with varying C_3A content of cements

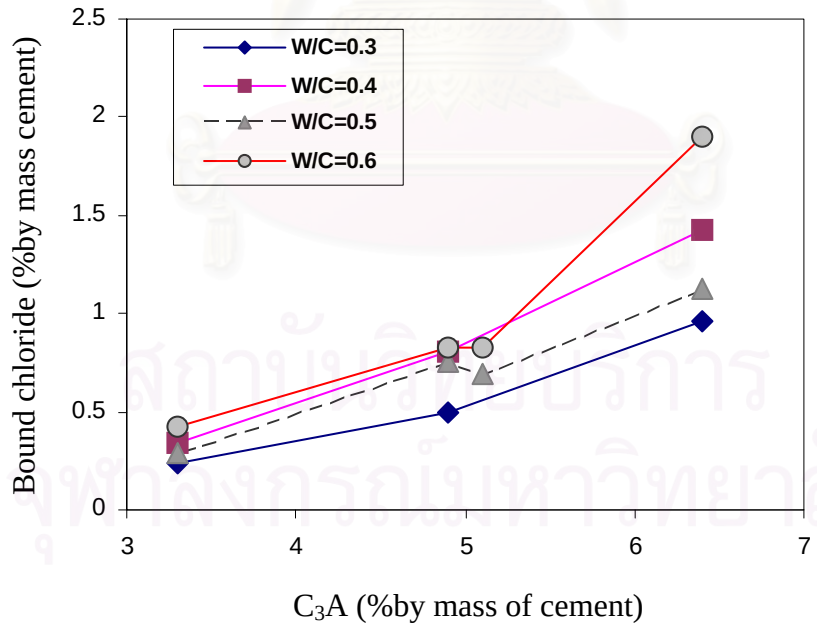

Figure 3.6 Relationship between bound chloride and C_3A content of cements

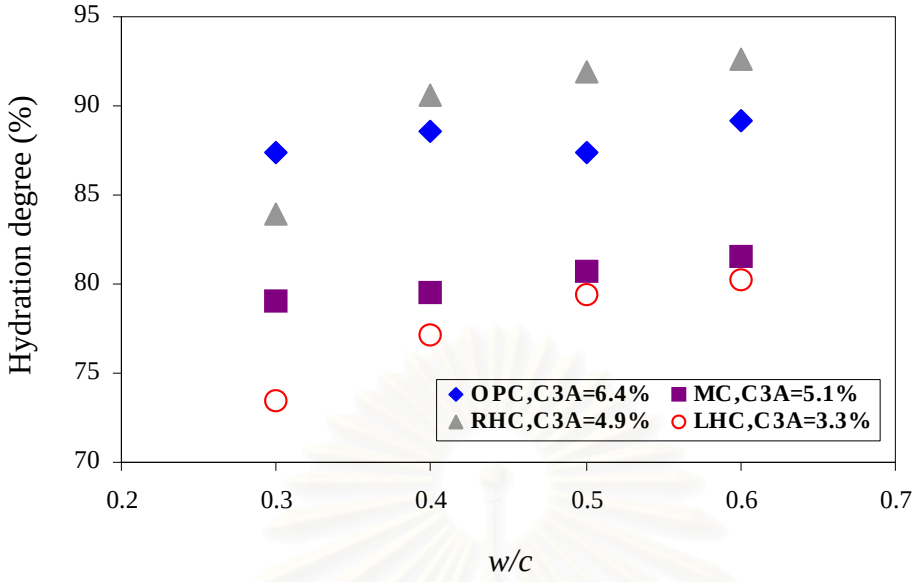

Figure 3.7 Hydration degrees of cements with varying *w/c* ratio

3.2.2 Contribution of physically and chemically bound chloride to the total chloride binding isotherms of various cement types

As mentioned above, bound chlorides were separated into physically bound chloride and chemically bound chloride so that the contributions of the physically bound chloride and chemically bound chloride to chloride binding were investigated. Figure 3.8 shows relationship between the free chloride content and the physically bound chloride content, while Figure 3.9 presents relationship between the free chloride content and the chemically bound chloride content. As can be seen from Figure 3.8, the contents of the physically chloride vary greatly with different cement types. This means that chloride adsorption behaviour of pastes made from different cements varies with specific surface area and structure of the hardened cement paste. From the viewpoint of chloride adsorption capacity, the rank of pastes made from cement types from highest to lowest is OPC, RHC, MC and LHC. In general, the chloride adsorption capacity of MC is comparable to that of RHC. Also, as the same tendency with the physically bound chloride, the contents of the chemically bound chloride change greatly with different cement types, see Figure 3.9. And, from the viewpoint of the capacity to form Friedel's salt, OPC has the highest capacity, whereas LHC has the lowest capacity, and MC is comparable to RHC to form Friedel's salt. This phenomenon reflects the contents of Al_2O_3 and C_3A in the cements, see Table 3.1, and that the chemically bound chloride content strongly depends on the type of cement. Moreover, it

is found that the contents of physically bound chloride are much higher than those of the chemically bound chloride in the different cement types and at the different *w/c* ratios, and that the physically bound chloride is the major part of the bound chloride. The content of the physically bound chloride, generally, ranges from 60% to 80% of the total amount of bound chloride, see Figure 3.10.

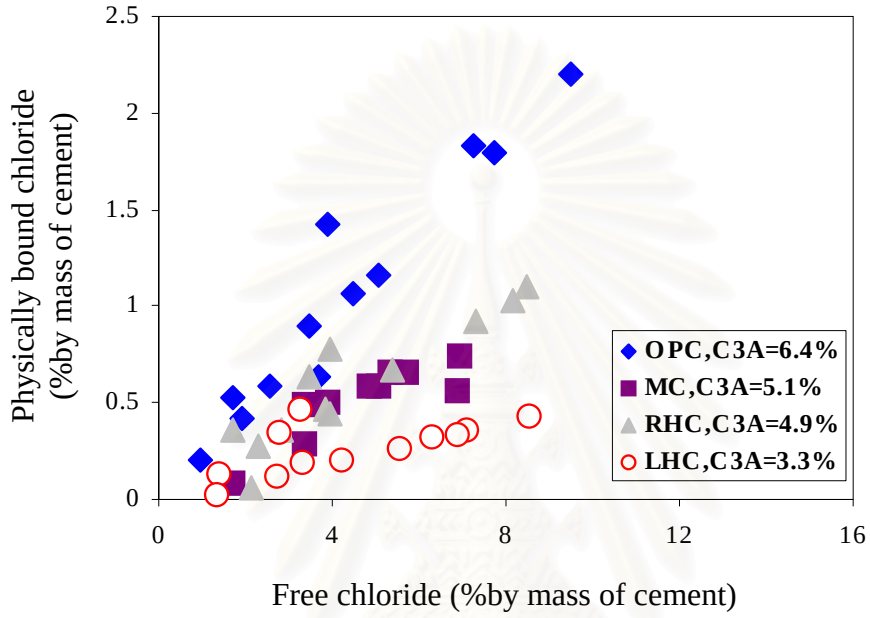

Figure 3.8 Relationship between physically bound chloride and free chloride of various cement types

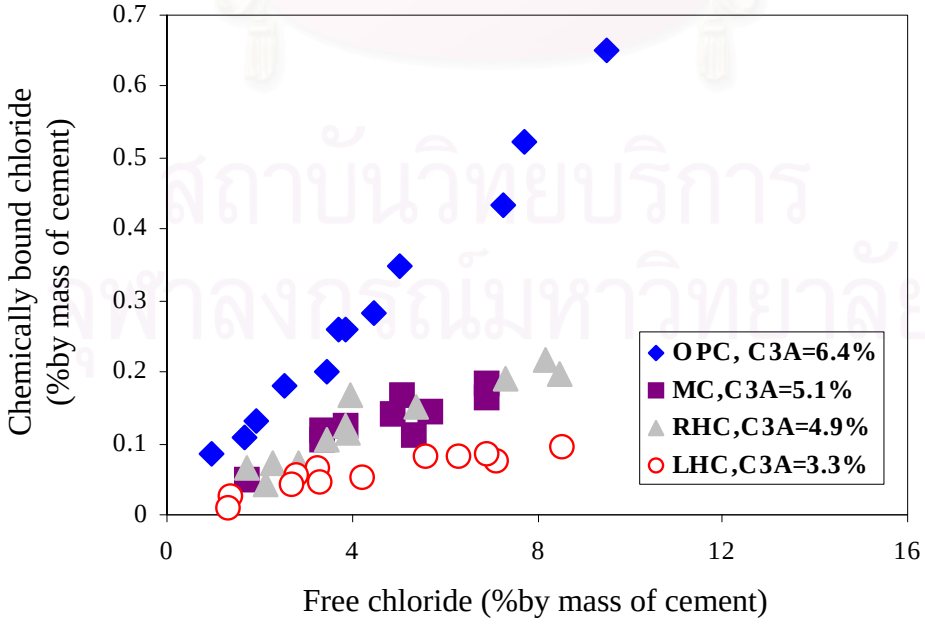

Figure 3.9 Relationship between chemically bound chloride and free chloride of various cement types

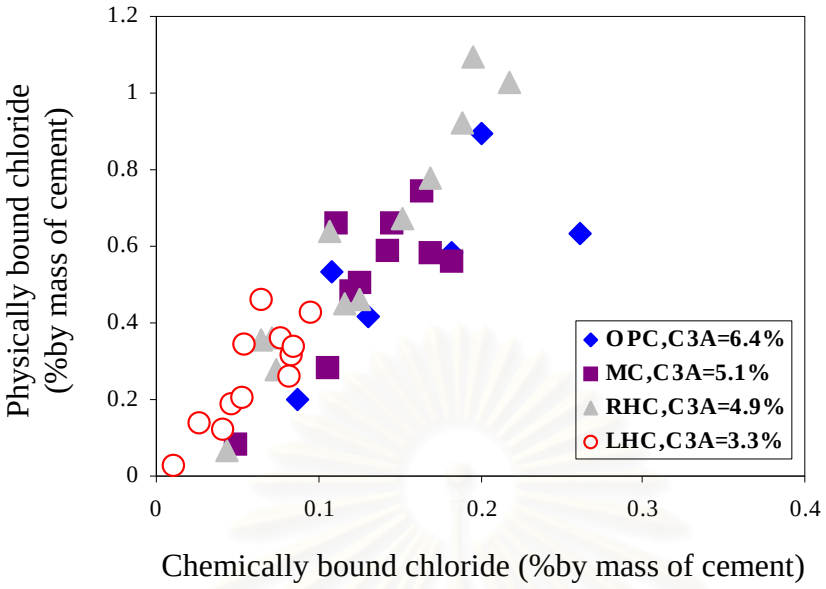

Figure 3.10 Relationship between chemically bound chloride and physically bound chloride of various cement types

Additionally, in this study, the chloride binding capacities of C-S-H and AFm hydrates in various cement types were calculated with assuming that C-S-H compounds are responsible for absorbing chloride ions, the physically bound chloride, on the large surfaces of C-S-H compounds; AFm is the major compound of paste that reacts with chloride ions, the chemically bound chloride, to form Friedel's salt; the content of AFm hydrate, which takes into account the reaction to form Friedel's salt, is the difference between the AFm hydrate content before immersing in chloride solution and the AFm hydrate content remaining at the end of the immersion period.

Figure 3.11 shows the isotherm of chloride bound by C-S-H. It is clearly shown that the amount of chloride bound by C-S-H increases with increases of the free chloride concentration, and the isotherm of chloride bound by C-S-H can be fitted to the curve of a Langmuir isotherm type. Moreover, the highest chloride binding capacity of C-S-H hydrate is around 33.58 mg per 1 g of C-S-H phase, this is 1/3 of the chloride bound by AFm hydrate, however the mass content of C-S-H hydrate in the cement paste is always much higher than that of the AFm phase, in some cases reaching nearly 66% weight of the cement paste. Consequently, the contribution of C-S-H hydrate to the chloride binding capacity of cement pastes is very significant. As shown in Figure 3.11, the isotherms of chloride bound by C-S-H for various cement types are different. The isotherms of chloride bound by C-S-H phase of the various cement types are expressed as follows:

$$\text{OPC: } y = 116.405\frac{0.0138x}{1+0.0138x} \tag{3.5}$$

$$\text{MC: } y = 20.355\frac{0.0805x}{1+0.0805x} \tag{3.6}$$

$$\text{RHC: } y = 133.156\frac{0.0064x}{1+0.0064x} \tag{3.7}$$

$$\text{LHC: } y = 10.0313\frac{0.0777x}{1+0.0777x} \tag{3.8}$$

here, x is the free chloride concentration (mmol/l) and y is the physically bound chloride content (mg/g C-S-H).

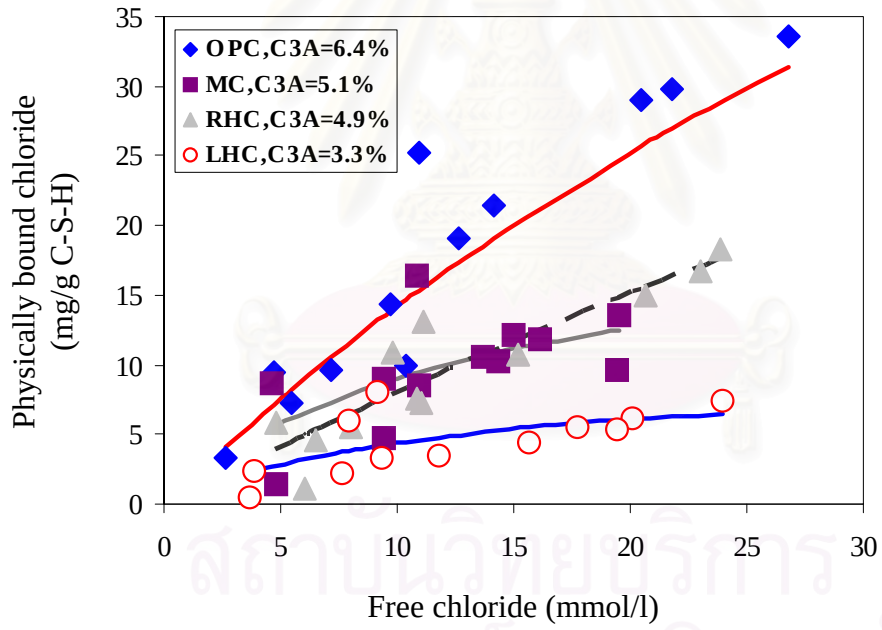

Figure 3.11 Chloride binding capacity of C-S-H hydrate of various cement types

Figure 3.12 shows the isotherm of chloride bound by AFm hydrate in cement pastes. The amount of the chemically bound chloride by AFm hydrate increases with the increase in the free chloride concentration. The highest chloride binding capacity of AFm hydrate is 1.4 mol per 1 mol of AFm at a free chloride concentration of 26.8 mmol/l. This value is lower than the stoichiometric value of 2 mol chloride per 1 mol of AFm hydrate, see Eq. (3.9).

Hirao et al 2005 found that 1 mol of AFm bound 1.1 mol of chloride, whereas, Saeki et al 2002 reported that this ratio was 5:1.

$$C_3A.CaSO_4.H_{12} + 2NaCl \rightarrow C_3A.CaCl_2.10H_2O + 2Na^+ + SO_4^{2-} + 2H_2O \quad (3.9)$$

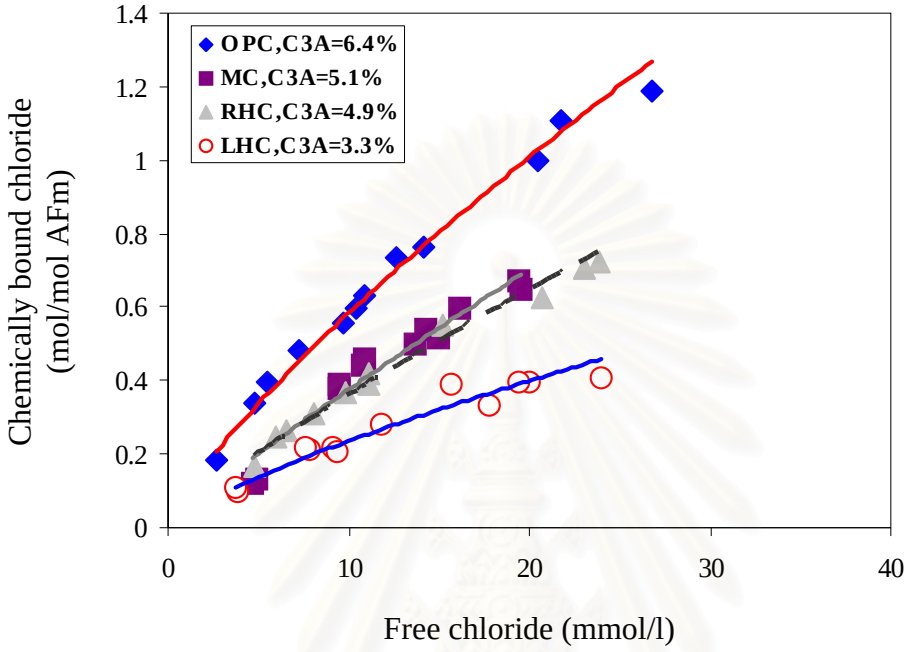

Figure 3.12 Chloride binding capacity of AFm hydrate of various cement types

As shown in Figure 3.12, isotherms of chloride bound by AFm of various cement types are different. The isotherm of chloride bound by AFm fits the Freundlich isotherm. Experimental data fit the isotherm of chloride bound by AFm of various cement types as below:

$$\text{OPC: } y = 0.0949x^{0.7888} \quad (3.10)$$

$$\text{MC: } y = 0.0473x^{0.901} \quad (3.11)$$

$$\text{RHC: } y = 0.0521x^{0.8408} \quad (3.12)$$

$$\text{LHC: } y = 0.0407x^{0.7623} \quad (3.13)$$

here, x is the free chloride concentration (mmol/l) and y is the chemically bound chloride content (mol/mol AFm).

3.2.3 Experimentally established equations to estimate the bound chloride of various cement pastes

Hirao et al 2005 reported that AFm and C-S-H hydrates are the major phases binding chloride ions. Tang et al 1993 showed that the chloride binding capacity of cement based solutions were strongly dependent on C-S-H gel. Also, as mentioned above, the C-S-H phase is responsible for the absorption of physically bound chloride, while the chemically bound chloride is formed due to the reaction of AFm hydrate with chloride ions present in the pore solution. Hence, the proposed equations used to estimate the bound chloride content of various cement pastes must be described based on the contents of AFm and C-S-H hydrates. The experimentally established equations are as follows:

$$\text{OPC: } y = 116.405\frac{0.0138x}{1+0.0138x}\frac{n}{100} + 0.0949x^{0.7888}.\frac{1000}{623}.\frac{35.5m}{100} \quad (3.14)$$

$$\text{MC: } y = 20.355\frac{0.0805x}{1+0.0805x}\frac{n}{100} + 0.0473x^{0.901}.\frac{1000}{623}.\frac{35.5m}{100} \quad (3.15)$$

$$\text{RHC: } y = 133.156\frac{0.0064x}{1+0.0064x}\frac{n}{100} + 0.0521x^{0.8408}.\frac{1000}{623}.\frac{35.5m}{100} \quad (3.16)$$

$$\text{LHC: } y = 10.0313\frac{0.0777x}{1+0.0777x}\frac{n}{100} + 0.0407x^{0.7623}.\frac{1000}{623}.\frac{35.5m}{100} \quad (3.17)$$

here, x is the free chloride concentration (mmol/l), y is the amount of chloride ions bound by hydrates (mg/g sample), n is the amount of C-S-H gel in cement paste (mass%), and m is the amount of AFm hydrate (mass%).

As shown in Equations (3.14) to (3.17), the content of chloride ions bound by hydrates includes functions of independent parameters: AFm content, C-S-H content and free chloride concentration. These experimental equations can be applied to all commonly used cement types with the assumptions that AFm is formed by the hydration of C_3A, that all AFm

reacts with chloride ions to form Friedel's salt, and that AFm does not change to AFt at low chloride concentrations. This assumption is consistent with other reported results (Hirao, 2005).

Several methods have been proposed to determine hydrated cement phases (JCI-C39, 1996), and applying the experimentally determined equations described above together with the methods of determining hydrated cement phases, makes it possible to estimate the bound chloride content of various cement pastes from the contents of (C_3S+C_2S) and C_3A in the cement, and from the free chloride concentration.

3.3 Concluding remarks

This chapter presents the chloride binding capacities of cements. Some concluding remarks for this chapter are as below:

1. The chloride binding capacity of cements can be fitted to Freundlich isotherm. Of four cement types, OPC has the highest capacity to bind chloride ion, whereas LHC has the lowest chloride binding capacity. The chloride binding capacities of MC and RHC are comparable.
2. The chloride binding capacity of cements is different because of the differences in chemical and mineral compositions of cements.
3. The bound chloride includes the chemically bound chloride and physically bound chloride. The content of the physically bound chloride is much higher than that of the chemically bound chloride. The physically bound chloride is adsorbed on the surface of C-S-H gel, whereas the chemically bound chloride is present in the solid phase of Friedel's salt which is the product of reaction of AFm hydrate with chloride ions.
4. Experimental equations were proposed for estimation of the bound chloride contents of different cement types basing on contents of AFm hydrate and C-S-H gel, and on the concentration of the free chloride ion.

CHAPTER IV

CHLORIDE PENETRATION INTO CONCRETE STRUCTURES UNDER FLEXURAL CYCLIC LOAD AND TIDAL ENVIRONMENT

This chapter shows numerical analysis of designed mechanical and physical properties of concretes, prediction of crack growth of plain concrete beam under flexural cyclic load, prediction of chloride diffusion coefficient under fatigue, and simulation of chloride penetration into plain concrete under fatigue and tidal environment.

4.1 Designed mechanical and physical properties of concretes

Mechanical and physical properties of concretes were predicted mainly basing on *w/c* ratios as mentioned in chapter II. In this study, *w/c* ratios are 0.4, 0.5 and 0.6 used for casting plain concretes. We assume that there is no crack at all in concrete beam before testing. It means that initial crack widths, w_0, are zero. The designed mechanical and physical properties of plain concrete beams, which were cured in water for 60 days, include compression strength, σ_c, tensile strength, σ_t, Young's modulus, E, ultimate bending load, P_{ult}, deflection of beam, δ_c, chloride diffusion coefficient at 28 days, D_{28}, and critical crack width, w_c. The designed mechanical and physical properties of concretes are shown in Table 4.1.

Table 4.1 Designed mechanical and physical properties of concrete

Series	*w/c*	σ_c, MPa	σ_t, MPa	E, GPa	P_{ult}, kN	δ_c, mm	w_c, μm	w_0, μm	D_{28}, 10^{-12} m^2/s
M1	0.40	47	3.9	32.2	15.7	1.34	60	0	7.8
M2	0.50	38	3.4	29.3	14.6	1.42	70	0	15.2
M3	0.60	29	2.8	25.0	13.2	1.78	90	0	19.7

Results of the designed mechanical and physical properties of concretes show that mechanical properties of concretes increase as *w/c* ratios decrease. However, physical properties, in terms of the deflection of concrete beams, δ_c, and the critical fictitious crack width, w_c, increase when *w/c* ratios increase. This means that the brittleness of concrete increases with decreasing *w/c* ratio.

4.2 Prediction of fatigue crack growth under flexural cyclic load

The crack growth process of plain concrete beam with depth *h*, width *b* and span *l* under flexural cyclic load can be generally divided into two stages: the fictitious crack initiation stage and the fictitious crack developing stage. The former will occur when bending load reaches the first crack load. In the later, stress distribution is nonlinear and linear in the cracked zone and uncracked zone, respectively.

The plain concrete beams were used with assumptions that there is no crack at all in concrete beams before bending, w_0=0, and a smear crack is supposed to appear as plain concrete beams are under flexural cyclic load. As explained in Chapter II, numerical solution of the system of nonlinear equations is applied to archive results of crack length, *ah*, and crack mouth opening, δ. In the first cycle, $\sigma_1(x)$ equals to σ_1 at N=1. In the second cycle, the stress degradation will occur in the cracked zone due to a closing and opening procedure of fatigue crack. A new fictitious crack is needed so that the external load, *P*, can reach $P_{app,\,max}$ in the zone where fictitious crack has been formed already. Hence, the stress degradation law will be applied to both the old cracked zone and the newly developed crack zone, with N = 2 and N = 1, respectively. This procedure will be continued until σ_N equals to zero.

In the fatigue test under load control procedure, bending load was ramped up to the desired $P_{app,\,max}$ over 20 cycles, the elastic displacement at this desired $P_{app,\,max}$, with SR=0.7, was about 0.01mm (Gontar, 2000). So, the numerical analyses of the fatigue deformation adopt 0.007, 0.008, 0.01 and 0.011mm as the initially ramped up crack width, w_i, these fatigue deformations are corresponding to *SR* of 0.5, 0.6, 0.7 and 0.8, respectively. Input parameters used to analyse the fatigue deformations of concrete beams under flexural cyclic load include the initially ramped up crack width, w_i, the applied bending load, $P_{app,\,max}$, the ultimate bending load, P_{ult}, the compression strength, σ_c, the tensile strength, σ_t and the Young's modulus, *E*. All the input parameters are shown in Table 4.2.

Table 4.2 Input Parameters of numerical analysis of fatigue deformations

Series	w_i, mm (*SR*)				$P_{app,\,max}$, kN (*SR*)				P_{ult}, kN	σ_c, MPa	σ_t, MPa	E, GPa
	0.5	0.6	0.7	0.8	0.5	0.6	0.7	0.8				
M1	0.007	0.008	0.01	0.011	7.85	9.42	11.0	12.56	15.7	47	3.9	32.2
M2	0.007	0.008	0.01	0.011	7.3	8.76	10.22	11.68	14.6	38	3.4	29.3
M3	0.007	0.008	0.01	0.011	6.6	7.92	9.24	10.56	13.2	29	2.8	25.0

Numerical analyses of relationships between crack width and the number of cycles for plain concrete beams subjected to fatigue tests with different *SR* are shown in Figure 4.1, 4.2 and 4.3. The theoretically calculated fatigue crack lengths of concrete beams under different load levels with the minimum applied load, $P_{app,min}$, equal to zero are shown in Figure 4.4, 4.5 and 4.6.

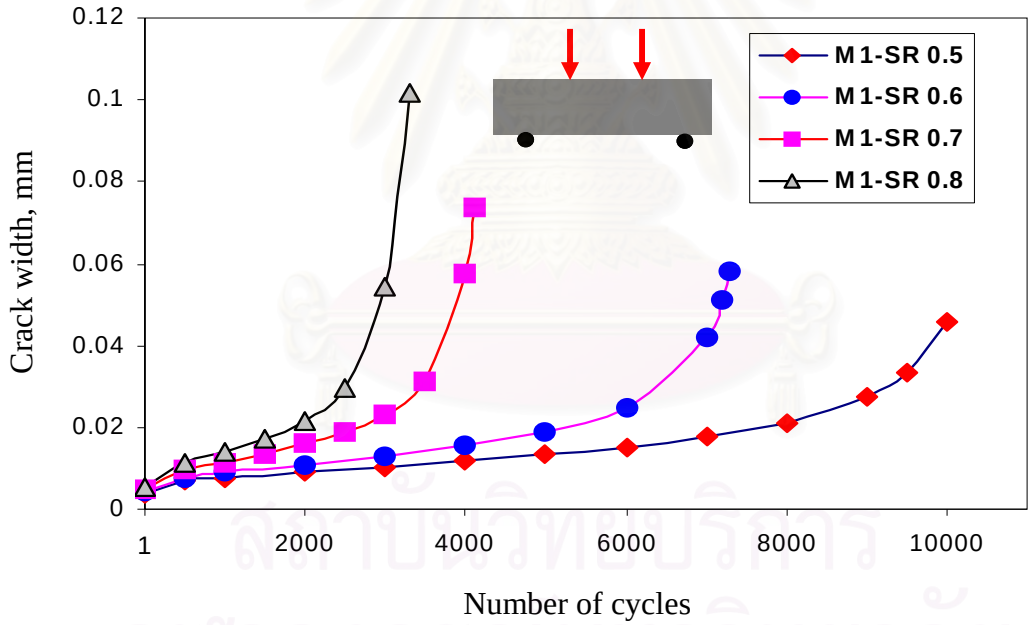

Figure 4.1 Predictions of relationships of crack width and number of cycles, M1

The fictitious crack width and crack length increased with increasing either the number of cycles, *N*, or the load level, *SR*, especially at the number of cycle where L-D curve starts changing and at the load levels, *SR*=0.7 and 0.8. The numerical simulation clearly showed that fictitious crack growth, in terms of crack width and crack length, can be divided

into three stages; a decelerated stage; a steady stage; an accelerated stage towards fracture. These results are consistent with other reports and with experimental data.

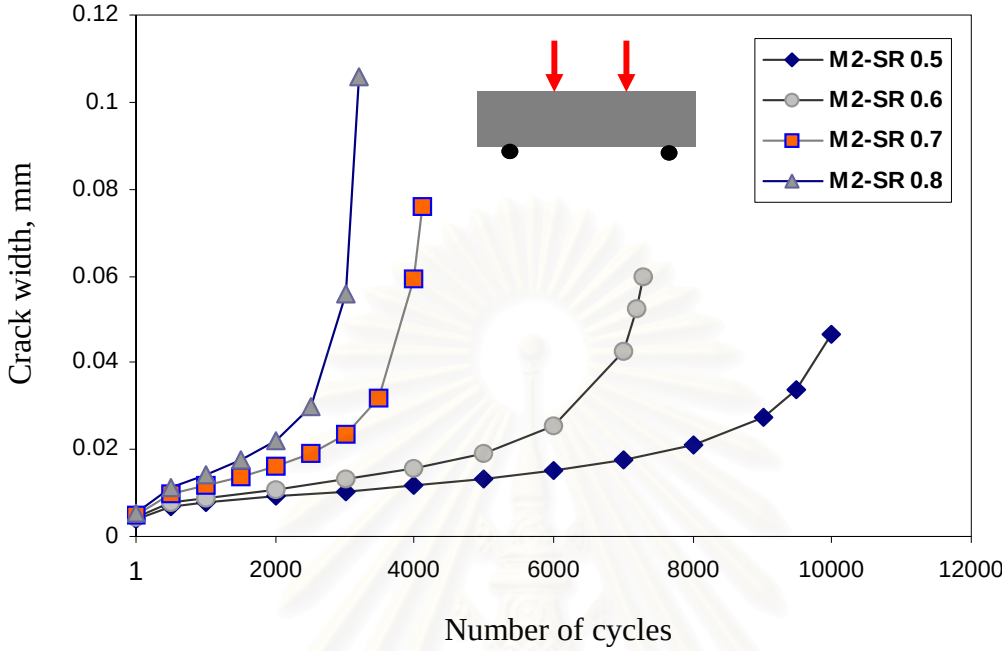

Figure 4.2 Predictions of relationships of crack width and number of cycles, M2

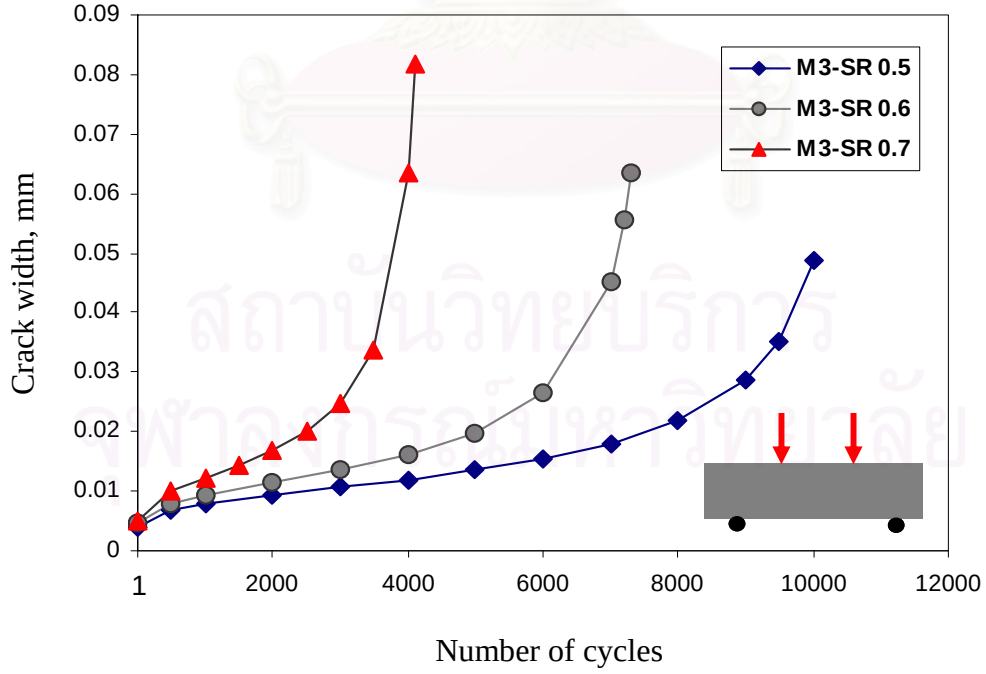

Figure 4.3 Predictions of relationships of crack width and number of cycles, M3

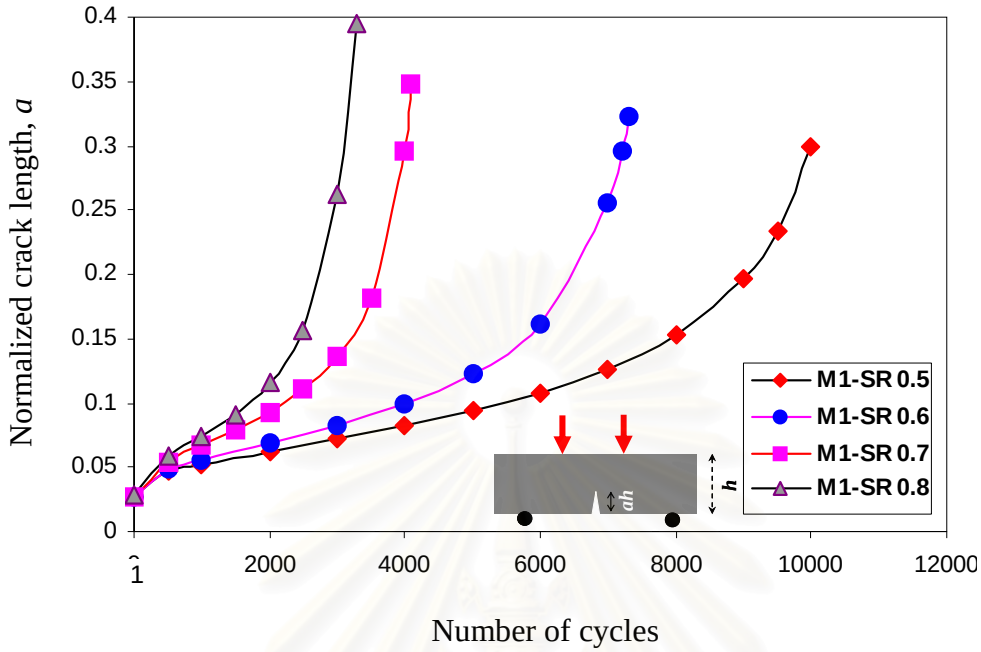

Figure 4.4 Predictions of relationships of crack length and number of cycles, M1

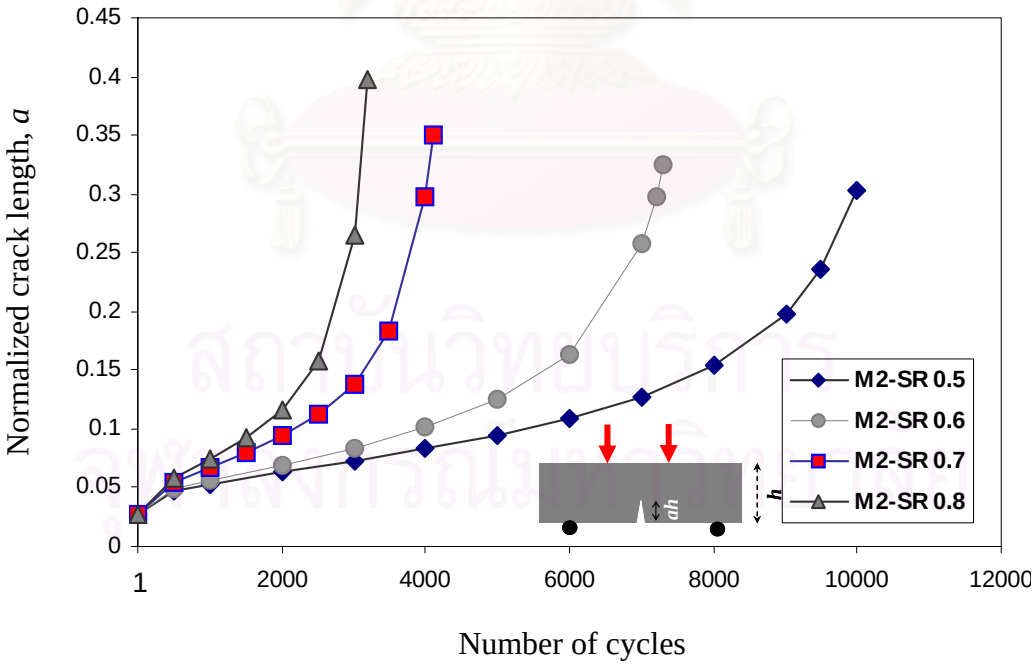

Figure 4.5 Predictions of relationships of crack length and number of cycles, M2

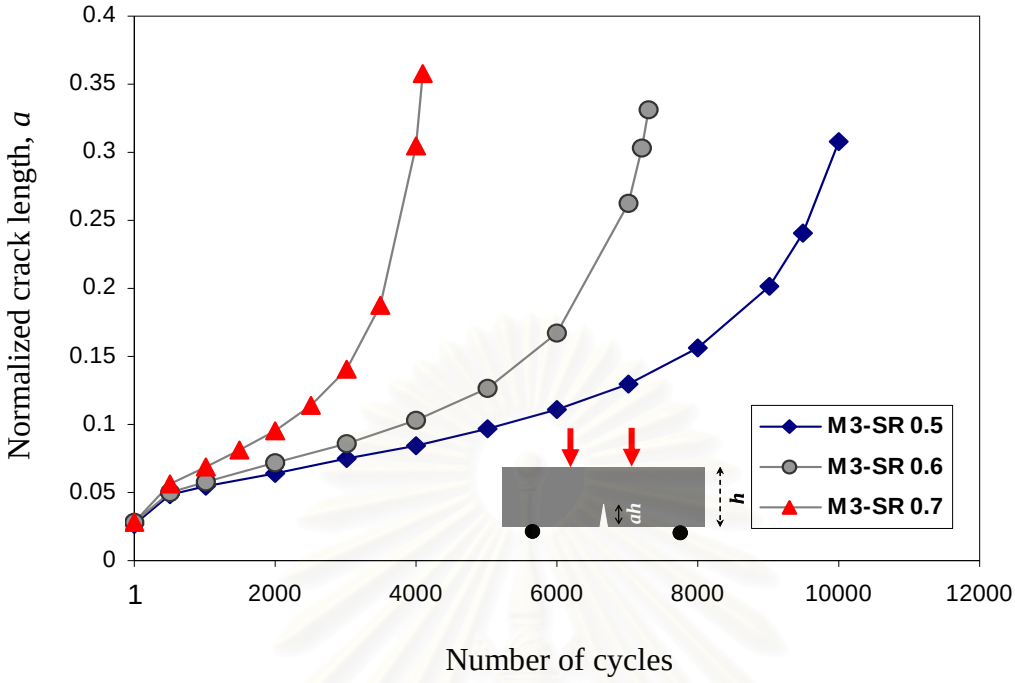

Figure 4.6 Predictions of relationships of crack length and number of cycles, M3

4.3 Prediction of chloride diffusion coefficient under fatigue

Considering a simple case of chloride flow through cracked concrete, total flow of chloride can be expressed as the sum of the flow through crack and flow through uncracked part of homogeneous material. For crack due to flexural cyclic load, the author adopts the simple assumption that a single-edge crack occurs; the crack shape is straight; the crack length at the edge side is equal to that at the bottom side of the beam.

Using theory of prediction of chloride diffusion in cracked concrete presented in chapter II, model prediction on the effect of number of cycles on the chloride diffusion, normalized D_{tot}, in the tension zone of plain concrete beams, which are under the flexural cyclic load, is shown in Figure 4.7, 4.8 and 4.9. Table 4.3 shows the model results of the calculated chloride diffusion coefficient in the tension zone with the number of cycles.

Model prediction data as shown in Figure 4.7 to 4.9 and in Table 4.3 clearly propose that the chloride diffusion in the tension zone increases with increasing either the number of cycles or the load level. Under fatigue loading with different load levels, the fictitious microcrack process involves the decelerated stage at which microcracks initiate as shown in Figure 4.1 to

4.6, however, during the decelerated stage of fictitious crack process, the chloride diffusion still seems to be monotonously increasing, see Figure 4.7, 4.8 and 4.9.

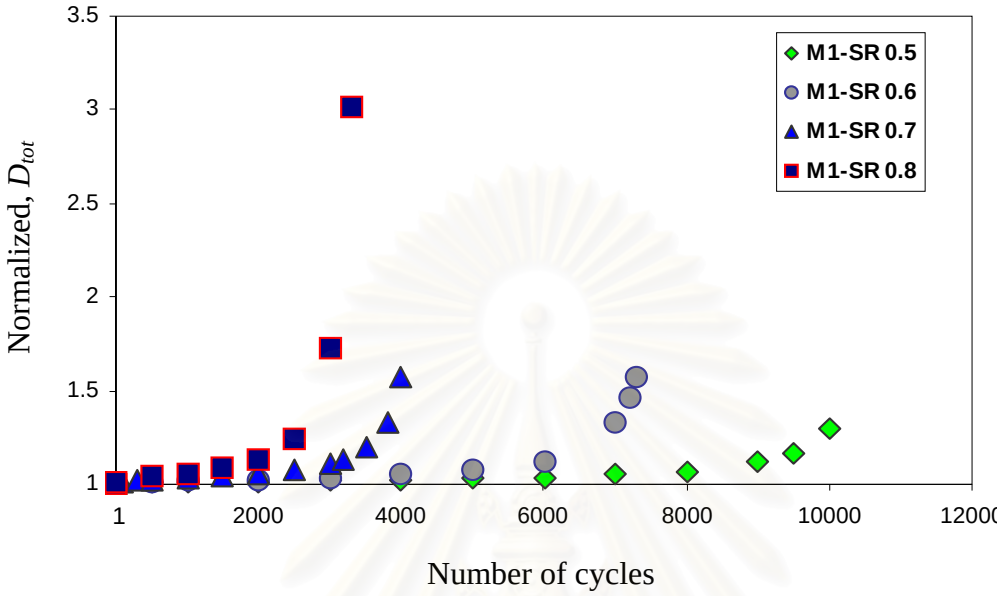

Figure 4.7 Model prediction for the influence of cyclic load on the chloride diffusion coefficient in tension zone of plain concrete beam, M1

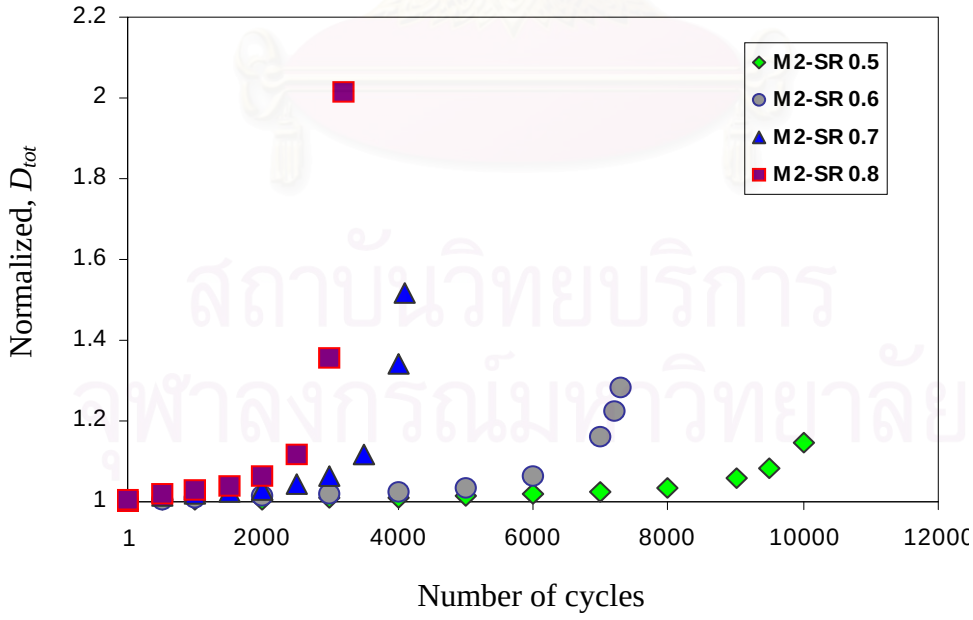

Figure 4.8 Model prediction for the influence of cyclic load on the chloride diffusion coefficient in tension zone of plain concrete beam, M2

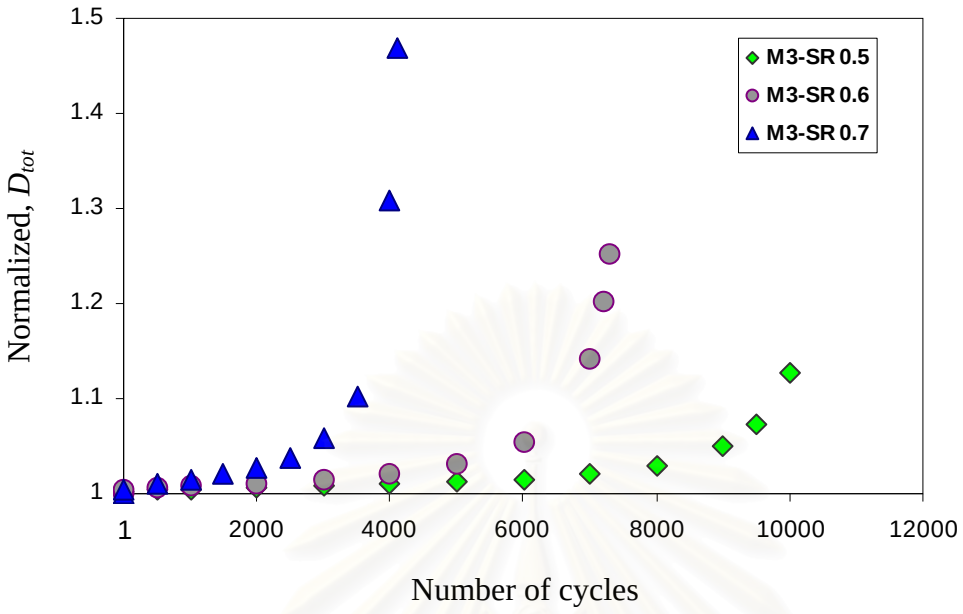

Figure 4.9 Model prediction for the influence of cyclic load on the chloride diffusion coefficient in tension zone of plain concrete beam, M3

One of the reasons is that decelerated microcracks are still so small that crack areas formed are still not large enough, compared to the whole surface area of the specimen, to change the chloride diffusion readily. After the decelerated stage of fictitious microcrack process, crack widths start to enhance up to the failure, which result in large crack areas corresponding with a so-called accelerated stage of the chloride diffusion. In this stage, cracks may not be able to heal in unloaded stage, or cracks become irreversible to contribute for widening accesses for the chloride diffusion. Thus, overall, flexural cyclic load makes the chloride diffusion coefficient, which is estimated in the tension zone of concrete beam, increase and be divided into two stages as the monotonously increasing and accelerated stage.

The effect of fatigue load level on the chloride diffusion coefficient in tension zone is shown in Figure 4.10. As can be seen in Figure 4.10, with the same mixture series and the same number of cycle, the experiments show an increasing tendency of the chloride diffusion with increasing the load level. The chloride diffusion increases significantly when we apply fatigue test with load level *SR* at 0.6, 0.7 and 0.8, especially at 0.7 and 0.8. The model prediction shows the same tendency of the chloride diffusion with measurements (Gontar, 2000).

Table 4.3 Prediction of D_{tot} of plain concrete in the tension zone with the number of cycles

Series	*SR*	$D_{tot} \times 10^{-12}$ m^2/s (*N*)													
M1	0.5	6.25 (0)	6.29 (1)	6.31 (500)	6.32 (1000)	6.34 (2000)	6.37 (3000)	6.39 (4000)	6.43 (5000)	6.48 (6000)	6.56 (7000)	6.70 (8000)	6.99 (9000)	7.31 (9500)	8.10 (10000)
	0.6	6.25 (0)	6.30 (1)	6.34 (500)	6.37 (1000)	6.41 (2000)	6.47 (3000)	6.56 (4000)	6.71 (5000)	7.03 (6000)	8.29 (7000)	9.11 (7200)	9.81 (7300)	-	-
	0.7	6.25 (0)	6.29 (1)	6.35 (100)	6.37 (300)	6.39 (500)	6.45 (1000)	6.51 (1500)	6.61 (2000)	6.74 (2500)	6.98 (3000)	7.14 (3200)	7.54 (3500)	8.45 (3800)	10.06 (4000)
	0.8	6.25 (0)	6.31 (1)	6.49 (500)	6.61 (1000)	6.78 (1500)	7.07 (2000)	7.74 (2500)	10.80 (3000)	18.90 (3300)	-	-	-	-	-
M2	0.5	13.10 (0)	13.10 (1)	13.20 (500)	13.20 (1000)	13.20 (2000)	13.20 (3000)	13.20 (4000)	13.30 (5000)	13.30 (6000)	13.40 (7000)	13.60 (8000)	13.80 (9000)	14.20 (9500)	15.0 (10000)
	0.6	13.10 (0)	13.10 (1)	13.20 (500)	13.20 (1000)	13.30 (2000)	13.30 (3000)	13.40 (4000)	13.60 (5000)	13.90 (6000)	15.20 (7000)	16.10 (7200)	16.80 (7300)	-	-
	0.7	13.10 (0)	13.20 (1)	13.30 (500)	13.30 (1000)	13.40 (1500)	13.50 (2000)	13.70 (2500)	14.00 (3000)	14.60 (3500)	17.60 (4000)	19.90 (4100)	-	-	-
	0.8	13.10 (0)	13.20 (1)	13.30 (500)	13.50 (1000)	13.60 (1500)	13.90 (2000)	14.60 (2500)	17.80 (3000)	26.40 (3200)	-	-	-	-	-
M3	0.5	15.90 (0)	15.90 (1)	16.00 (500)	16.00 (1000)	16.00 (2000)	16.00 (3000)	16.10 (4000)	16.10 (5000)	16.10 (6000)	16.20 (7000)	16.40 (8000)	16.70 (9000)	17.10 (9500)	17.90 (10000)
	0.6	15.90 (0)	16.00 (1)	16.00 (500)	16.00 (1000)	16.10 (2000)	16.10 (3000)	16.20 (4000)	16.40 (5000)	16.80 (6000)	18.20 (7000)	19.10 (7200)	19.90 (7300)	-	-
	0.7	15.90 (0)	16.00 (1)	16.10 (500)	16.10 (1000)	16.20 (1500)	16.30 (2000)	16.50 (2500)	16.80 (3000)	17.50 (3500)	20.80 (4000)	23.40 (4100)	-	-	-

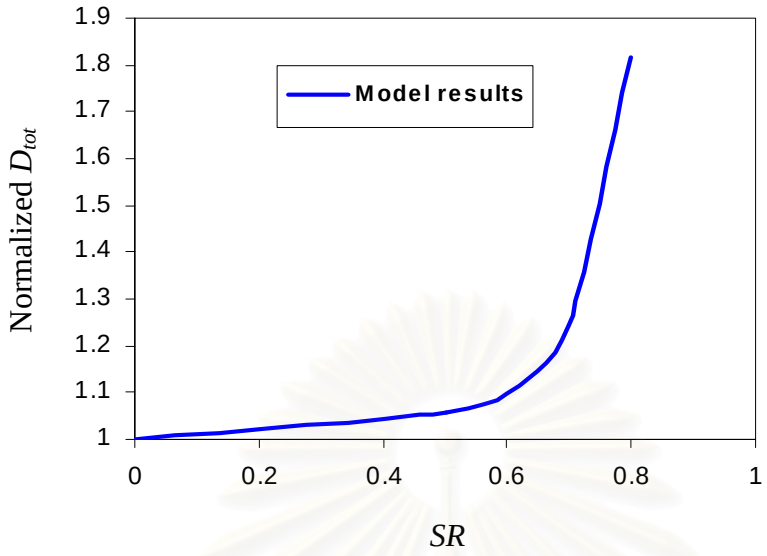

Figure 4.10 Relationships of load level and normalized D_{tot}, model prediction results, M1, N=3500

4.4 Prediction of chloride penetration under fatigue and tidal environment

As mentioned in chapter II, the governing equation describing the chloride penetration in the drying-wetting condition can be written as:

$$\frac{\partial C_t}{\partial t} = D_a \frac{\partial^2 C_t}{\partial x^2} + \frac{C_t}{\phi} w_{sat} D_h \frac{\partial^2 h}{\partial x^2} \tag{4.1}$$

The finite difference method and Crank-Nicholson algorithm are used to discretize and solve the one-dimensional problem as Eq.(4.1). The second-order parts of the second-order parabolic partial differential Eq.(4.1) are approximated with a standard method that has second-order accuracy as shown in Eq.(4.2) and (4.3). And, the first-order part is approximated with the first-order accuracy as shown in Eq.(4.4).

$$D_a \frac{\partial^2 C}{\partial x^2} = D_a \frac{1}{2}\left[\frac{C_{i+1}^{l+1} - 2C_i^{l+1} + C_{i-1}^{l+1}}{(\Delta x)^2} + \frac{C_{i+1}^{l} - 2C_i^{l} + C_{i-1}^{l}}{(\Delta x)^2}\right] \tag{4.2}$$

$$D_h \frac{\partial^2 h}{\partial x^2} = D_h \frac{1}{2}\left[\frac{h_{i+1}^{l+1} - 2h_i^{l+1} + h_{i-1}^{l+1}}{(\Delta x)^2} + \frac{h_{i+1}^{l} - 2h_i^{l} + h_{i-1}^{l}}{(\Delta x)^2}\right] \tag{4.3}$$

$$\frac{\partial C}{\partial t} = \frac{C_i^{l+1} - C_i^{l}}{\Delta t} \tag{4.4}$$

Applying the Crank-Nicholson algorithm, the discretization of Eq.(5.2) became:

$$\begin{aligned}\frac{C_i^{l+1} - C_i^{l}}{\Delta t} = {} & D_a \frac{1}{2}\left[\frac{C_{i+1}^{l+1} - 2C_i^{l+1} + C_{i-1}^{l+1}}{(\Delta x)^2} + \frac{C_{i+1}^{l} - 2C_i^{l} + C_{i-1}^{l}}{(\Delta x)^2}\right] + \\ & + \frac{w_{sat}}{\phi} C_i^{l} D_h \frac{1}{2}\left[\frac{h_{i+1}^{l+1} - 2h_i^{l+1} + h_{i-1}^{l+1}}{(\Delta x)^2} + \frac{h_{i+1}^{l} - 2h_i^{l} + h_{i-1}^{l}}{(\Delta x)^2}\right]\end{aligned} \tag{4.5}$$

4.4.1 Numerical analysis

After formation of prediction of chloride diffusion under fatigue, a numerical simulation of chloride penetration, which couples fatigue and tidal effects, is analyzed basing on one-dimensional chloride penetration. The humidity, *h*, and surface chloride content, C_s, incorporated in the numerical solution changed in the time domain to simulate tides.

Numerical analysis is applied to predict chloride penetration into plain concretes with *w/c*=0.4 and 0.5, using 4 common cement types as OPC, MC, RHC and LHC, and subjected to both flexural cyclic loads and tidal conditions. Firstly, numerical analysis predicts chloride profiles of concrete beams, which are exposed to tidal environment and without loading, cast with *w/c*=0.4 and 0.5, and using 4 common cement types. These model results of chloride profiles will specify which type of cement is the best. Then, the numerical analysis of chloride penetration into concrete beams, using the best cement, exposed to tidal environment and under flexural cyclic load with different load levels will be proposed.

During the numerical analysis, the temperature is assumed constant, however, humidity *h* and the surface chloride content C_s changed in step rise in the time domain. Using the Crank-Nicholson algorithm, the results of the numerical analysis has good convergence with time steps of 8×10^6s, and very good with time steps of 4×10^6s (Tralla and Silfwerbrand, 2002), and 4.32×10^4s (12 hours) (Tran, Stitmannaithum and NAWA, 2006). Moreover, taking account tidal conditions, the time step of the time domain is chosen as 12 hours to

include 12 hour wet and 12 hour dry which is representative of the daily tidal cycle periods. Further, space steps of Δx = 5mm are chosen to ensure good convergence of the numerical solution. In this numerical analysis, the proposed chloride binding isotherm is linear. The values of input parameters used in the numerical analysis for predictions of the chloride profiles of concrete beams exposed to tidal environment for 5 years, using different cement types, are shown in Table 4.4.

Table 4.4 Input parameters used in the numerical analysis of chloride penetration into plain concrete using different cements and exposed to tidal environment

Input parameters	Concrete mixture							
	w/c=0.4				*w/c*=0.5			
Cement type	OPC	MC	RHC	LHC	OPC	MC	RHC	LHC
Concrete age, days	60							
	Humidity diffusion							
*Liquid content, w_{sat} (%)	11				13			
*Humidity diffusion coefficient, D_h (m^2/s)	1.0×10^{-12}				5.0×10^{-12}			
Initial humidity, h (%)	100							
Boundary conditions of time step	h_{max}=100, h_{min}=0 Time step, Δt=12 hr							
	Chloride diffusion							
Binding capacity factor, ϕ	1.3218	1.12	1.17	1.08	1.3218	1.12	1.17	1.08
Diffusion coefficient, $D_{i,ref}$ (m^2/s)	6.25×10^{-12}				13.58×10^{-12}			
Initial chloride content (wt % of cement)	$C_{i,0}$ = 0							
Boundary conditions of time step	C_s^{max} = 2.6; C_s^{min} = 0 Time step, Δt=12 hr				C_s^{max} = 3.1; C_s^{min} = 0 Time step, Δt=12 hr			
Temperature, t (^{0}C)	25±2							

* Data from Saetta et al, 1993

Generally, in tidal environments, the surface chloride content, C_s, is considered as 13kg/m^3 concrete, equal to 2.6% and 3.1% of the cement content of the concrete mix at *w/c*=0.4 and 0.5, respectively. Figure 4.11 and 4.12 show numerical results of the effect of types of cement on the total chloride content of concrete beams exposed to tidal cycles for 5 years with *w/c*=0.5 and 0.4. The curves of the chloride profile are nonlinear with *w/c*=0.4 and 0.5. Also, at a specific depth, the chloride content of concrete with *w/c*=0.4 is lower than that of concrete with *w/c*=0.5. This is due to the different chloride diffusion coefficients, $D_{i,ref}$ =6.25×10^{-12} m^2/s (*w/c*=0.4) and 13.58×10^{-12} m^2/s for *w/c*=0.5. Showing that for lower *w/c*, there is less pore volume and connective paths, consequently making the chloride penetration in concrete more difficult.

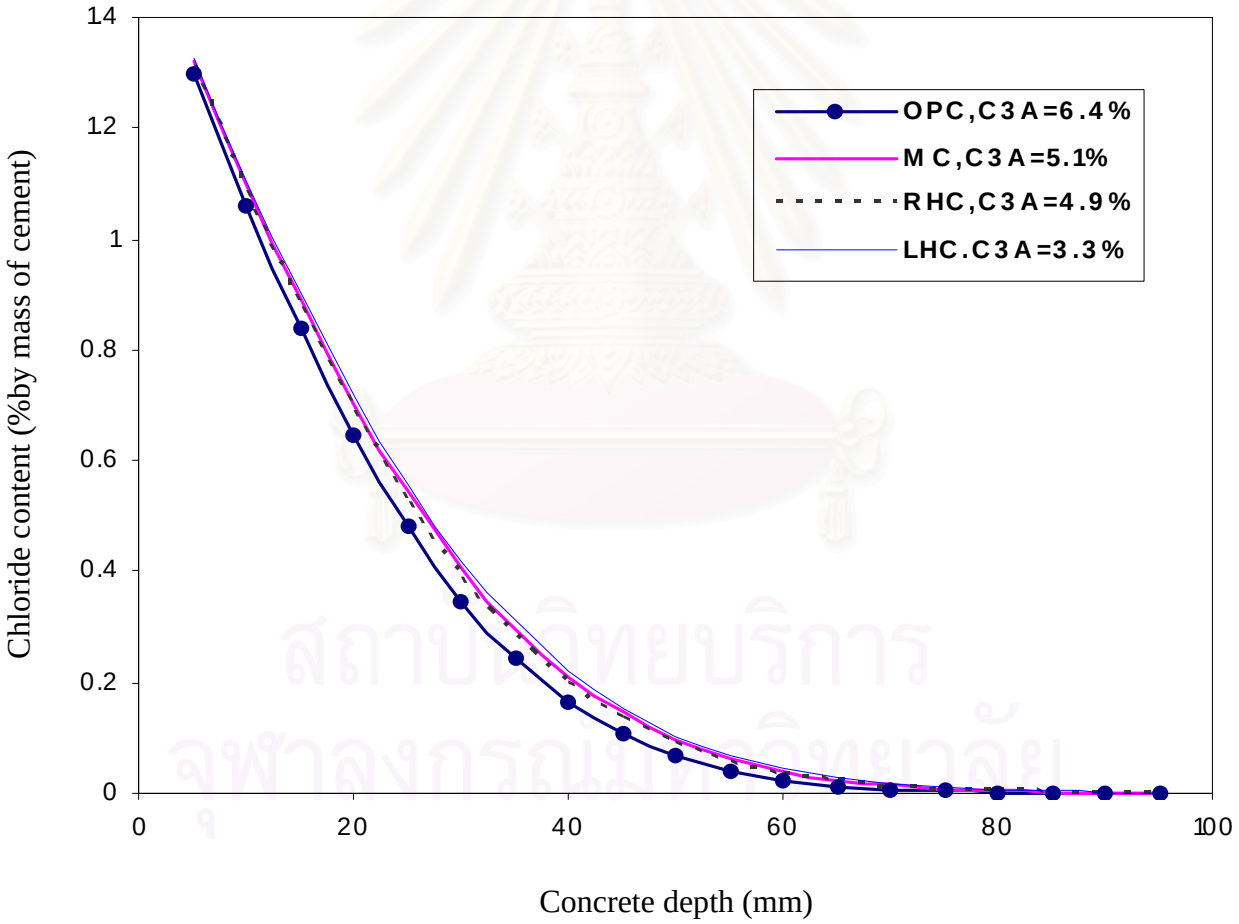

Figure 4.11 Chloride profiles of concrete beams using 4 different cements and exposed to tidal environment for 5 years, *w/c*=0.5

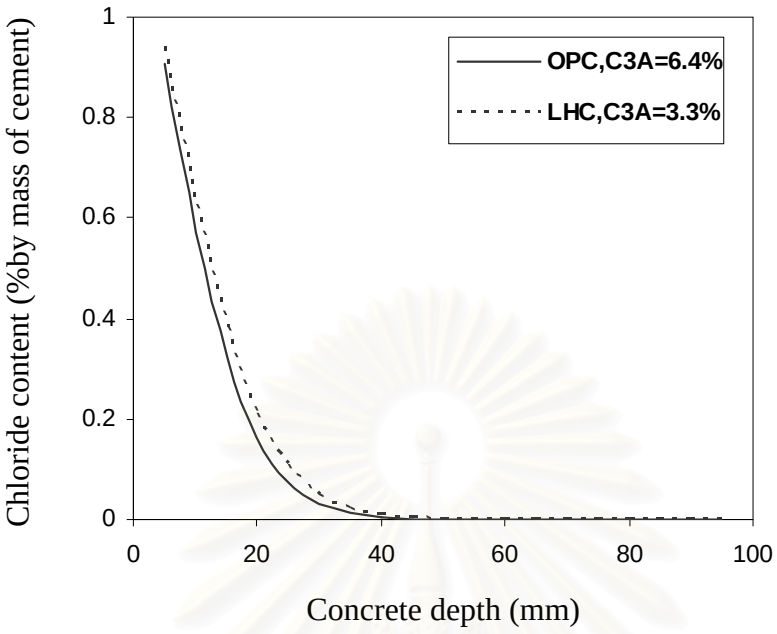

Figure 4.12 Chloride profiles of concrete beams using OPC and LHC, and exposed to tidal environment for 5 years, *w/c*=0.4

Model results indicated that the chloride penetration into concrete is different with different cement types. The chloride penetration was faster, and the acceleration rates of the chloride penetration into concretes became more distinct with cement types as MC, RHC, especially with LHC, see Figure 4.11 and 4.12. The chloride penetration is the lowest as concrete beam uses OPC, whereas the chloride penetration is the highest with LHC. The difference in the chloride penetrations of concretes is due to difference in cement types used for casting concrete beams. OPC has the highest chloride binding capacity and LHC has the lowest chloride binding capacity, as presented in chapter III. This makes chloride profiles predicted by numerical analysis highest and lowest in case we use LHC and OPC, respectively, see Figure 4.12. The predicted chloride penetration of concrete beams using MC and RHC are almost similar because the chloride binding capacities of MC and RHC are comparable, see Figure 4.11. This is consistent with the results of the experiments which described the chloride binding isotherms of various cements in chapter III. Therefore, OPC is the best cement type of four common cement types, in term of chloride induced corrosion, used for concrete structures.

Further numerical analysis presents the effect of flexural cyclic load, in term of load level, *SR*, on the chloride penetration in to concrete beams using OPC exposed to tidal

environment for 5 years. The input parameter used for predictions are shown in Table 4.5. The numerical analysis of the influence of the flexural cyclic load on the chloride penetration into concrete beams is shown in Figure 4.13 and 4.14.

Table 4.5 Input parameters used in the numerical analysis of chloride penetration into plain concrete subjected to coupling flexural cyclic loads and tidal cycles

Input parameters	Concrete mixture	
	w/c=0.4	w/c=0.5
Cement type	Ordinary Portland cement	
Concrete age, days	60	
	Humidity diffusion	
*Liquid content, w_{sat} (%)	11	13
*Humidity diffusion coefficient, D_h (m^2/s)	1.0×10^{-12}	5.0×10^{-12}
Initial humidity, h (%)	100	
Boundary conditions of time step	h_{max}=100, h_{min}=0 Time step, Δt=12 hr	
	Chloride diffusion	
Binding capacity factor, ϕ	1.3218	
Diffusion coefficient, $D_{i,ref}$ (m^2/s)	6.25×10^{-12}	13.58×10^{-12}
Initial chloride content (wt % of cement)	$C_{i,0}$ = 0	
Boundary conditions of time step	C_s^{max} = 2.6; C_s^{min} = 0 Time step, Δt=12 hr	C_s^{max} = 3.1; C_s^{min} = 0 Time step, Δt=12 hr
	Flexural cyclic load	
Cyclic flexural loading level, SR	0; 0.5; 0.6; 0.7 and 0.8	
Temperature, t (^{0}C)	25±2	

* Data from Saetta et al, 1993

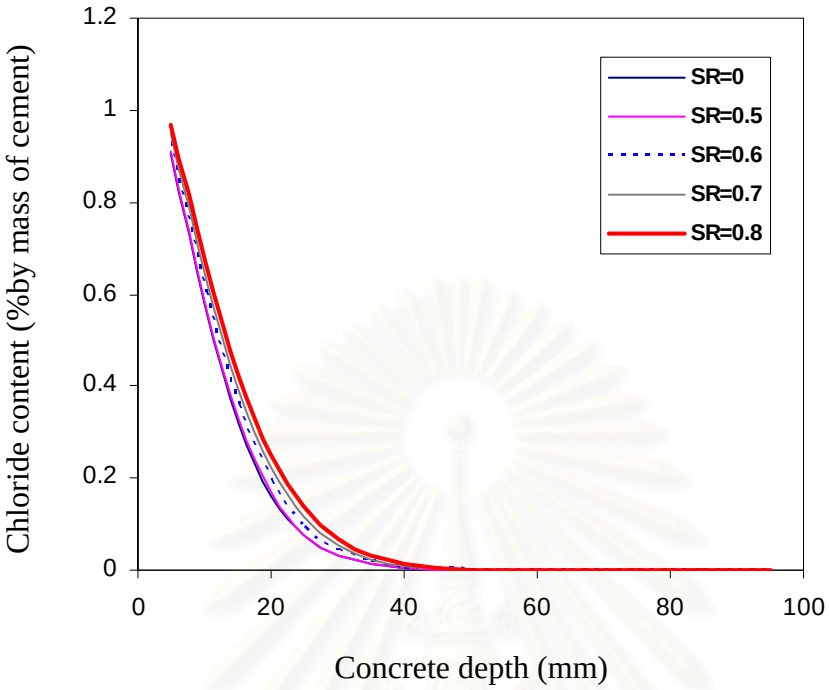

Figure 4.13 Prediction of chloride profiles of concretes subjected to cyclic loads and 5 year exposure to tidal environment, *w/c*=0.4

Model results indicated that the cyclic flexural load accelerated the chloride penetration into concrete. At higher cyclic flexural load levels, the chloride penetration was faster, and the acceleration rates of the chloride penetration into concretes became more distinct with cyclic flexural load levels, *SR*, of 0.6, 0.7, and, especially, 0.8, see Figure 4.13. This is consistent with the results of the experiments which described the effect of flexural cyclic loads on the chloride diffusion coefficient of plain concrete. Regarding the time till corrosion starts, considering a concrete mixture with *w/c*=0.4, it is assumed that the critical chloride content is 0.4% cement by weight to initiate corrosion, this critical chloride content is obtained at specific concrete depths of about 12mm, 15mm, and 16mm for *SR* 0, 0.7, and 0.8, respectively, see Figure 4.13. At a specific depth, applying flexural cyclic load with load level as 0.8 can make the chloride content increase 35% to 45% compared to the case without loading, see Figure 4.14.

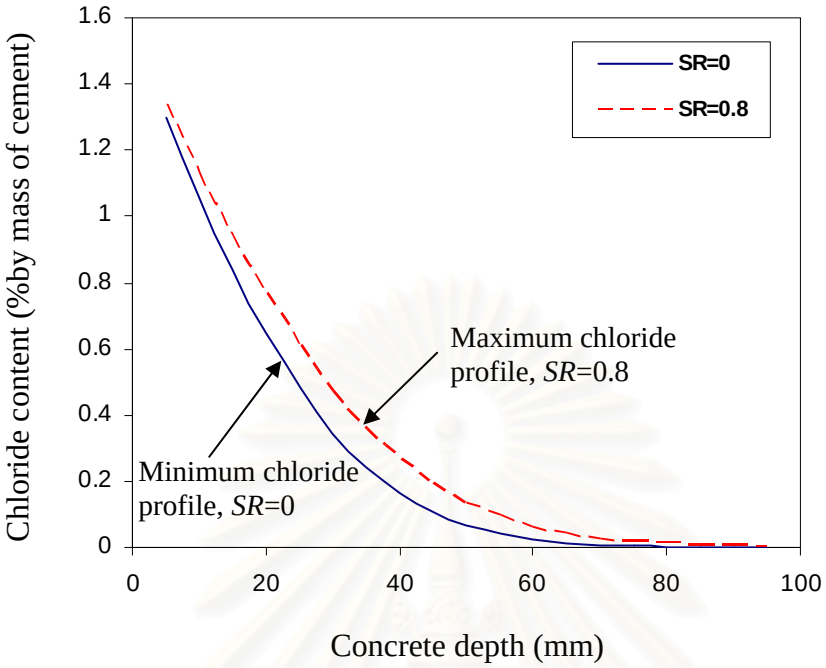

Figure 4.14 Prediction of chloride profiles of concretes subjected to cyclic loads and 5 year exposure to tidal environment, *w/c*=0.5

Concern with the initial time of corrosion, the chloride penetration into a concrete structure, which is exposed to tide and under flexural cyclic load having different load level, with different exposure time was simulated so that the initial corrosion was determined. BS8110 and RILEM codes imply that the critical chloride content at which the initial corrosion starts is 0.4% by weight of binder. The tidal exposed condition has the surface chloride content, C_s, of 13kg/m^3 or 3.1% by weight of cement. The concrete structure, according to ACI 201.2R-22, which is exposed to tidal environment, has a required depth of cover of 50mm, the chloride diffusion coefficient and the humidity diffusion coefficient are 13.58×10^{-12} and 5×10^{-12} m^2/s, respectively (Saetta, 1993). In the numerical prediction, the space step is 5mm, and the time step is 12 hours. All input data used to predict the chloride profiles of the concrete structure exposed to the tidal condition for different time is shown in Table 4.6.

The chloride profiles of the concrete, which is exposed to tide and under different load levels of flexural cyclic load, are shown in Figure 4.15. It can be clearly seen that at the requested cover depth of 50mm, no matter concrete beams subjected to flexural cyclic load or

not, the chloride content increases with increasing the exposed time, and this increase is nonlinear. At the first two years, the chloride content at 50mm required depth increases slowly. This slow increase of the chloride content may be adopted as the accumulative stage of chloride ions, then on the chloride content increases faster. Also, from Figure 4.15, with assumption that the critical chloride content is 0.4% by weight of cement, the higher load level is, the shorter the initial corrosion time is.

Table 4.6 Input parameters used to predict the initial corrosion time of the concrete exposed to tidal cycles and flexural cyclic load

Input parameters	Concrete mixture
	w/c=0.5
Cement type	Ordinary Portland cement
Exposed time, year	0, 1, 2, 3, 4, 5, 6, 7, 8, 9, 10, 11, 12, 13, 14, 15, 16, 17, 18, 19, 20, 21, 22, 23, 24, 25
	Humidity diffusion
*Liquid content, w_{sat} (%)	13
*Humidity diffusion coefficient, D_h (m^2/s)	5.0×10^{-12}
Initial humidity, h (%)	100
Boundary conditions of time step	h_{max}=100, h_{min}=0
	Time step, Δt=12 hr, space step, Δx=5mm
	Chloride diffusion
Binding capacity factor, ϕ	1.3218
Diffusion coefficient, $D_{i,ref}$ (m^2/s)	13.58×10^{-12}
Initial chloride content (wt % of cement)	$C_{i,0}$ = 0
Boundary conditions of time step	C_s^{max} = 3.1; C_s^{min} = 0
	Time step, Δt=12 hr
	Flexural cyclic load
Cyclic flexural loading level, SR	0; 0.5; 0.6; 0.7 and 0.8
Temperature, t (^{0}C)	25±2

* Data from Saetta et al, 1993

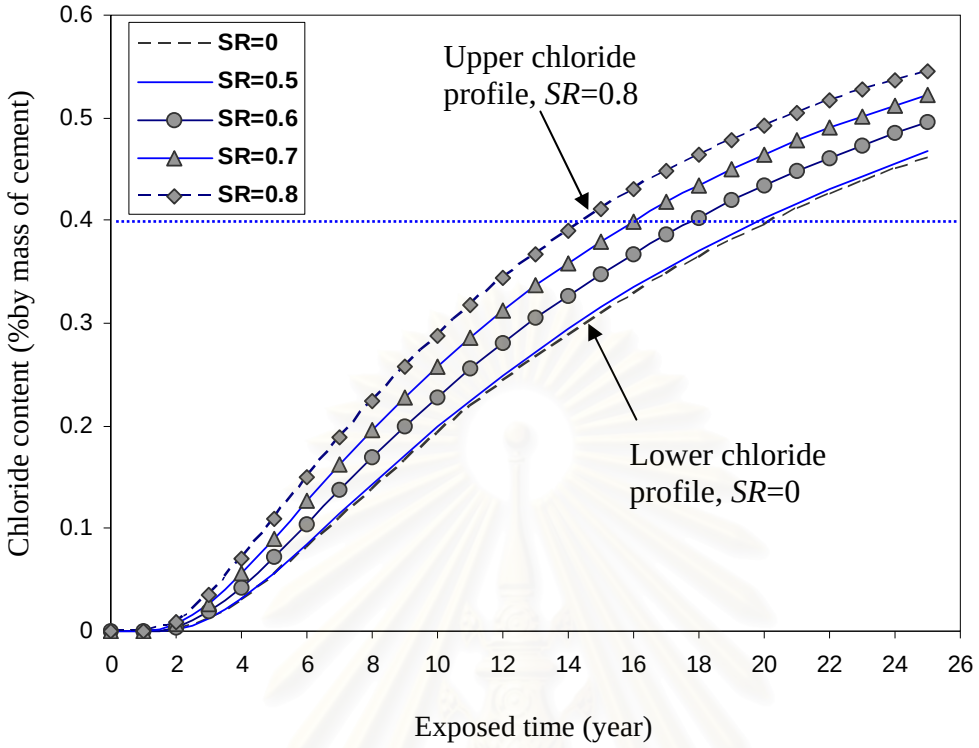

Figure 4.15 Chloride profiles of the concrete at 50mm required cover depth exposed to tide and different load levels of flexural cyclic load

Applying different load levels to concrete beams, the difference of the chloride profiles is insignificant as load level, *SR*, is 0 and 0.5, however, this difference becomes significant when the load level, *SR*, is over 0.5. At the required cover depth of 50mm, the initial corrosion time of concrete beams exposed to tide without cyclic load and with cyclic load having load level, *SR*=0.5, is almost the same and around 20 years, see Figure 4.16. However, this initial corrosion time is only 18 years when the load level, *SR*, increases to 0.6, see Figure 4.17. Likewise, the time at which corrosion starts is reduced to 16 and 14 years as applying flexural cyclic load to concrete beams with the load level, *SR*, of 0.7 and 0.8 respectively, see Figure 4.18 and 4.19. It can be concluded that applying flexural cyclic load to concrete beams with the load level of 0.5 may not reduce significantly durability of concretes, however, the durability of concretes are decreased significantly as the load levels, *SR*, are over 0.5. Overall, the simulation of chloride profiles of concrete exposed to different load levels and different periods makes clear that at a specific depth, cyclic loads make the time till corrosion is initiated becomes shorter; the durability of actual concrete structures subjected to service load, particularly cyclic flexural loads, is shorter than assumed in

conventional design standards where the effect of service loads on the chloride penetration is not considered.

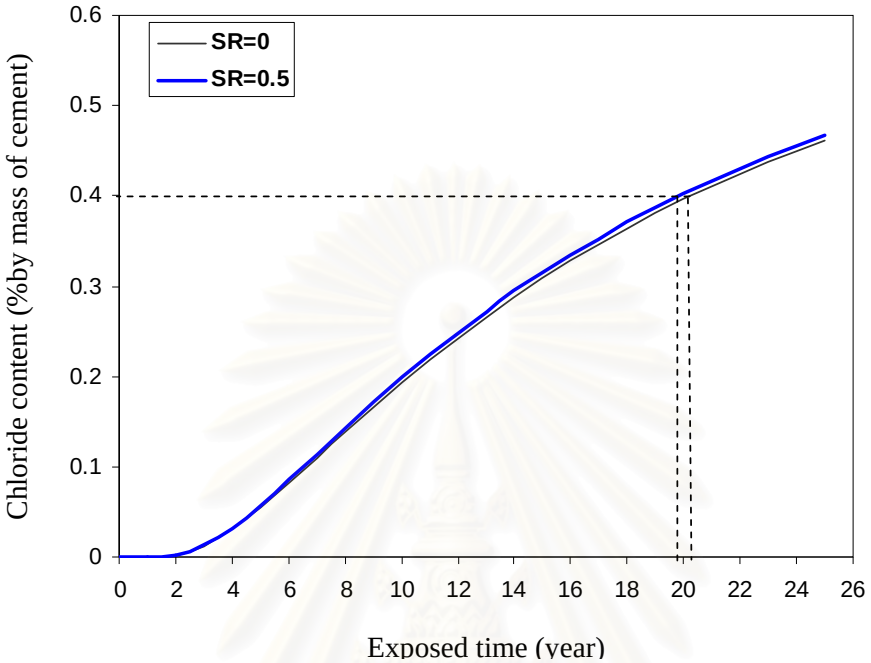

Figure 4.16 Chloride profiles of concrete at 50mm cover depth exposed to tide and *SR*=0, 0.5

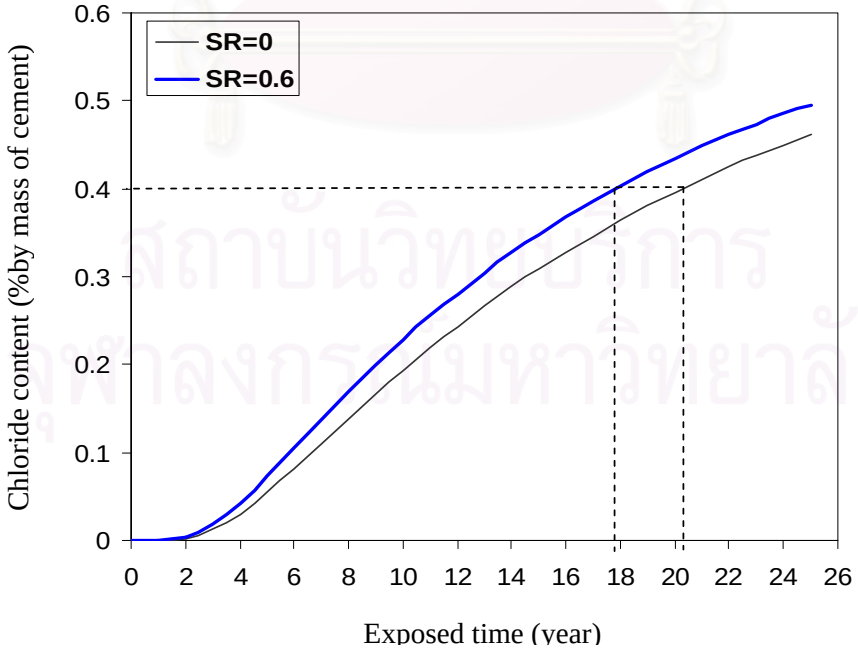

Figure 4.17 Chloride profiles of concrete at 50mm cover depth exposed to tide and *SR*=0, 0.6

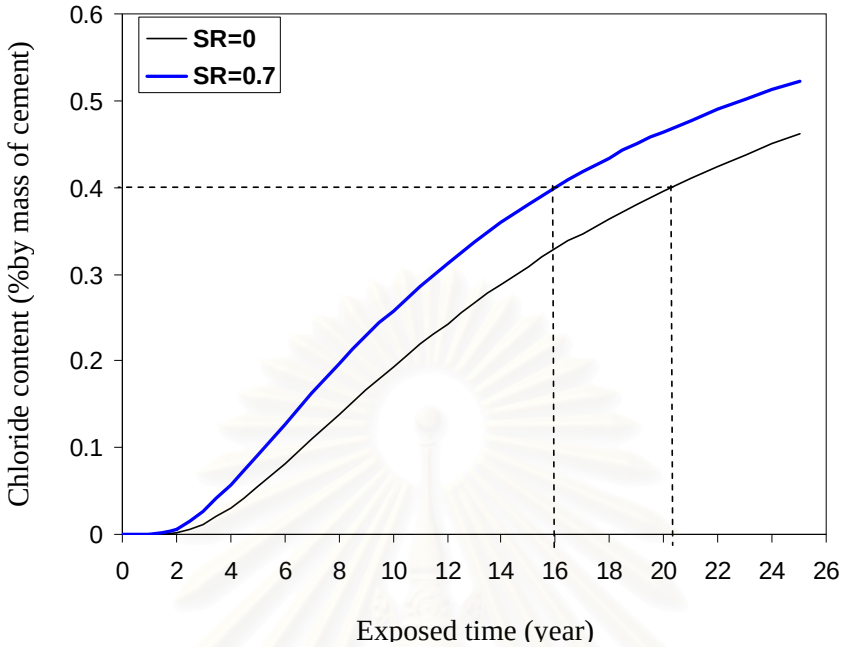

Figure 4.18 Chloride profiles of concrete at 50mm cover depth exposed to tide and *SR*=0, 0.7

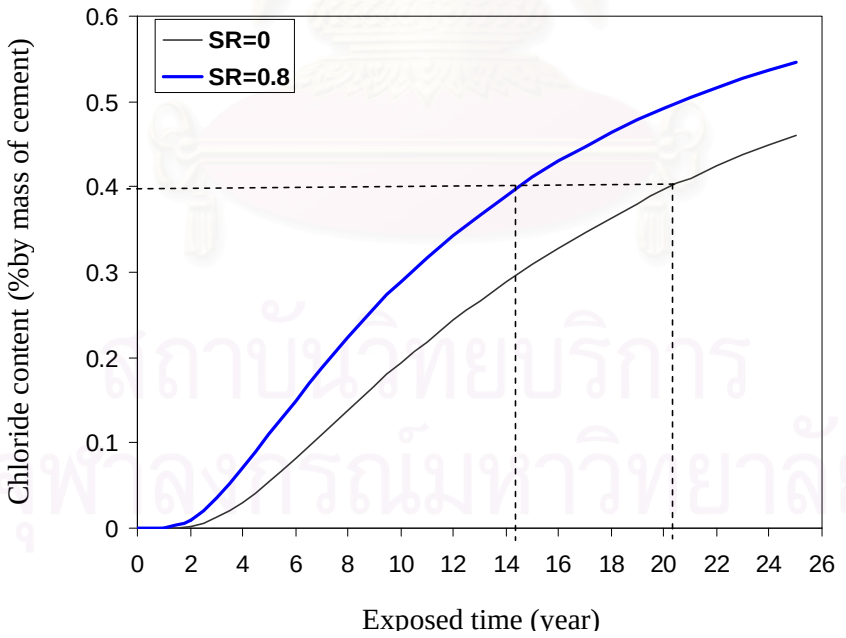

Figure 4.19 Chloride profiles of concrete at 50mm cover depth exposed to tide and *SR*=0, 0.8

4.5 Concluding remarks

This chapter describes simulation of chloride penetration into concretes using different cements under flexural cyclic load and tide. The simulation was proposed via prediction of fatigue crack growth of plain concrete beam and prediction of effects of flexural cyclic load on the chloride diffusion coefficient. Some concluding remarks issued from this chapter are as following:

1. The crack growth of plain concrete beam under flexural cyclic load can be divided into three stages as decelerated stage, steady state stage and accelerated stage. The fatigue crack growth, in terms of crack length and crack with increase with increasing either the number of cycles and the load level, especially with load levels, SR=0.7 and 0.8.
2. Under flexural cyclic load, the chloride diffusion coefficient in the tension zone increases with increasing the number of cycles and the load level, especially at the number of cycles where the crack width start accelerating and at the load levels of 0.7 and 0.8. The chloride diffusion coefficient predicted in the tension zone can be divided into two stages as monotonously increasing stage and accelerated stage.
3. At the same conditions of environment and materials used, the flexural cyclic load accelerates the chloride penetration into concretes. The higher the load level, especially with load levels, SR=0.7 and 0.8, the higher the chloride contents. At a given exposed condition and load imposing, the chloride profiles of concrete beams using different cements are different. At a give concrete depth, the concrete beam using OPC cement has the lowest chloride content, whereas it is found highest in case of using LHC. Therefore, of four common cement types, OPC is the best cement used to retard the chloride penetration into concrete structures exposed to marine environment.

CHAPTER V

EXPERIMENTAL VERIFICATION

Normally, the results predicted from the model are different from measured results. The magnitude of this difference depends on the complexity of input parameters. As a result, in modeling, in order to make the model reliable, the proposed model is always verified by comparison with experimental data. This chapter presents verification of model used for predictions as following:

1. Verification of designed mechanical and physical properties of concretes.
2. Verification of model for prediction of fatigue deformation of plain concrete beam.
3. Verification of model for prediction of the influence of flexural cyclic load on chloride diffusion coefficient of concrete in tension zone.
4. Verification of model of prediction of the chloride penetration into concretes under flexural cyclic load and tidal environment.

The global steps of verifications presented in this chapter are shown in Figure 5.1.

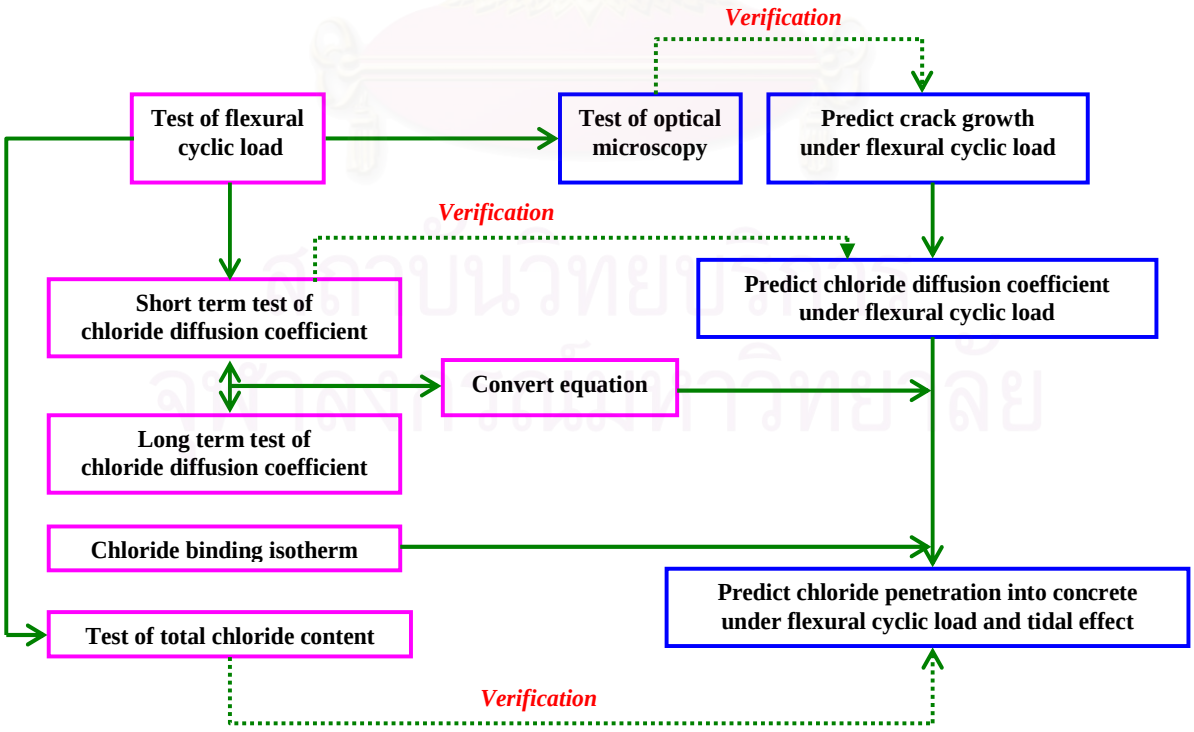

Figure 5.1 Global steps of verifications of model

5.1 Experimental program

In this study, materials used include cements, fine aggregate and coarse aggregate. Ordinary Portland cement (OPC) is used to cast concrete specimens for experiments of compression strength, flexural cyclic load, chloride diffusion coefficient and chloride content. Coarse aggregate, which satisfies ASTM C33-84, is crushed limestone aggregate with a maximum size of 20mm. Fine aggregate is river sand having fineness modulus of 2.8. Mixture concrete design follows ACI 211 (Standard practice for selecting proportions for normal concrete). Water-cement ratios, *w/c*, change as 0.40, 0.50 and 0.60. The mixture proportions are shown in Table 5.1.With each mixture, cylinder specimens, ϕ100 x 200mm, were prepared for the evaluation of the compression strength and the chloride diffusion coefficient. The concretes were cast in steel moulds and covered with plastic sheets after casting. The cylinder specimens were demoulded at one day of age and after that cured in lime saturated up to 28, 60 and 90 day age for determination of chloride diffusion coefficients at 28, 60 and 90 days, respectively. Concrete beams with dimensions of 400mm in length, 100mm in depth, and 100mm in width, which were used for flexural cyclic test, were cast in two layers in steel moulds, covered by plastic sheets and also demoulded at the age of one day. Then, the prisms were cured in lime saturated for other 60 days for tests of flexural strength and flexural cyclic load. Mixing and casting were performed in the control room with temperature of 22 ± 2^{0}C and relative humidity of 60±5%.

Table 5.1 Mixture proportions used in research

Series	*w/c*	OPC, kg	Mixing water, litre	Coarse aggregate, kg	Fine aggregate, kg
M.1	0.40	512	205	992	636
M.2	0.50	410	205	992	738
M.3	0.60	342	205	992	806

5.1.1 Testing procedures of chloride diffusion coefficient

About the apparent chloride diffusion coefficient following ASTM C1556, after 28, 60 and 90 days of water curing, cylindrical specimens are cut into slides with 100mm of diameter and 75mm of depth. All sides of the test specimen are sealed except the finished surface. Saturate the sealed specimen in a calcium hydroxide solution, rinse with tap water,

and then place in a sodium chloride solution of 10% concentration. After 35 days of exposure, the test specimen is removed from the sodium chloride solution and thin layers are ground off parallel to the exposed face of the specimen. The acid-soluble chloride content of each layer is determined. The apparent chloride diffusion coefficient and the projected surface chloride-ion concentration are then calculated using the initial chloride-ion content, and at least six related values for chloride-ion content and depth below the exposed surface.

Concern with accelerated test of chloride diffusion coefficient, also, after 28, 60 and 90 days of curing, cylindrical specimens with a diameter of 100 mm and a thickness of 50 mm are sliced from cast cylinders. Then, all sides of the test specimen are sealed with epoxy except two exposed surfaces. The sealed specimens are saturated in a calcium hydroxide solution and rinsed with tap water. After that specimens are placed between two chambers: a chamber with 3% sodium chloride and the other chamber with 0.3N sodium hydroxide, and an external electrical potential of 30V is applied axially across the specimen for 12 hours to force the chloride ions outside to migrate into the specimen, as mentioned in Chapter II. After 12 hours of test duration, the specimen is split axially and a silver nitrate solution sprayed onto one of the freshly split sections. The chloride penetration depth can then be measured from the visible white silver chloride precipitation, after which the chloride migration coefficient can be calculated from this penetration depth.

5.1.2 Testing procedures of chloride content

For the tests of total chloride content – ASTM C1152, 10g of powder sample passing a 850μm sieve is dispersed in a 250ml beaker with 75ml of deionized water, 25ml of dilute (1+1) nitric acid added slowly, then 3ml of hydrogen peroxide (30% solution), and 20 drops of acid nitric (1+1) added in excess, and heat the covered beaker rapidly to boiling. After removal of the beaker from the hot plate and filtering the solution, the chloride concentration in the filtrate will be analyzed by titration method or by ion chromatography.

Experimental procedures of tests of the free chloride content – ASTM C1218 are very similar to those of the total chloride content test. However, only 50ml of deionized water is used instead of 75ml, and boiling of the solution in the beaker is for 5 min. Then left to stand for 24 h for filtering by gravity or suction through a fine-texture. Adding 3 ml of (1:1) nitric acid and 3 ml of hydrogen peroxide (30% solution) to the filtrate, covering the beaker with a

watch glass and allow it to stand for 1 to 2 min. Then heating the covered beaker rapidly to boiling, and the chloride concentration in the filtrate will be also analyzed by titration or by ion chromatography.

5.1.3 Testing procedures of flexural strength and flexural cyclic load in tidal zone

After curing in lime saturated condition for 60 days, concrete beams, which are 400mm in length, 100mm in width and 100mm in depth, are dried in the atmosphere condition for further 2 days. Then, the flexural strength test of concrete followed ASTM C78 is conducted for determination of flexural ultimate load, P_{ult}, of concrete under four-point bending through Instron machine 1200kN. Then, the test of flexural cyclic load using Instron machine 1200kN conducts four-point bending cyclic loads to concrete beams over span of 300mm, see Figure 5.2. The flexural cyclic test is performed with different load levels, *SR*, which is ratio of maximum applied load, $P_{app,\ max}$, to ultimate load, P_{ult}. Bending load is ramped up to the desired $P_{app,\ max}$ over about 20 cycles, then one-stage constant applitude fatigue loading between $P_{app,\ max}$ and $P_{app,\ min}$, where $P_{app,\ min}$ equals to zero, is conducted. Deflection values of beams at middle bottom position are measured by LVDT. The load control test with low frequency of 0.01Hz and load levels, *SR*, of 0.5, 0.6, 0.7 and 0.8 is used in this research. With each mixture, *SR*=0.7 is adopted as standard *SR* to determine the number of cycle N_1 and N_2, at which irreversible crack and fracture occurs, respectively. Cubic specimens of 100mm are taken from the middle bottom position of beams by sawing, see Figure 5.3, to identify the effect of flexural cyclic load on diffusion characteristic of plain concrete in tension as well as in compression zone. Also, crack widths of plain concrete in tension zone are measured by optical microscopy. This test procedure applied to all concrete mixtures M1, M2 and M3.

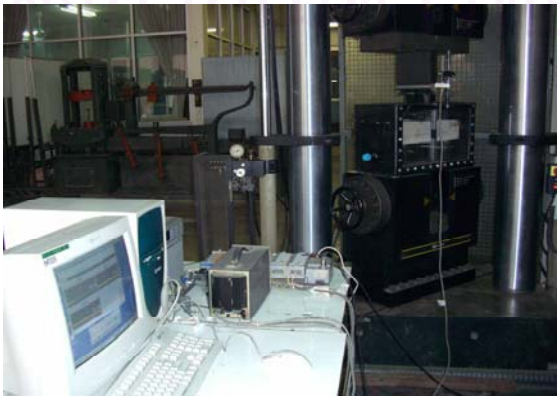

Figure 5.2 Experimental set up and equipments used for tests of flexural cyclic load

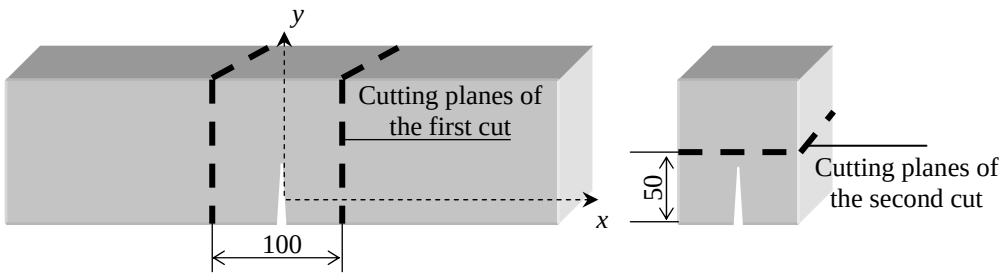

Figure 5.3 Schematic representation of cutting planes

Regarding to the test of flexural cyclic load in tidal zone, concrete beams are both subjected to flexural cyclic load and simulated tidal zone, which include 12 hour wetting in NaCl 10% solution and 12 hour drying in atmosphere, see Figure 5.4. This kind of testing is used to verify the proposed model of chloride penetration into concrete under cyclic load and tidal effect. In this test, 400mm long, 100mm thick, and 100mm wide beams are cast with OPC concrete, *w/c* = 0.5. After curing for 60 days in water, the beams where all surfaces, except the bottom face, are covered by epoxy subjected to flexural cyclic loads with low frequency, 0.01Hz, for *SR* values of 0.5; 0.6; 0.7; and 0.8 up to N_1 cycles. Simultaneously, the simulated tidal conditions are applied to concrete beams so that the concrete beams are subjected to condition resembling the couple of loading and a tidal environment. After finishing N_1 cycles of flexural cyclic load, cored concrete specimens at the middle bottom of beams are used to analyze total chloride contents at different depths.

a *b*

Figure 5.4 Flexural cyclic load in simulated tidal environment
(a) 12 hour wetting ; (b) 12 hour drying

5.2 Experimental results and verifications of model

5.2.1 Chloride diffusion coefficients of concretes in long term and short term tests

Chloride diffusion tests include both short-term and Long-term chloride diffusion. These tests are conducted following testing procedures mentioned in section 5.1. Results of the chloride diffusion coefficients are shown in Table 5.2, 5.3 and Figure 5.5. In Table 5.2 and 5.3, one can see that values of chloride diffusion coefficient as well as surface chloride content increase when *w/c* increases because more pores and diffusing paths may form as *w/c* increases. This trend is observed both in the short-term and long-term test.

Table 5.2 Diffusion coefficient values given by short-term test, concrete cured at 28 days

Series	Chloride diffusion coefficient value, $D\times10^{-12}$, m^2/s			Average value, $D\times10^{-12}$, m^2/s
	(1)	(2)	(3)	
M1	11.2	12.5	13.1	12.3
M2	21.3	23.2	20.6	21.7
M3	27.5	25.2	28.1	26.9

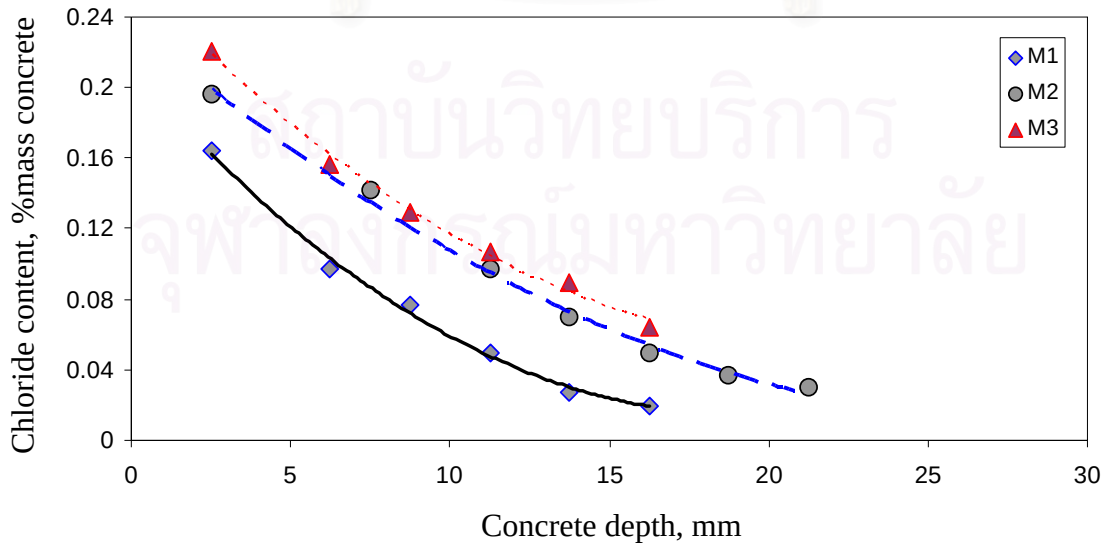

Figure 5.5 Chloride profiles of concretes in the long term diffusion coefficient tests

Table 5.3 Diffusion coefficient values given by long-term test, concrete cured at 28 days

Series	Concrete depth, mm	Chloride content, %mass concrete	Surface chloride content, %mass concrete	Apparent chloride diffusion coefficient, $D_a \times 10^{-12}$, m^2/s	Average value, $D_a \times 10^{-12}$, m^2/s
M1	2.50	0.1638	0.21	8.4	8.9
	6.25	0.0968		7.5	
	8.75	0.0769		9.8	
	11.25	0.0496		9.4	
	13.75	0.0273		8.5	
	16.25	0.0199		9.9	
M2	2.50	0.1960	0.24	14.8	17.4
	7.50	0.1414		12.8	
	11.25	0.0968		17.4	
	13.75	0.0694		17.5	
	16.25	0.0496		18.0	
	18.75	0.0372		19.4	
	21.25	0.0298		21.6	
M3	2.50	0.2209	0.26	22.2	23.1
	6.25	0.1563		18.3	
	8.75	0.1290		21.2	
	11.25	0.1067		23.9	
	13.75	0.0893		26.9	
	16.25	0.0645		25.3	

With the same mixture, the chloride diffusion coefficient got from the long-term test, D_a, is always lower than that given by the short-term test, D. There is a relationship between short-term test and long-term test, and that this relationship is linear, see Figure 5.6. By linear regression, the empirical relationship between D and D_a was derived as:

$$D_a = 0.9061D - 2\times10^{-12} \quad (5.1)$$

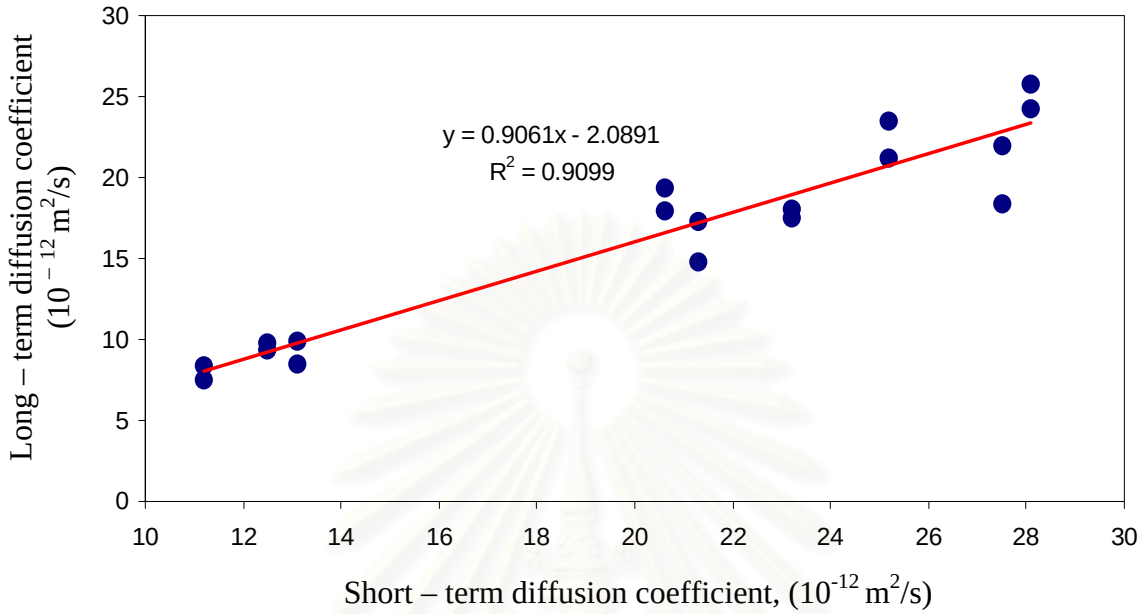

Figure 5.6 Relationship between long-term and short-term test of chloride diffusion coefficient

5.2.2 Time dependent chloride diffusion coefficients

By the time, as concrete matures, the mass transfer of concrete will decrease since the capillary pore system becomes denser as hydration products continue to form. This reduces the diffusion paths for the penetration of ions, including chloride ions, through concrete cover. As a result, chloride diffusion coefficient of concrete is time dependent, it is decreased by time. Time dependent diffusion of concrete is modeled as:

$$D(t) = D_{28}\left(\frac{28}{t}\right)^m \quad (5.2)$$

where $D(t)$ is diffusion coefficient at time t; D_{28} is diffusion coefficient at 28 days; m is constant which depends on mixture proportions.

Best fitting values of chloride diffusion coefficients measured at 28 days with ones measured at 60 and 90 days results in a power relationship, whose power variables, m, depend on the mixture proportion, the power variables, m, are shown in Table 5.4 and Figure

5.7. The table and figure clearly propose that the chloride diffusion coefficients, which are determined by both short term and long term tests, decrease with increasing curing time.

Table 5.4 Best fitted values of D_{28} and *m* for concrete mixtures

Series	$D_{28}\times10^{-12}$, m^2/sec	*m*
M1	12.4	0.45
M2	21.9	0.35
M3	27.1	0.36

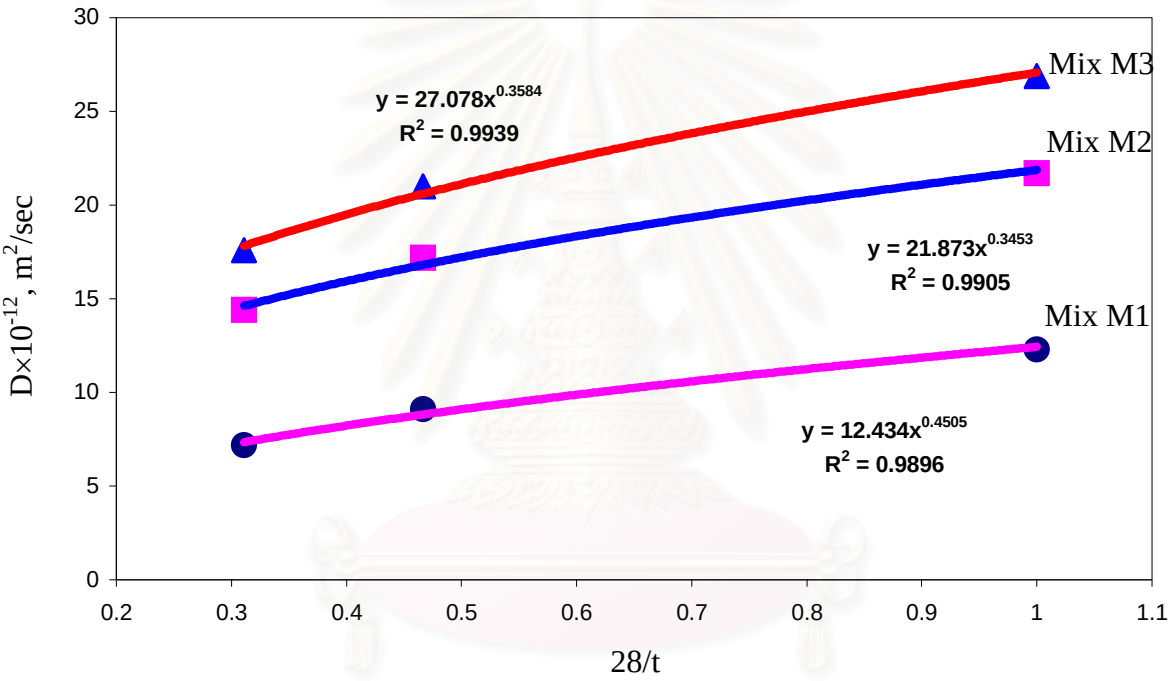

Figure 5.7 Time dependent of chloride diffusion coefficients

5.2.3 Mechanical and physical properties of concrete

Mechanical and physical properties of concrete include compression strength, σ_c, tension strength, σ_t, flexural strength, P_{ult}, Young's modulus, E, deflection of beam, δ_c, and chloride diffusion coefficient at 28 days, D_{28}. The compression strength and flexural strength are conducted for 60 day aged concrete following ASTM C39 and C78, respectively. The tension strength and Young's modulus are determined indirectly via the compression strength by recommendations of ACI.

Comparisons between results of mechanical and physical properties of concretes predicted basing on *w/c* and experimental results are shown in Table 5.5. The performance of concrete beams under four point bending is shown in Figure 5.8.

Table 5.5 Mechanical and physical properties of concrete

Series	*w/c*	P_{ult}, kN	σ_c, MPa	σ_t, MPa	E, GPa	δ_c, mm	$D_{28}\times10^{-12}$, m^2/s
M1	0.40	16 (15.7)	48 (47)	3.9 (3.9)	32.5 (32.2)	1.13 (1.34)	8.9 (7.8)
M2	0.50	15 (14.6)	40 (38)	3.5 (3.4)	29.8 (29.3)	1.28 (1.42)	17.4 (15.2)
M3	0.60	13 (13.2)	27 (28)	2.7 (2.8)	24.5 (25.0)	1.61 (1.78)	23.1 (19.7)

( ) Predicted results

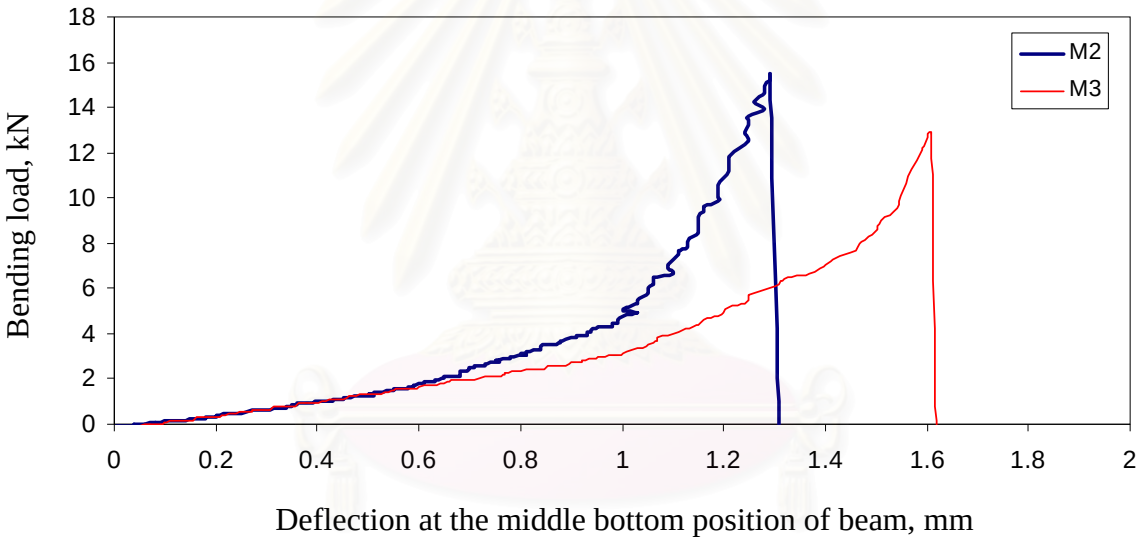

Figure 5.8 Flexural behavior of concrete beams under four point bending

Table 5.5 clearly shows that mechanical properties of concrete mainly depend on *w/c*. Strengths of concrete increase with decreasing *w/c*. This is due to the denser microstructure of concrete as *w/c* reduces. However, the physical properties of concretes, in terms of the deflection of beam and the chloride diffusion coefficient, increase with increasing *w*/c ratio. Figure 5.8 also confirms the trend that the flexural strength of concrete beam increases as *w/c* decreases. Moreover, based on flexural performance, decreasing *w/c* makes concrete more brittle and concrete beams fracture at a lower deflection.

Predicted results and experimental results of mechanical and physical properties of concretes fit well with each other. Therefore, the designed mechanical and physical properties of concretes predicted basing on *w/c* ratio are reliable for using as input parameters in modelling chloride penetration into concretes under flexural cyclic load and tidal environment.

5.2.4 Verification of model of fatigue deformation of concrete beam under flexural cyclic load

The verification is performed by comparison results between experiments and predictions. In the flexural cyclic testing, firstly, the test of the flexural strength of concrete beam was conducted by ASTM C78 for determination of flexural ultimate load, P_{ult}. Then, the flexural cyclic test was performed with different load levels, *SR*, which is ratio of maximum applied load, $P_{app,\ max}$, to ultimate load, P_{ult}. Load levels, *SR*, of 0.5, 0.6, 0.7 and 0.8 are used in this research. The load levels, *SR*, flexural ultimate load, P_{ult}, and maximum applied load, $P_{app,\ max}$, of different mixture series are shown in Table 5.6. The load level, *SR*=0.7, is adopted as standard load level. The flexural cyclic testing will be performed with standard load level till concrete beams fracture. Results of this test are curves of relationship of load and deflection (herein after it is referred as to L-D curve). Based on L-D curves, the specific number of cycles where the L-D curve changes or not is determined. The number of cycles, at which L-D curve changes and concrete beam is broken, are shown in Table 5.7.

Table 5.6 Flexural cyclic loads applied to concrete beams with different load levels

Series	P_{ult}, kN	*SR*			
		0.5	0.6	0.7	0.8
		$P_{app,\ max}$, kN			
M1	16	8.0	9.6	11.2	12.8
M2	15	7.5	9.0	10.5	12.0
M3	13	6.5	7.8	9.1	10.4

Table 5.7 Cyclic flexural behaviour of plain concrete beams of different mixture proportions

Series	*w/c*	*SR*	P_{ult}, (kN)	$P_{app,\,max}$, (kN)	Number of cycle, N_1	Number of cycle, N_2
M1	0.4	0.7	16	11.2	3500	4800
M2	0.5	0.7	15	10.5	3200	4300
M3	0.6	0.7	13	9.1	3000	4000

N_1 is the number cycle at which the L-D curve changes.

N_2 is the number cycle at which concrete beam fractures.

The typical L-D curve, where concrete beams of series are under flexural cyclic load with standard load level, is shown in Figure 5.9.

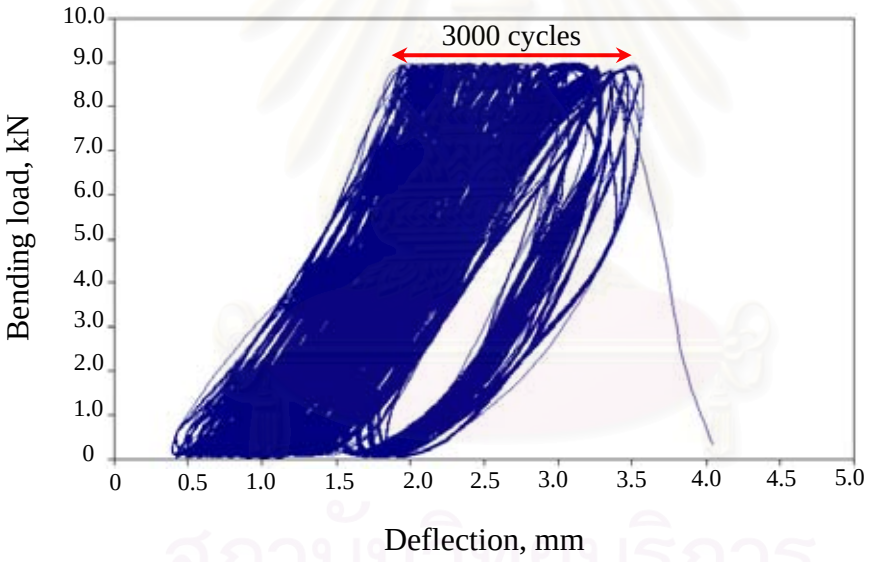

Figure 5.9 Typical destructive flexural fatigue results for a load control test, M3, *SR* 0.7

Loading in flexure gives a localized tensile stress field and produces wide, localized cracks that may not heal upon over elastic stage. When deformation due to cyclic flexure is in elastic stage, microcrack is able to heal. By increasing the numbers of cycle, however, microcrack becomes so-called irreversible crack that can not heal, it is continuously widen still failure of concrete beam. Irreversible crack can be indicated by measurement of plastic distortion in the member shape or indirect measurement of decreasing flexural stiffness (flatten of load-deflection or load-displacement curve changes, see Figure 5.9).

Cyclic flexural behaviour of concrete beam depends on compression strength, which has close relation with mixture proportion, especially with *w/c*. One can see that at the same loading level, fracture load increases with decreasing *w/c*. Also, the number of cycles, N_1 and N_2, at which L-D curve changes and concrete beam is fractured, respectively, increase as *w/c* reduces, see Table 5.7.

In order to investigate influences of the load level on the fatigue crack width, with each mixture series, the flexural cyclic load, whose load level includes 0.5; 0.6; 0.7 and 0.8, is applied to concrete beams up to 3500; 3200 and 3000 cycles corresponding to mixture series M1, M2 and M3, respectively. The influence of number of cycles on crack width of beams is also investigated, where crack widths are measured at cycles which are smaller than N_2. Effects of load level and number of cycles on the crack width of the concrete beam are shown in Figure 5.10 and 5.11, respectively.

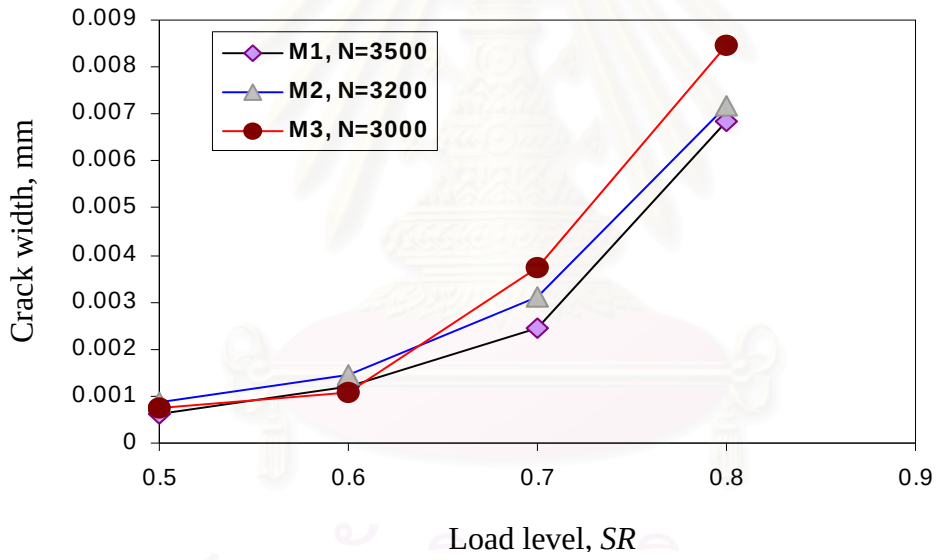

Figure 5.10 Relationships of crack width and load level

Regarding to load level, *SR*, crack width increases significantly as *SR* increases from 0.6 to 0.8, especially at 0.7 and 0.8. At the same load level, crack width of concrete beam made with lower *w/c* is lower than that of concrete beam made with higher *w/c*. This phenomena is clearer as we apply flexural cyclic load with *SR*=0.7 and 0.8. One reason for this is that concrete beam made with lower *w/c* has higher compression strength, higher flexural strength and higher Young's modulus, as a result, with the same stress level in the tension zone, concrete beam made with lower *w/c* has lower deformation compared to that of concrete beam with higher *w/c*. Figure 5.11 shows that the fictitious crack width increases

with increasing the number of cycles. The experimental results clearly showed that fictitious crack growth, in terms of crack width, can be divided into two stages; a steady stage; an accelerated stage towards fracture. Crack width develops gradually up to N_1 cycles, where microcracks are supposed not to heal, and then it develops fast from N_1 cycles up to fracture of concrete beam.

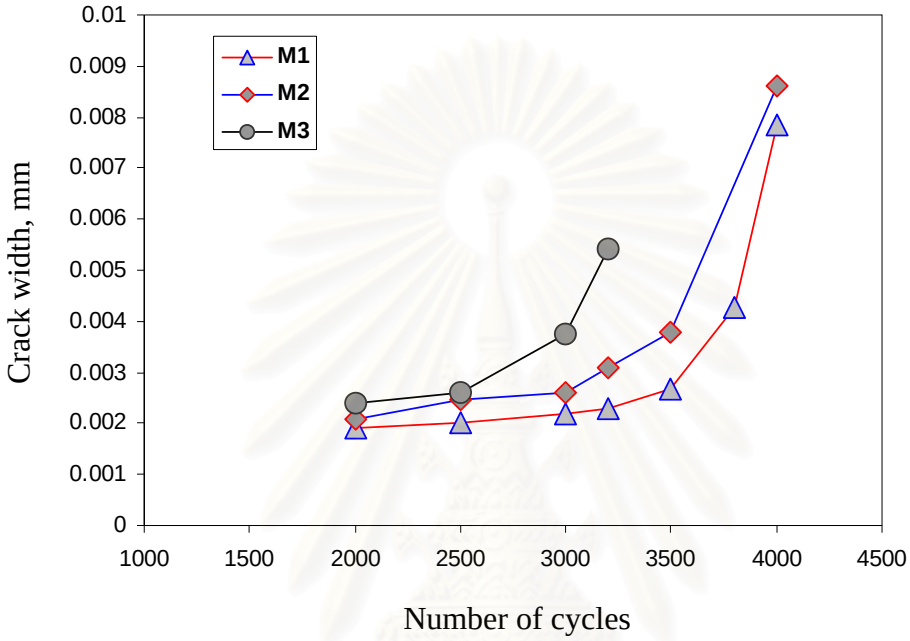

Figure 5.11 Relationships of crack width and number of cycles, experimental results, *SR*=0.7

Table 5.8 Predictions of crack widths and experimental crack widths

Series	*SR*	Cycle	Crack width-Model, mm	Crack width-Measured, mm
M1	0.5	3500	0.0110	0.00064
	0.6	3500	0.0141	0.00120
	0.7	3500	0.0258	0.00246
	0.8	3500	0.0544	0.00684
M2	0.5	3200	0.0107	0.00087
	0.6	3200	0.0136	0.00146
	0.7	3200	0.0263	0.00310
	0.8	3200	0.1058	0.00718
M3	0.5	3000	0.0106	0.00075
	0.6	3000	0.0135	0.00107
	0.7	3000	0.0247	0.00375
	0.8	3000	0.0599	0.00846

In numerical prediction, the fictitious crack width and crack length also increased with increasing either the number of cycles, *N*, or the load level, *SR*. The numerical simulation clearly showed that fictitious crack growth, in terms of crack width and crack length, can be divided into three stages; a decelerated stage; a steady stage; an accelerated stage towards fracture. However, as shown in Figure 5.12 and Table 5.8, the numerical results of crack widths do not fit well with experimental data obtained by optical microscopy. One reason for this is that the fatigue load may cause multiple microcracks in concrete than results of the numerical prediction with a single crack, see Figure 5.13. Indeed, the numerical predicted crack width is larger than the measured crack width. As shown in Figure 5.12 and 5.14, good fitting between the model estimation and experimental data is found when the authors introduce a so-called crack density parameter, μ, which takes into account microcracks beside the main crack. μ is a function of the number of cycles, *N*, and load level, *SR*, as below:

$$\mu = \left(\frac{1}{SR}\right)^2 \log(N) + 2.2 \qquad (5.3)$$

with, $0.5 \le SR \le 0.8$

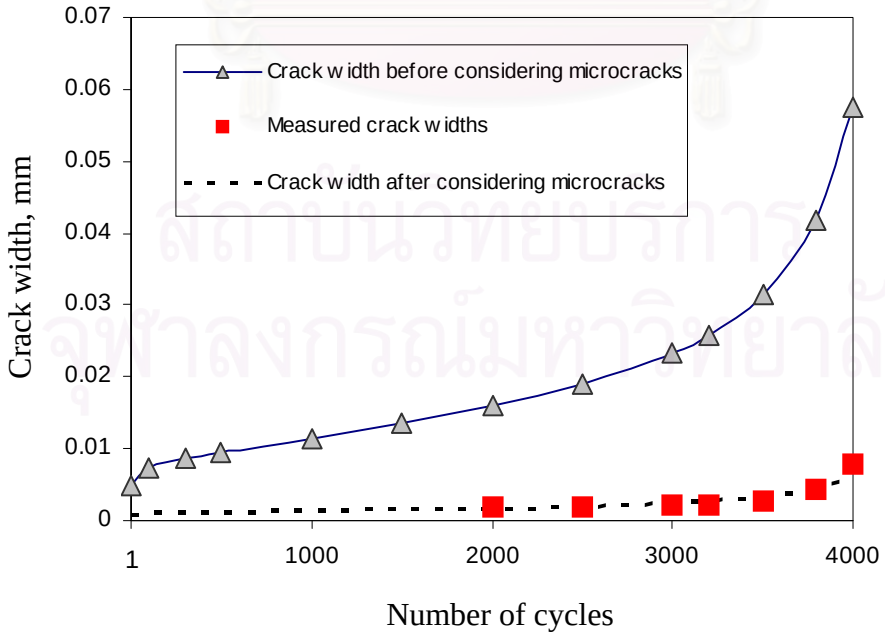

Figure 5.12 Relationships of crack width and number of cycles, model prediction and experimental results, M1, *SR*=0.7

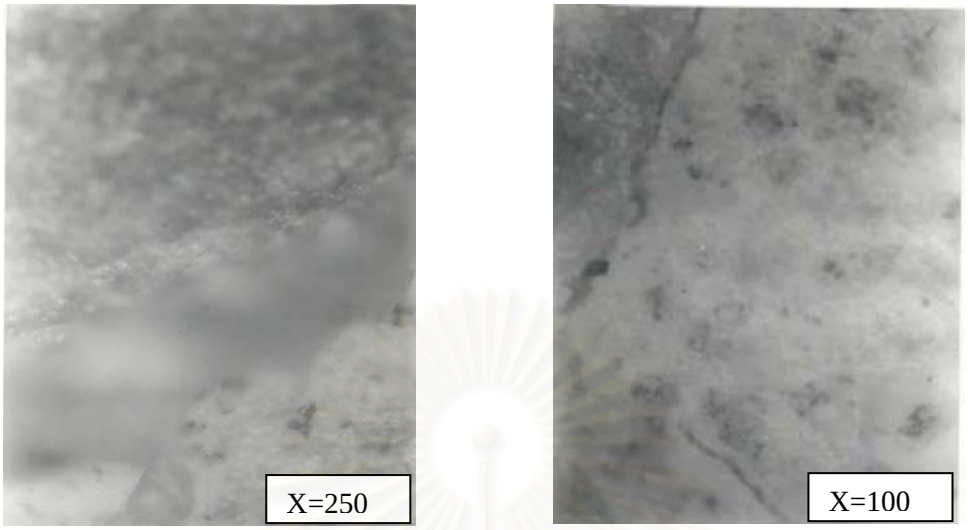

Figure 5.13 Microcrack of concrete from optical microscopy,

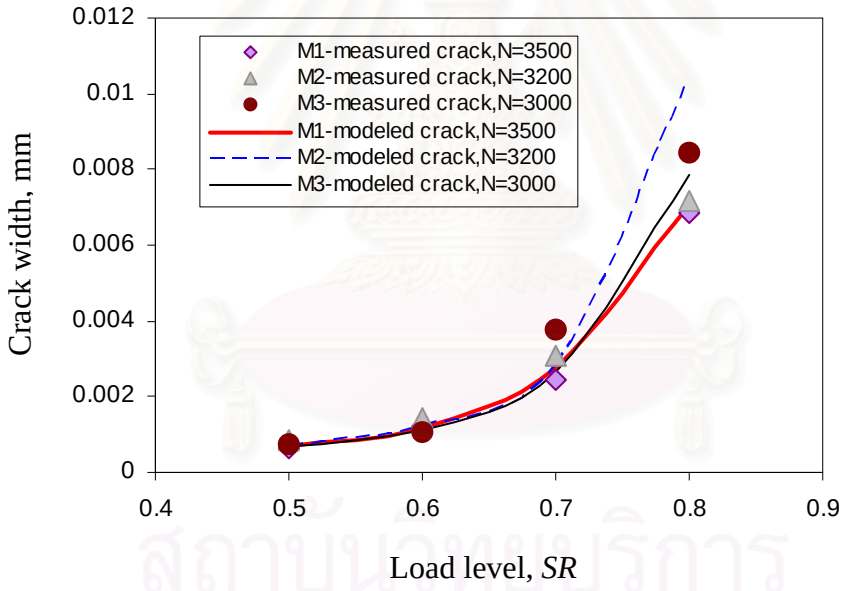

Figure 5.14 Relationship of crack width and load level, experimental results and model predictions after considering microcracks

5.2.5 Verification of model of effect of flexural cyclic load on chloride diffusion coefficient

Load level, *SR*=0.7, is adopted as standard *SR* to determine the number of cycle N_1 and N_2, at which irreversible crack and fracture occur, respectively. After that all beams are subjected to the flexural cyclic load using the number of cycle, N_1, with *SR* changing as 0.5, 0.6, 0.7 and 0.8, then specimens, which are sawn both at the middle bottom and middle top

positions of beams, are used to identify the effect of flexural cyclic load on diffusion characteristic of plain concrete in tension as well as in compression zone by the short term chloride diffusion test. This test procedure applied to all concrete mixtures M1, M2 and M3. Undergoing flexural cyclic load, stress of beam is divided to tension zone and compression zone with a specific applied load, the effects of flexural cyclic load level on diffusion coefficients of plain concrete in the tension and the compression zone were shown in Table 5.9 and Figure 5.15.

Table 5.9 The effects of flexural cyclic load on the chloride diffusion coefficients

Series	SR	$D\times10^{-12}$, m^2/s (Tension zone)	$D\times10^{-12}$, m^2/s (Compression zone)	Normalized D (Tension zone)	Normalized D (Compression zone)
M1	0	9.10	9.10	1.000	1.000
	0.5	9.41	9.19	1.034	0.979
	0.6	9.20	9.19	1.118	0.958
	0.7	9.21	9.18	1.208	0.898
	0.8	9.22	9.17	1.321	0.816
M2	0	17.20	13.58	1.000	1.000
	0.5	18.21	13.71	1.052	0.97
	0.6	18.21	13.71	1.128	0.939
	0.7	18.21	13.70	1.242	0.857
	0.8	18.21	13.69	1.458	0.804
M3	0	21.00	17.03	1.000	1.000
	0.5	21.22	17.19	1.041	0.955
	0.6	21.23	17.19	1.094	0.942
	0.7	21.27	17.17	1.298	0.851
	0.8	21.32	17.16	1.504	0.773

From Figure 5.15, it is seen that as the load level, *SR*, increases, the chloride diffusion coefficients in tension zone increase, whereas, it is a decreased trend in compression zone. Generally, the effect of flexural cyclic load on the chloride diffusion coefficient can be expressed as an exponential function in the tension zone and a polynomial function compatible to the compression zone. This may be supposed that compression stress, one is generated in compression face of concrete beam undergoing flexural cyclic load, makes

concrete microstructure become denser, and accordingly reduce porous connectivity, providing low diffusion of chloride. On the contrary, when microcracks are widen even to become irreversible microcracks at high flexural cyclic load levels that generate tensile stresses beyond elastic stress of concrete, porous volume as well as connectivity of concrete increases so that chloride diffusion coefficient increases. The exponential function is composed of three distinctive portions. The first portion, which includes the lowest slope, at *SR* from 0.5 to 0.6, the second one starts from *SR* of 0.6 to 0.7 to generate the higher slope compared to the first one, and the last portion has the highest slope at *SR* from 0.7 to 0.8. On the other hand, flexural cyclic load has much effect on the chloride diffusion coefficient of plain concrete at *SR* from 0.7 to 0.8.

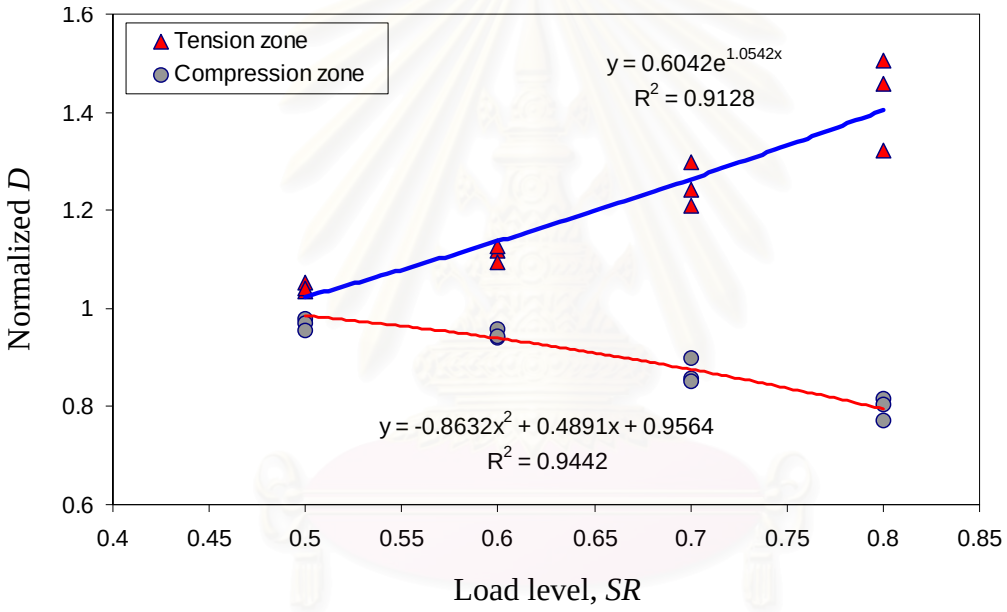

Figure 5.15 Relationship between the chloride diffusion coefficient and load level in flexural cyclic load

Obviously, under flexural cyclic load, the compression zone of the concrete beam is in safety stage because the chloride diffusion coefficient in this zone is decreased with increasing either the load level or the number of cycles. Whereas, the tensile zone of the concrete beam becomes dangerous due to increasing the chloride diffusion coefficient with increasing the load level or the number of cycle. On the other hands, the tension zone is severed to the chloride induced corrosion. Therefore, the verification presented in this section will concentrate only on the tension zone where the predicted influence of the flexural cyclic load on the chloride diffusion coefficient, *D*, was predicted in chapter IV.

The verification is performed by comparing the predicted results with experimental results of the influence of the flexural cyclic, in terms of the load level and the number of cycle, on the chloride diffusion coefficient, *D*, in the tension zone. The verification is shown in Figure 5.16 and 5.17. As can be seen in Figure 5.16, with the same mixture series and the same number of cycle, the experiments show an increasing tendency of the chloride diffusion with increasing the load level. The chloride diffusion increases significantly when we apply fatigue test with load level *SR* at 0.6, 0.7 and 0.8, especially at 0.7 and 0.8. The model prediction shows the same tendency of the chloride diffusion with measurements. However, at any the load level of fatigue test, the normalized D_{tot} (against the control without fatigue test, *SR*=0) predicted by the model is always higher than that measured by the experiment. A main reason is that the author use the assumption of the singly straight crack developed with the number of cycles. Practically, with the number of cycles, the crack is tortuous and the width of the crack along the path varies significantly. When tortuosity parameter, τ, with τ=1.65, is introduced to account for the intrinsic tortuosity of the crack, good agreement between model predictions and measured results, simulated crack width after considering the crack density divided by τ, can be found, see Figure 5.16 and 5.17.

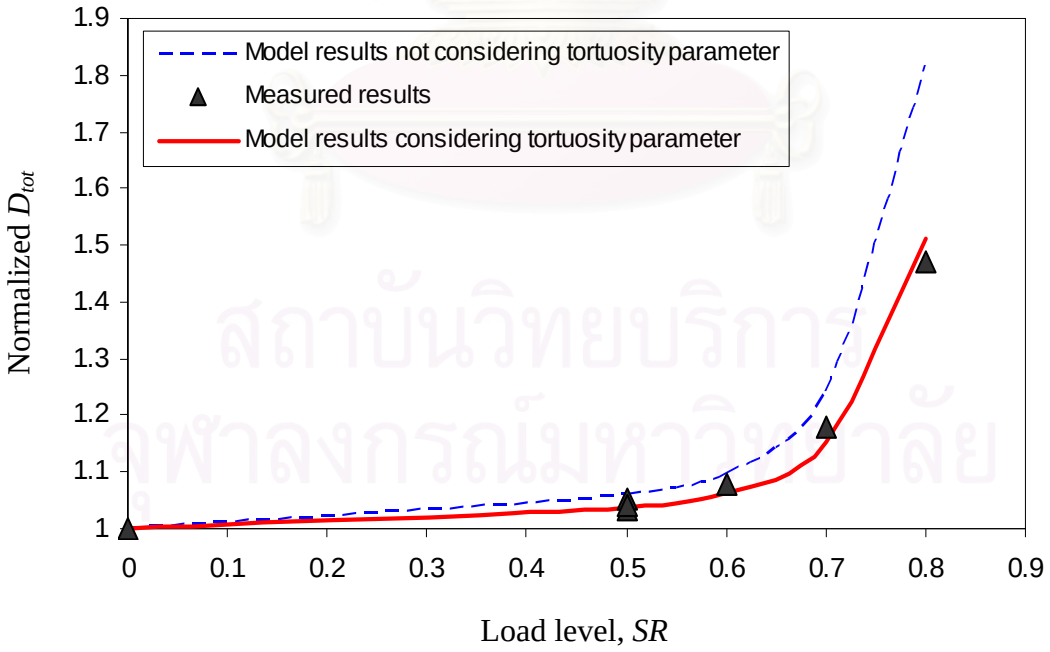

Figure 5.16 Relationships of load level and normalized D_{tot}, model prediction and experimental results, M1, *N*=3500

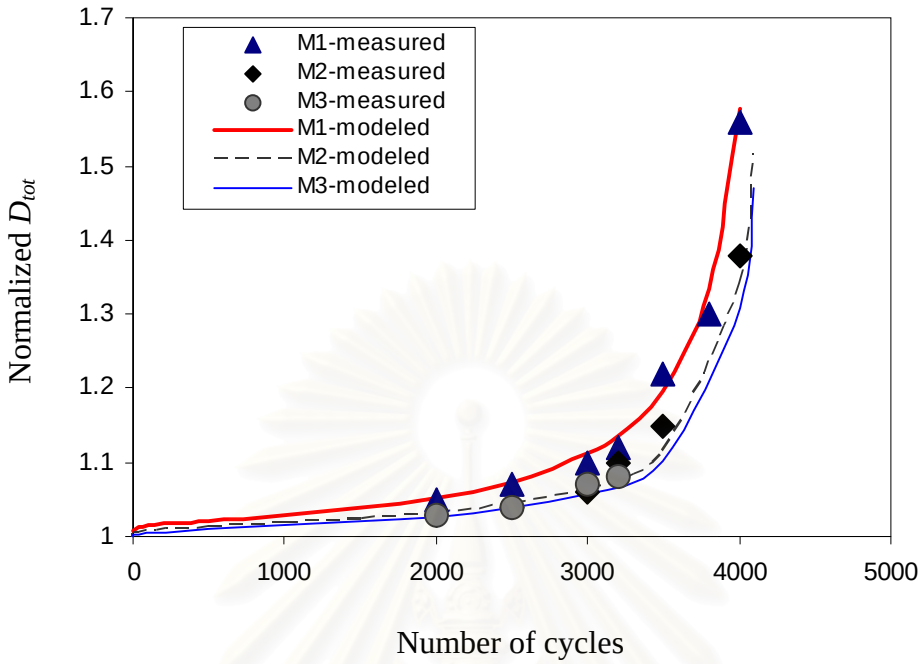

Figure 5.17 Relationships of number of cycles and normalized D_{tot}, model prediction and experimental results, SR=0.7

5.2.6 Verification of model of chloride penetration into concretes under flexural cyclic load and tidal environment

The reliability of the numerical analysis of prediction chloride penetration into concretes under flexural cyclic load and tidal environment is verified by the results of the experiments and measured results of other researchers. Firstly, the numerical analysis is verified by measured results of Uji et al 1990 to confirm that the numerical analysis, which uses finite difference method (FDM), of chloride penetration without loading is reliable or not. The final verification consists of comparisons between numerical results accounting for flexural cyclic loads and experimental results. The first verification is shown in Figure 5.18, in which a concrete specimen has D_a=1.89×10^{-12} m^2/s, D_h=1.0×10^{-12} m^2/s and is exposed to tidal environment in 7.6 years. Figure 5.18 shows that results of the numerical analysis fit quite well with those measured by Uji et al 1990, in which concretes were exposed to tidal environment and without loading. The numerical analysis mentioned above, thus, is reliable and capable of applying to predict chloride penetration into plain concrete subjected to both

flexural cyclic loads and tidal environments. Also, from Figure 5.18, once can see that accounting for flexural cyclic load with load level, *SR*=0.8, make the chloride penetration into concretes accelerated significantly compared to the chloride profile measured by Uji with condition of unloading, *SR*=0.

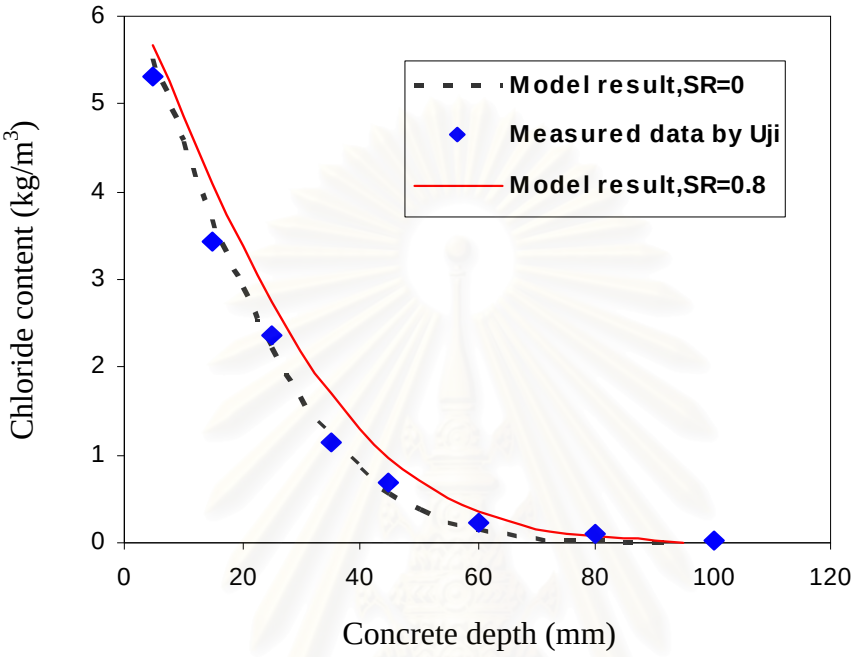

Figure 5.18 Comparison between results of numerical solution and measured results of concrete exposed to tidal environment for 7.6 years

In experiments of the second verification, 400mm long, 100mm thick, and 100mm wide beams are cast with OPC concrete, *w/c*=0.4. After curing for 60 days in water, the beams where all surfaces, except the bottom face, are covered by epoxy subjected to flexural cyclic loads with low frequency, 0.01Hz, for *SR* values of 0.5; 0.6; 0.7; and 0.8 up to 3500 cycles. Simultaneously, the simulated tidal conditions, which include 12 hour wetting in NaCl 10% solution and 12 hour drying in atmosphere, are applied to concrete beams so that the concrete beams are subjected to condition resembling the couple of loading and a tidal environment. After finishing 3500 cycles of flexural cyclic load, equivalent to 10 days of cyclic flexural load, sliced concrete specimens at the middle bottom of beams were used to analyze total chloride contents at different depths. In the second verification, an experimental equation (Uji, 1990) is used to determine the surface chloride content, C_s = 5.1% weight of cement. 60 day aged concrete beams have D_a=6.25×10^{-12} m^2/s, D_h=1.0×10^{-12} m^2/s used as input parameters in the numerical analysis accounting for flexural cyclic loads.

The chloride ion profiles of concretes with the couple of different cyclic flexural load levels and simulated tidal environments working for 10 days are shown in Figure 5.19. It could be concluded that the experimental results and those of the proposed model fitted well in all cases when applying the cyclic flexural load levels at *SR* 0.5; 0.6; 0.7 and 0.8. The effect of flexural cyclic loads on the chloride penetration is clear in both the measured and the numerical results. At a given depth, the higher *SR* value, the higher chloride content is due to widening crack width and appearance of irreversible crack. These results suggest that the proposed numerical simulation possibly evaluates the chloride penetration into concrete structures subjected to both tidal environment and flexural cyclic load, when the flexural cyclic load levels, *SR*, changed from 0.5 to 0.8, and the numerical analysis used is FDM combining with Crank-Nicholson algorithm.

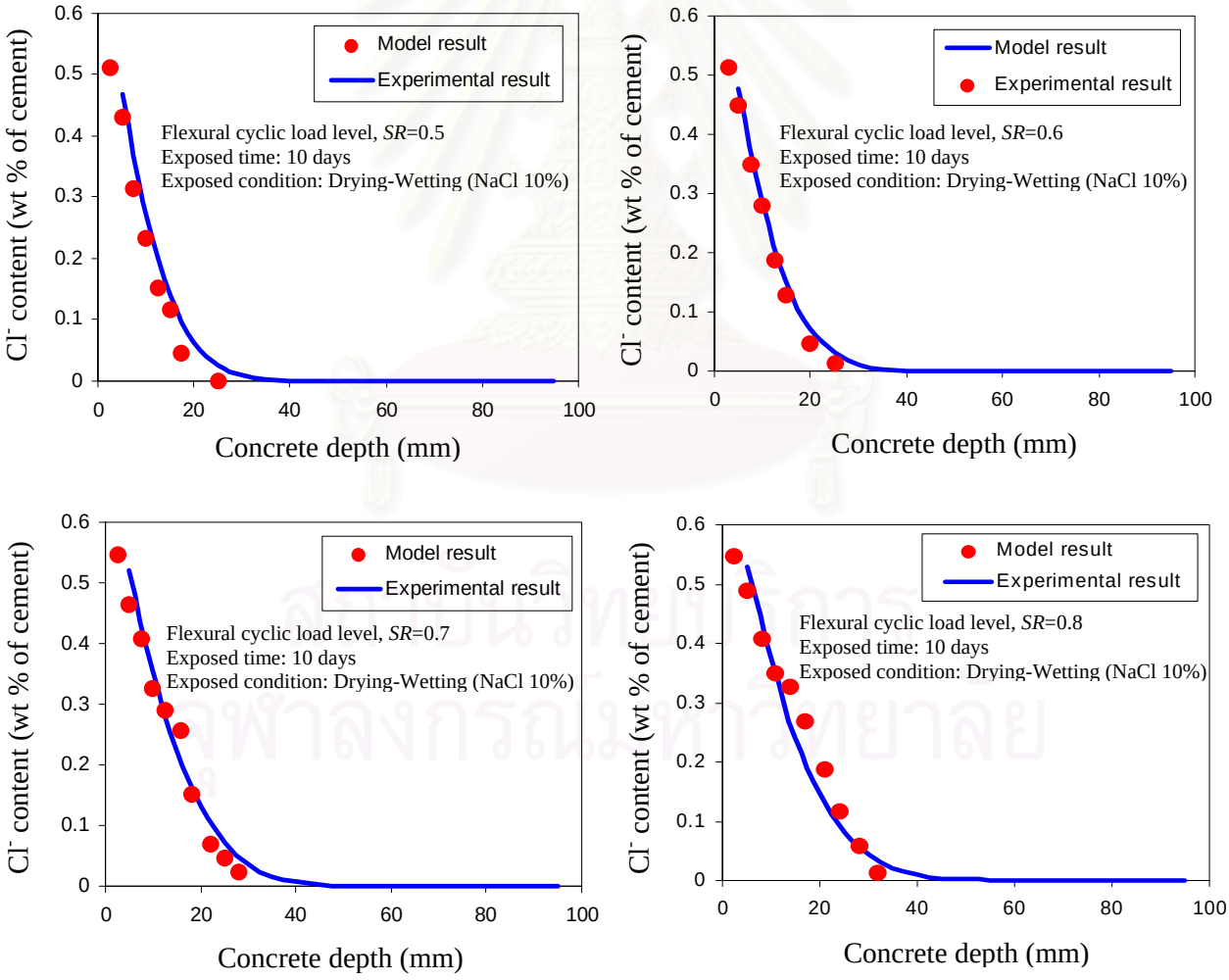

Figure 5.19 Verification of chloride penetration into concrete subjected to both cyclic load and tidal environment

5.3 Concluding remarks

This chapter presents verifications of predictions of designed mechanical and physical properties of concretes, crack growth under flexural cyclic load, the chloride diffusion coefficient under fatigue and the chloride penetration into concretes under flexural cyclic load and tide. The chapter has concluding remarks as following:

1. The predictions, basing on *w/c* ratio, of physical and mechanical properties of concretes fitted well with experimental results. Therefore, these data can be used as initial data or input parameters for the prediction of the durability of concrete exposed to aggressive media.
2. The prediction of crack growth of plain concrete beam, in terms of crack width and crack length, fitted well with measurements as the crack density parameter, μ, which is a function of the number of cycles and the load level, was introduced.
3. The prediction of effects of flexural cyclic load on the chloride diffusion coefficient of plain concrete beam showed that the flexural cyclic load, in terms of the number of cycles and the load level, accelerated the chloride diffusion coefficient in the tension zone. The model of effect of flexural cyclic load on the chloride diffusion coefficient of plain concrete beam fitted well with experimental results when the tortousity parameter, τ=1.65, was introduced to account for the tortuous characteristic of the crack surface.
4. The simulation of chloride penetration into concretes under flexural cyclic load and tidal effect, using finite different method (FDM) fitted well with measured data of other researcher (Uji, 1990) and with experimental data of this investigation.

CHAPTER VI

CONCLUSIONS

6.1 Conclusions

This research models the chloride penetration into concrete under flexural cyclic load and tidal environment. In addition, chloride binding isotherms of various cement types were determined. Also, the effect of flexural cyclic load on the chloride diffusion coefficient of plain concrete was investigated. The results suggest the following conclusions:

1. An analytical approach for modeling the influence of flexural cyclic load on the chloride diffusion coefficient in the tension zone of plain concrete that depends on the stress degradation law and the steady-stead transport of chloride ions as the fundamental assumptions was presented. When we introduced the crack density parameter, μ, and the tortuosity parameter, τ, the model predictions fit well with experimental results.
2. Under flexural cyclic load, the non-linear relationship between load level, *SR*, and the chloride diffusion coefficient in the tension zone of plain concrete is found both in model predictions and experiments. Model predictions show an increasing tendency of the chloride diffusion coefficient, in the tension zone, with increasing the number of cycles and load level, *SR*, especially at *SR*=0.7 and 0.8. Flexural cyclic load applied with load levels, *SR*, from 0.5 to 0.8 makes the chloride diffusion coefficient of plain concrete increase in the tension zone, however, it makes the diffusion coefficient decrease in the compression zone.
3. Values of the chloride diffusion coefficients got from short-term test (D) are always higher those got from long-term test (D_a). There is the linear relation between results of short-term and long-term test. One can apply this linear equation to determine more precisely the chloride diffusion coefficient of concrete as converting values of short term test to those of long term test.
4. Of the four cement types, OPC has the highest capacity to bind chloride ions, whereas LHC has the lowest chloride ion binding capacity. The chloride binding capacities of MC and RHC are very similar. The chloride binding isotherms of the four cement

types can be fitted to Freundlich isotherms. The amount of bound chloride increases with increases in the free chloride concentration.

5. The AFm is responsible for binding chemically bound chloride by the formation of Friedel's salt, the isotherm of chloride bound by AFm can be fitted to the Freundlich isotherm. The C-S-H binds the physically bound chloride, the isotherm of chloride bound by C-S-H can be fitted to a Langmuir isotherm. At a given bound chloride content, the amount of physically bound chloride is always much higher than that of the chemically bound chloride.
6. A model of the chloride penetration into plain concretes coupling cyclic flexural load and tidal environments is proposed. A new experiment was conducted to describe the simultaneous effect of both cyclic flexural loads and tidal environments. Results from this experiment were used to verify the model. Using a numerical analysis with the finite difference method, results obtained with this model fit well with the experimental data.
7. The proposed model showed that the flexural cyclic load accelerated chloride penetration into concrete. The higher the flexural cyclic load level or the number of cycles, the faster chloride penetration occurred, especially with *SR* of 0.6, 0.7, and 0.8. This means a reduction in the durability of concrete structures subjected to coupling service loads, particularly cyclic flexural loads, and aggressive environments. As a result, it will be necessary to modify conventional design procedures of concrete structures in marine environments. And that, it is essential to account for coupling service loads and aggressive environments in modelling to predict the service life of such concrete structures more accurately.

6.2 Applications of results

The results archived in this research propose the applications as following:

1. Proposed chloride binding isotherms of cements help engineers choose the best cement type used for constructions in marine environment.
2. In research or inspection, in order to accelerate the testing tine, the chloride diffusion coefficient of concrete can be measured by the modified short-term test. Then, the real results of the chloride diffusion coefficient measured by the long term test can be predicted by using the converted equation proposed from this research.

3. In this research, the proposed model for prediction of fatigue deformations of plain concrete beams under flexural cyclic load can refer to the initial step for other researches to develop models of fatigue deformations of reinforced concretes under fatigue.
4. The proposed model for prediction of the chloride penetration into concrete using FDM can apply to predict the service life of concrete structures, in term of the chloride profile, under mechanical load and tide, tidal effect only, or in the submerged zone by changing the boundary conditions in the algorithm of numerical analysis.
5. With the present reinforced concrete structures, we can measure easily the number of cracks, crack widths and crack lengths of these structures. Then, these data of crack properties are used as input parameters in the proposed model of this research to predict the chloride profiles of RC structures. By this way, investors of concrete structures can know how long the service life of RC structures is left, or propose suitable methods to protect or maintain RC structures.

6.3 Limitations

The current study is conducted with the time restraint. Therefore, it has some limitations as proposed expressions and application of investigation in the field.

This investigation was performed in the conditions of laboratory which is quite different from the real conditions at field, where temperature and humidity change by time. Moreover, the specimens used in this research are concrete beams 100mm in width, 100mm in depth and 400mm in length, which are not full scale concrete structures. Also, these concrete beams are only subjected to flexural cyclic load, however, at field, the loading history applied to concrete is more complex, at which there are more than one kind of load as bending, compression or torsion loaded on concretes at the same time.

About chemical point of view, this study considered the chloride penetration only. However, in the marine environment, there are some other phenomena besides the chloride penetration such as sulphate attack and carbonation. Generally, these phenomena occur at time, and they have influence and reaction to each other. Obviously, the degradation of concrete structures are accelerated as we consider phenomena at the same time in stead of the considering the chloride penetration alone.

6.4 Recommendations

Based on the results of the investigation of chloride penetration into concrete under flexural cyclic load and tidal environment, some recommendations can be drawn out as following

1. We should use OPC and the kinds of cement which have high content of C_3A compound to increase the chloride binding capacity, or use other mineral additive materials such as silica fume and fly ash to reduce the chloride diffusion coefficient, so that the chloride penetration into concrete is prolonged, as a result, the service life or the durability of concrete structure is better.
2. With the proposed convert equation, the accelerated testing of chloride diffusion coefficient can be used to determine the diffusion coefficient of concrete.
3. The model will be reliable and precise if we can integrate many phenomena, such as chloride penetration, sulphate attack and carbonation at the same time.
4. The chloride penetration into concrete structures is accelerated as we integrate mechanical load and climatic load. Therefore, in modelling to predict the durability of concrete structures used in a certain environment, we should consider both mechanical load and climatic load.
5. Basing on or developing from this investigation, future studies can concentrate on prediction of chloride ingress into reinforced concretes under loading and marine environment, in which the environment may be the atmosphere zone, tidal zone or submerged zone, and loading condition can be cyclic compression, flexural cyclic load or combination of loading conditions.

REFERENCES

American Society for Testing and Materials Standards. **ASTM Standard test Methods for chemical analysis of hydraulic cement: ASTM C114.** Philadelphia: ASTM Committee on Standards, 1997.

American Society for Testing and Materials Standards. **ASTM Standard test Methods for Acid-Soluble chloride in mortar and concrete: ASTM C1152.** Philadelphia: ASTM Committee on Standards, 1997.

American Society for Testing and Materials Standards. **ASTM Standard test Methods for Electrical indication of Concrete's ability to resist chloride ion penetration: ASTM C1202.** Philadelphia: ASTM Committee on Standards, 1997.

American Society for Testing and Materials Standards. **ASTM Standard test Methods for determining the apparent chloride diffusion coefficient of cementitious mixtures by bulk diffusion: ASTM C1556.** Philadelphia: ASTM Committee on Standards, 1997.

American Society for Testing and Materials Standards. **ASTM Standard test Methods for Flexural strength of concrete (Using simple beam with third-point loading): ASTM C78.** Philadelphia: ASTM Committee on Standards, 1997.

Boulfiza, M., Sakai, K., Banthia, N., and Yoshida, H. Prediction of Chloride ions ingress in Uncracked and Cracked Concrete. **ACI Materials Journal.** 100, 1 (2003): 38-48.

Byung Hwan Oh and Seung Jup Yang. Effects of material and environmental parameters on chloride penetration profiles in concrete structures. **Cement Concrete Research.** 37, 1 (2007): 47 – 53.

Byung, B., Oh, H. Fatigue analysis of plain concrete in flexure. **Journal of Structural Engineering.** 112, 2 (1986): 273 – 288.

C. C. Yang and L. C. Wang. The diffusion characteristic of concrete with mineral admixtures between salt ponding test and accelerated chloride migration test. **Materials chemistry and physics.** 85, (2004): 266 - 272.

Chun Qing Li. Initiation of chloride-induced reinforcement corrosion in concrete structural members-experimentations. **ACI Structural Journal.** 98, 4 (2001): 502-510.

Crank J. **The Mathematics of Diffusion.** Oxford Press, London, 1975.

Delagrave, A., Marchand, J., Ollivier, J.P., Julien, S., and Hazrati, K. Chloride binding capacity of various hydrated cement paste systems. **Cement Concrete Composites.** 6, (1997): 28 – 35.

Gérard, B., Marchand, J. Influence of cracking on the diffusion properties of cement-based materials, Part I: Influence of continuous cracks on the steady-state regime. **Cement and Concrete Research.** 30, 1 (2000): 37 – 43.

Glass, G.K., and Buenfeld. The influence of chloride binding on the chloride induced corrosion risk in reinforced concrete. **Corrosion Science.** 42, (2000): 329 – 344.

Glass, G.K., Stevenson, G.M., and Buenfeld, N.R. Chloride-binding isotherms from the diffusion cell test. **Cement and Concrete Research.** 28, 7 (1998): 939 – 945.

Gontar, W.A., Martin, J.P. and Popovics, J.S. Effects of cyclic loading on chloride permeability of plain concrete. **Proceeding of ASCE International Conference of Condition monitoring of Materials and Structures**, 95 – 107. Austin-Texas: ASCE Press, 2000.

Gowripalan, N., Sirivivatnanon, V., Lim, C.C. Chloride diffusivity of concrete cracked in flexure. **Cement and Concrete Research.** 30, 5 (2000): 725-730.

Hirao, H., Yamada, K., Takahashi, H. and Zibara, H. Chloride binding of cement estimated by binding isotherms of hydrates. **Journal of Advanced Concrete Technology.** 3, 1 (2005): 77-84.

Japan Concrete Institute. **Proceedings of JCI Symposium on Chemical Reaction and Process Analysis of Cement Concrete**, JCI-C39, 1996.

Johannesson, B., Yamada, K. and Nilsson, L-O. Multi-species ionic diffusion in concrete with account to interaction between ions in the pore solution and the cement hydrates. **Materials and Structures.** 40, (2007): 651-665.

Jun Zhang, Henrick Stang and Victor, C.L. Fatigue life prediction of fiber reinforced concrete under flexural load. **International Journal of Fatigue.** 21, 10 (1999): 1033–1049.

Kato, E., Kato, Y., Uomoto, T. Development of simulation model of chloride ion transportation in cracked concrete. **Journal of Advanced Concrete Technology.** 3, 1 (2005): 85 – 94.

Kyle Stanish and Michael Thomas. The use of bulk diffusion tests to establish time-dependent concrete chloride diffusion coefficients. **Cement and Concrete Research .** 33, (2003): 55-62.

Luca Bertolini, Bernhard Elsenser, Pietro Pedeferri and Rob Polder. **Corrosion of steel in concrete: prevention, diagnosis and repair.** Wiley-VCH, 2003.

Mehta, P. Kumar. **Concrete Structure, Properties and Materials.** Prentice Hall Inc, Englewood Cliffs, N. J. 07632, 1993.

Michelle Nokken, Andrea Boddy, Hooton, R.D. and Thomas, M.D.A. Time dependent diffusion in concrete – three laboratory stuies. **Cement and Concrete Research .** 36, (2006): 200-2007.

Mohamed, T.U. and Hamada, H. Relationship between free chloride and total chloride contents in concrete. **Cement and Concrete Research.** 33, 9 (2003): 1487 – 1490.

Nakhi, A., Xie, Z., Asiz, A., Ababneh, A., and Xi, Y. Chloride penetration under coupled hygromechanical loadings. **Proceeding of International Conference of Condition monitoring of Materials and Structures**, 84-94. Austin-Texas: ASCE Press, 2000.

Nielsen, E.P., Herfort, D., and Geiker, M.R. Binding of chloride and alkalis in Portland cement systems. **Cement and Concrete Research.** 35, (2005): 117 – 123.

Nordtest method NT Build 492. **Concrete, mortar and cement-based repair materials: Chloride migration coefficient from non-steady-state migration experiments**. Approved 1999-11.

Reinhardt, H.W., Cornelissen, H.A.W. Post-peak cyclic behavior of concrete in uniaxial tensile and alternating tensile and compressive loading. **Cement Concrete Research**. 14, (1984): 263-272.

Rui Luo, Yuebo Cai, Changyi Wang, and Xiaoming Huang. Study of chloride binding and diffusion in GGBS concrete. **Cement and Concrete Research.** 33, (2003): 1 – 7.

Saetta, A.V., Scotta, R.V., and Vitaliani, R.V. Analysis of chloride diffusion into partially saturated concrete. **ACI Materials Journal.** 90, 5 (1993): 441-451.

Sang-Hun Han. Influence of diffusion coefficient on chloride ion penetration of concrete structure. **Construction and Building Materials.** 21, 2 (2007): 370 – 378.

Scheidegger, A.E. **The physics of flow through porous media**. University of Toronto Press, Toronto, 1974.

Suryavanshi, AK., Scantlebury, J.D., and Lyon, S.B. Mechanism of Friedel's salt formation in cements rich in Tri-Calcium Aluminate. **Cement and Concrete Research.** 26, 5 (1996): 717 – 727.

Tang, L., and Nilsson, L.O. Chloride binding capacity and binding isotherms of OPC pastes and mortars. **Cement and Concrete Research.** 23, (1993): 247 – 253.

Taylor, H.F.W. **Cement Chemistry**. Academic Press, London, 1990.

Tralla, J.P., and Silfwerbrand, J. Estimation of chloride ingress in uncracked and cracked concrete using measured surface concentrations. **ACI Materials Journal.** 99, 1 (2002): 27-36.

Tran, M.V., Stitmannaithum, B. and NAWA, T. Effect of flexural cyclic load on chloride diffusion coefficient of plain concrete**. Cement and Concrete Composites**, Submitted for publication, (2007).

Tran, M.V., Stitmannaithum, B., and NAWA, T. Numerical solution to predict the chloride penetration into concrete structures in tidal environment. **Proceedings of the Nineteenth KKCNN Symposium on Civil Engineering**, 417 – 420. Kyoto, December, 2006.

Uji, K., Tsutsumi, T. and Maruya, T. Formulation of an equation for surface chloride content of concrete due to permeation of chloride. **Proceedings of the third International Symposium on Corrosion of Reinforcement in Concrete Construction**, Warwickshire, UK, 1990.

Ulfkjær, J.P., Krenk, S., Brincker, R. Analytical model for fictitious crack propagation in concrete beams. **Journal of Engineering Mechanics.** 121, 1 (1995): 7 – 14.

Wittmann, F.H., Roelfstra, P.E, Mihashi, H., Huang, Y.Y., Zhang, X.H. and Nomura, N. Influence of age of loading, water-cement ratio and rate of loading on fracture energy of concrete. **Materials and Structures**. 20, 116 (1987): 103-115.

Xing Feng, Leng Fa-guang, and Nai-qian Feng. Chloride Diffusivity of Plain Concrete Subjected to Sustained Flexural Loading. **Proceeding of International Workshop on Durability of reinforced concrete under combined Mechanical and Climatic Loads**, 133 – 139. Quingdao: Aedificatio Press, 2005.

APPENDIX

APPENDIX A: Concrete beam under flexural cyclic load

Figure A1. Equipments used to collect bending load and deflection of concrete beam under flexural cyclic load

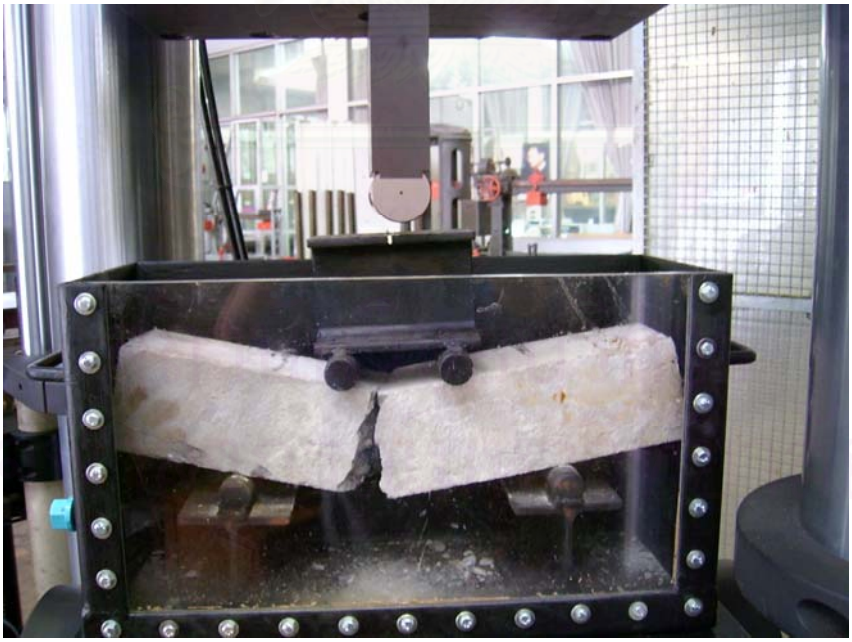

Figure A2. Fracture of concrete beam under bending load

Figure A3. Power supply and chamber used in the accelerated test of chloride diffusion coefficient

Figure A4. Chloride penetration depth of specimen M2 subjected to the accelerated test of chloride diffusion coefficient

Figure A5. Optical microscopy

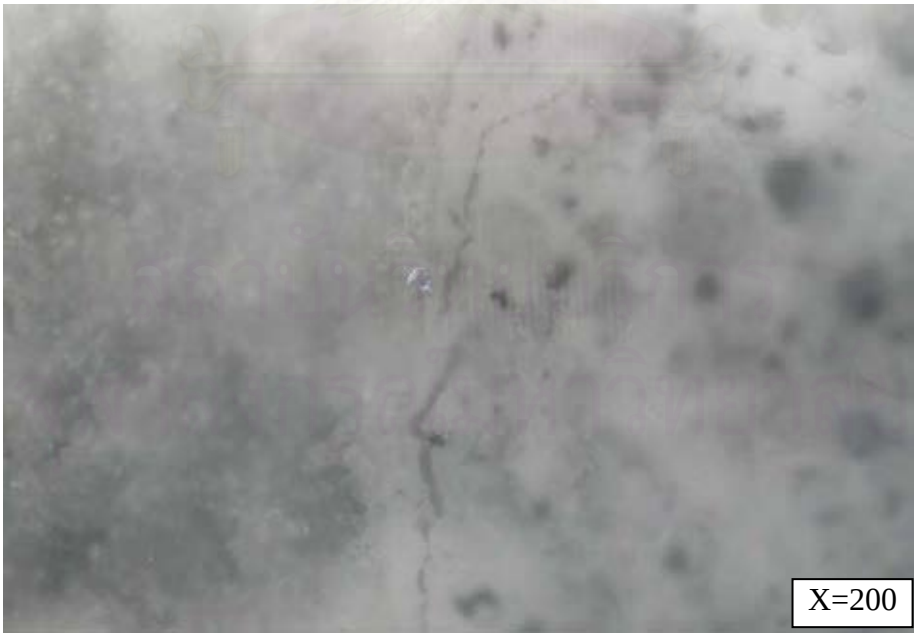

Figure A6. Microcrack of specimen, M2

APPENDIX B: Chloride binding analysis of various cements

Table B1. The results of XRD-Rietveld analysis of sample I-1

Name of component	Content (%by weight of sample)		
	Sample		
	I-1(1)	I-1(2)	I-1(3)
C3S (Triclinic Belov mode)	2.753	3.457	2.393
C3S (mono)	6.119	6.456	4.395
C2S	-	1.666	2.089
C2S	3.147	2.874	4.787
C3A (cubic)	0.481	0.458	-
C4AF	2.185	1.874	0.957
Gypsum	0.262	0.500	0.261
Periclase	0.656	0.583	0.609
Portlandite	10.795	10.329	12.533
Ettringite	2.579	0.666	0.870
Calcite (hex. cell)-use i	-	-	-
Calcite (rhomb. cell)	0.306	0.292	1.001
Calcium-Al- sulphate hyd.	-	0.333	0.348
Anhydrite	-	-	0.305
Friedel'sSalt3	-	0.250	-
Friedel'sSalt1	3.497	1.208	2.393
Katoite	0.830	0.750	0.479
Corundum	10.009	9.996	10.009

Table B2. The results of XRD-Rietveld analysis of sample I-2

Name of component	Content (%by weight of sample)		
	Sample		
	I-2(1)	I-2(2)	I-2(3)
C3S (Triclinic Belov mode)	2.545	4.891	5.113
C2S	3.430	1.920	1.767
C2S	2.286	1.051	2.782
C4AF	1.844	-	
Gypsum	0.184	-	
Periclase	0.700	-	0.827
Portlandite	12.467	12.355	14.248
Ettringite	0.811		
Calcite (hex. cell)-use i	-	-	0.602
Calcite (rhomb. cell)	0.995	0.761	0.526
Calcium-Al- sulphate hyd.	-	2.572	0.639
Friedel'sSalt3	0.442	0.435	0.489
Friedel'sSalt1	0.516	1.739	-
Katoite	0.700	0.507	0.602
Corundum	9.996	10.000	10.000

Table B3. The results of XRD-Rietveld analysis of sample I-3

Name of component	Content (%by weight of sample)		
	Sample		
	I-3(1)	I-3(2)	I-3(3)
C3S (Triclinic Belov mode)	-	-	5.801
C3S (mono)	8.775	6.917	-
C2S	0.711	0.000	0.909
C2S	1.067	0.949	0.649
C3A (cubic)	-	-	0.303
C4AF	-	1.660	0.043
Gypsum	-	0.040	0.996
Periclase	-	-	-
Portlandite	13.478	13.676	0.519
Ettringite	-	-	14.459
Calcite (hex. cell)-use i	-	-	5.281
Calcite (rhomb. cell)	0.395	-	0.043
Calcium-Al- sulphate hyd.	-	3.913	0.606
Anhydrite	-	-	-
Friedel'sSalt3	0.514	0.553	0.390
Friedel'sSalt1	4.585	1.107	2.381
Katoite	-	0.711	0.519
Corundum	10.000	10.000	10.000

Table B4. The results of XRD-Rietveld analysis of sample I-4

Name of component	Content (%by weight of sample)		
	Sample		
	I-4(1)	I-4(2)	I-4(3)
C3S (Triclinic Belov mode)	-	1.939	-
C3S (mono)	11.458	3.349	8.532
C2S	0.833	2.688	0.917
C2S	0.500	-	1.468
C3A (cubic)	-	0.705	1.239
C4AF	-	-	-
Gypsum	-	0.264	-
Portlandite	13.542	16.395	17.477
Ettringite	1.250	0.926	0.642
Calcium-Al- sulphate hyd.	-	-	1.468
Calcite (hex. cell)-use i	0.750	1.807	0.642
Calcite (rhomb. cell)	-	-	0.596
Friedel'sSalt3	0.500	0.485	0.505
Friedel'sSalt1	2.833	4.672	1.927
Katoite		0.793	0.459
Corundum	10.000	10.004	10.000

Table B5. The results of XRD-Rietveld analysis of sample II-1

Name of component	Content (%by weight of sample)		
	Sample		
	II-1(1)	II-1(2)	II-1(3)
C3S (Triclinic Belov mode)	3.649	4.273	4.552
C3S (mono)	-	-	-
C2S	3.659	2.952	5.115
C2S	6.757	8.678	5.537
C3A (cubic)	0.721	-	0.939
C4AF	2.523	2.678	2.393
Gypsum	0.676	0.529	0.704
Portlandite	10.000	10.176	11.122
Ettringite	1.532	0.837	1.032
Calcium-Al- sulphate hyd.	1.441	1.101	2.206
Calcite (hex. cell)-use i	0.811	-	-
Calcite (rhomb. cell)	0.991	1.542	1.549
Anhydrite	-	-	-
Friedel'sSalt3	-	-	0.282
Friedel'sSalt1	1.667	0.705	0.892
Katoite	0.631	0.573	0.657
Corundum	10.000	10.000	9.995

Table B6. The results of XRD-Rietveld analysis of sample II-2

Name of component	Content (%by weight of sample)		
	Sample		
	II-2(1)	II-2(2)	II-2(3)
C3S (Triclinic Belov mode)	-	0.361	0.444
C3S (mono)	-	-	-
C2S	4.664	6.265	3.388
C2S	6.513	5.663	6.333
C3A (cubic)	-	-	0.766
C4AF	3.739	2.771	3.025
Gypsum	0.420	0.723	0.363
Portlandite	10.546	10.964	10.972
Ettringite	1.429	0.884	1.331
Calcium-Al- sulphate hyd.	-	-	-
Calcite (hex. cell)-use i	1.134	-	1.089
Calcite (rhomb. cell)	0.714	1.566	0.444
Anhydrite	-	-	-
Friedel'sSalt3	-	0.442	-
Friedel'sSalt1	2.311	-	1.452
Katoite	0.546	0.522	0.686
Corundum	10.000	10.000	10.004

Table B7. The results of XRD-Rietveld analysis of sample II-3

Name of component	Content (%by weight of sample)		
	Sample		
	II-3(1)	II-3(2)	II-3(3)
C3S (Triclinic Belov mode)	-	0.476	1.147
C3S (mono)	-	-	-
C2S	5.154	4.589	2.890
C2S	5.771	6.147	7.385
C3A (cubic)	-	-	0.872
C4AF	5.639	3.377	6.101
Gypsum	0.485	0.779	0.550
Portlandite	11.278	11.775	10.963
Ettringite	1.101	1.429	1.284
Calcium-Al- sulphate hyd.	-	-	-
Calcite (hex. cell)-use i	1.233	3.333	1.789
Calcite (rhomb. cell)	1.189	1.385	0.963
Anhydrite	-	-	-
Friedel'sSalt3	-	-	-
Friedel'sSalt1	1.806	-	1.514
Katoite	0.396	-	0.413
Corundum	10.000	10.000	10.000

Table B8. The results of XRD-Rietveld analysis of sample II-4

Name of component	Content (%by weight of sample)		
	Sample		
	II-4(1)	II-4(2)	II-4(3)
C3S (Triclinic Belov mode)	0.796	-	1.121
C3S (mono)	-	-	-
C2S	5.221	4.294	4.437
C2S	5.796	6.715	5.424
C3A (cubic)	-	-	-
C4AF	4.425	5.528	5.513
Gypsum	0.796	1.919	0.583
Portlandite	10.265	11.284	10.847
Ettringite	1.062	1.233	0.807
Calcium-Al- sulphate hyd.	-	-	-
Calcite (hex. cell)-use i	3.540	1.964	2.824
Calcite (rhomb. cell)	0.664	0.914	1.255
Anhydrite	-	-	-
Friedel'sSalt3	-	-	-
Friedel'sSalt1	1.018	1.325	2.062
Katoite	0.664	0.457	-
Corundum	10.000	10.005	9.996

Table B9. The results of XRD-Rietveld analysis of sample III-1

Name of component	Content (%by weight of sample)		
	Sample		
	III-1(1)	III-1(2)	III-1(3)
C3S (Triclinic Belov mode)	0.938	2.381	-
C3S (mono)	8.894	7.460	11.404
C2S	-	-	-
C2S	1.224	1.706	0.979
C3A (cubic)	0.734	0.556	0.766
C4AF	2.407	2.262	3.191
Gypsum	0.408	0.357	0.468
Portlandite	11.506	11.111	11.106
Ettringite	1.754	1.310	1.149
Calcium-Al- sulphate hyd.	-	1.468	-
Calcite (hex. cell)-use i	-	-	-
Calcite (rhomb. cell)	0.734	-	0.681
Anhydrite	0.204	-	-
Friedel'sSalt3	-	-	-
Friedel'sSalt1	0.816	-	1.787
Katoite	0.734	0.516	0.511
Corundum	9.996	10.000	10.000

Table B10. The results of XRD-Rietveld analysis of sample III-2

Name of component	Content (%by weight of sample)		
	Sample		
	III-2(1)	III-2(2)	III-2(3)
C3S (Triclinic Belov mode)	2.872	2.866	1.198
C3S (mono)	-	-	6.529
C2S	0.689	0.968	-
C2S	2.719	0.426	-
C3A (cubic)	-	-	-
C4AF	1.072	2.014	3.471
Gypsum	0.306	0.232	-
Portlandite	13.443	12.432	11.364
Ettringite	3.600	2.130	1.529
Calcium-Al- sulphate hyd.	0.881	4.493	3.182
Calcite (hex. cell)-use i	0.689	-	-
Calcite (rhomb. cell)	1.072	1.239	1.116
Anhydrite	-	-	-
Friedel'sSalt3	-	-	0.372
Friedel'sSalt1	0.115	0.930	1.612
Katoite	0.881	0.658	0.537
Corundum	9.996	9.992	10.000

Table B11. The results of XRD-Rietveld analysis of sample III-3

Name of component	Content (%by weight of sample)		
	Sample		
	III-3(1)	III-3(2)	III-3(3)
C3S (Triclinic Belov mode)	1.544	-	-
C3S (mono)	6.909	2.335	1.597
C2S	-	2.948	0.555
C2S	0.463	0.306	2.534
C3A (cubic)	-	-	-
C4AF	0.926	0.421	0.625
Gypsum	-	-	-
Portlandite	13.277	15.046	15.654
Ettringite	1.698	0.613	1.250
Calcium-Al- sulphate hyd.	-	2.642	-
Calcite (hex. cell)-use i	-	0.651	0.451
Calcite (rhomb. cell)	0.965	0.574	0.764
Anhydrite	-	-	-
Friedel'sSalt3	0.463	0.498	0.555
Friedel'sSalt1	1.930	1.302	0.069
Katoite	0.463	0.498	0.694
Corundum	9.996	9.992	9.997

Table B12. The results of XRD-Rietveld analysis of sample III-4

Name of component	Content (%by weight of sample)		
	Sample		
	III-4(1)	III-4(2)	III-4(3)
C3S (Triclinic Belov mode)	0.847	0.222	-
C3S (mono)	8.226	0.185	1.031
C2S	-	1.592	0.952
C2S	1.734	1.148	0.555
C3A (cubic)	-	-	0.476
C4AF	-	1	0.912
Gypsum	-	-	0.674
Portlandite	15.121	17.556	16.779
Ettringite	-	1.815	1.825
Calcium-Al- sulphate hyd.	-	-	1.269
Calcite (hex. cell)-use i	1.210	1.037	1.626
Calcite (rhomb. cell)	0.968	0.815	0.516
Anhydrite	-	-	-
Friedel'sSalt3	0.645	0.556	0.397
Friedel'sSalt1	0.927	0.037	1.904
Katoite	0.645	1.074	0.793
Corundum	10.000	10.000	9.996

Table B13. The results of XRD-Rietveld analysis of sample IV-1

Name of component	Content (%by weight of sample)		
	Sample		
	IV-1(1)	IV-1(2)	IV-1(3)
C3S (Triclinic Belov mode)	3.937	3.530	4.8
C3S (mono)	-	-	-
C2S	3.683	4.849	2.0
C2S	11.346	11.655	13.333
C3A (cubic)	-	-	-
C4AF	3.048	3.275	3.156
Gypsum	0.296	0.298	0.400
Portlandite	5.673	6.593	6.311
Ettringite	1.693	1.191	2.222
Calcium-Al- sulphate hyd.	-	-	0.311
Calcite (hex. cell)-use i	-	-	-
Calcite (rhomb. cell)	1.228	1.191	1.022
Anhydrite	-	-	-
Friedel'sSalt3	-	-	-
Friedel'sSalt1	1.270	-	0.311
Katoite	0.254	-	0.578
Corundum	9.992	9.996	10.000

Table B14. The results of XRD-Rietveld analysis of sample IV-2

Name of component	Content (%by weight of sample)		
	Sample		
	IV-2(1)	IV-2(2)	IV-2(3)
C3S (Triclinic Belov mode)	-	3.464	-
C3S (mono)	-	-	-
C2S	5.086	5.304	8.978
C2S	10.047	9.367	8.850
C3A (cubic)	-	-	-
C4AF	3.091	3.122	3.634
Gypsum	0.601	0.556	-
Portlandite	8.115	7.913	7.781
Ettringite	2.190	0.941	1.283
Calcium-Al- sulphate hyd.	-	-	-
Calcite (hex. cell)-use i	1.374	-	1.026
Calcite (rhomb. cell)	0.644	1.454	0.299
Anhydrite	-	-	-
Friedel'sSalt3	-	-	-
Friedel'sSalt1	1.202	0.556	0.855
Katoite	0.558	-	-
Corundum	10.004	10.009	10.004

Table B15. The results of XRD-Rietveld analysis of sample IV-3

Name of component	Content (%by weight of sample)		
	Sample		
	IV-3(1)	IV-3(2)	IV-3(3)
C3S (Triclinic Belov mode)	-	-	-
C3S (mono)	-	-	-
C2S	3.79	4.504	5.031
C2S	9.954	9.587	10.391
C3A (cubic)	-	-	-
C4AF	3.374	3.719	3.565
Gypsum	0.583	0.620	0.739
Portlandite	7.497	8.017	7.783
Ettringite	1.666	1.157	1.304
Calcium-Al- sulphate hyd.	-	-	-
Calcite (hex. cell)-use i	2.582	2.107	3.435
Calcite (rhomb. cell)	0.375	0.579	-
Anhydrite	-	-	-
Friedel'sSalt3	-	-	-
Friedel'sSalt1	1.208	0.702	0.565
Katoite	0.666	0.331	0.565
Corundum	9.996	10.000	10.000

Table B16. The results of XRD-Rietveld analysis of sample IV-4

Name of component	Content (%by weight of sample)		
	Sample		
	IV-4(1)	IV-4(2)	IV-4(3)
C3S (Triclinic Belov mode)	3.23	0.414	1.189
C3S (mono)	-	-	-
C2S	3.789	3.159	4.264
C2S	8.872	9.101	8.364
C3A (cubic)	-	-	-
C4AF	3.058	2.933	3.034
Gypsum	0.517	0.827	0.738
Portlandite	6.934	7.033	8.241
Ettringite	0.560	0.451	0.984
Calcium-Al- sulphate hyd.	-	-	0.000
Calcite (hex. cell)-use i	3.962	3.310	2.870
Calcite (rhomb. cell)	0.646	0.338	0.451
Anhydrite	-	-	-
Friedel'sSalt3	-	-	0.082
Friedel'sSalt1	1.593	-	0.369
Katoite	-	-	0.369
Corundum	9.991	10.004	10.004

Table B17. Experimental data of chloride binding isotherms of four cement types

Mix series	Total Cl (mol/l)	Free Cl (mol/l)	Bound Cl (mg/g C-S-H)	C-S-H (%)	Friedel's salt (%)	AFm reaction (%)	Chemical bound Cl (mol/mol AFm)	Physical bound Cl (mg/g C-S-H)	Hydration degree (%)
MI-1(1)	0.0157	0.0109	29.86	56.38	2.40	7.0	0.65	25.23	86.90
MI-1(2)	0.0070	0.0055	9.42	58.3	1.20	5.8	0.39	7.18	87.89
MI-1(3)	0.0065	0.0047	11.32	56.57	1.00	5.8	0.33	9.40	87.23
MI-2(1)	0.0269	0.0205	35.98	63.07	4.00	7.5	1.02	29.08	88.45
MI-2(2)	0.0129	0.0104	14.06	63.77	2.40	7.5	0.61	9.97	88.74
MI-2(3)	0.0128	0.0097	17.60	62.4	1.85	6.3	0.56	14.37	88.62
MI-3(1)	0.0283	0.0218	38.38	60.47	4.80	8.2	1.12	29.75	87.80
MI-3(2)	0.0094	0.0072	12.68	60.47	1.67	7.9	0.40	9.68	86.28
MI-3(3)	0.0035	0.0027	4.71	60.47	0.80	8.2	0.19	3.27	88.10
MI-4(1)	0.0349	0.0268	43.53	65.6	6.00	8.2	1.40	33.58	90.20
MI-4(2)	0.0165	0.0127	24.08	55.97	2.60	6.7	0.74	19.03	89.54
MI-4(3)	0.0185	0.0142	27.93	54.13	3.20	7.8	0.78	21.51	87.75
MII-1(1)	0.0141	0.0108	19.04	61.30	1.46	6.2	0.45	16.45	79.31
MII-1(2)	0.0052	0.0049	2.22	58.33	0.45	6.2	0.14	1.38	78.69
MII-1(3)	0.0063	0.0046	9.66	61.40	0.55	7.1	0.15	8.68	79.31
MII-2(1)	0.0215	0.0194	12.78	57.98	1.68	4.8	0.67	9.63	80.12
MII-2(2)	0.0127	0.0109	10.53	59.84	1.15	4.8	0.46	8.44	79.68
MII-2(3)	0.0105	0.0094	6.52	59.70	0.97	4.8	0.39	4.75	78.74
MII-3(1)	0.0157	0.0137	13.08	55.95	1.31	5.0	0.50	10.53	80.65
MII-3(2)	0.0164	0.0143	13.24	56.70	1.55	5.5	0.54	10.27	82.62
MII-3(3)	0.0111	0.0094	11.16	54.13	1.10	5.5	0.38	8.95	78.81
MII-4(1)	0.0184	0.0161	14.43	55.75	1.34	4.2	0.61	11.82	82.15
MII-4(2)	0.0172	0.0150	14.19	54.36	1.02	3.8	0.51	12.15	80.67
MII-4(3)	0.0221	0.0195	16.46	55.13	1.50	4.2	0.68	13.51	81.96

Table B17. Experimental data of chloride binding isotherms of four cement types (Continued)

MIII-1(1)	0.0138	0.0112	15.99	59.16	1.55	6.3	0.47	13.14	84.74
MIII-1(2)	0.0063	0.0060	1.81	60.32	0.40	4.0	0.19	1.09	84.55
MIII-1(3)	0.0060	0.0048	6.97	60.00	0.60	6.3	0.18	5.88	82.56
MIII-2(1)	0.0238	0.0206	17.99	61.66	1.74	5.2	0.64	14.92	91.57
MIII-2(2)	0.0127	0.0111	9.21	61.19	1.07	5.2	0.39	7.31	92.64
MIII-2(3)	0.0119	0.0098	12.71	58.68	0.98	5.0	0.37	10.89	87.72
MIII-3(1)	0.0265	0.0230	20.31	61.37	2.00	5.4	0.71	16.77	89.07
MIII-3(2)	0.0125	0.0109	9.54	61.64	1.15	5.4	0.41	7.51	92.90
MIII-3(3)	0.0092	0.0080	6.65	65.26	0.66	4.0	0.31	5.56	93.60
MIII-4(1)	0.0275	0.0238	21.64	59.68	1.80	4.7	0.73	18.36	88.10
MIII-4(2)	0.0175	0.0152	13.08	62.96	1.40	4.8	0.56	10.66	94.77
MIII-4(3)	0.0075	0.0065	5.84	60.29	0.68	4.8	0.27	4.61	94.99
MIV-1(1)	0.0107	0.0092	9.15	57.58	0.60	4.0	0.29	8.02	75.43
MIV-1(2)	0.0043	0.0038	2.85	57.42	0.24	4.0	0.11	2.39	74.10
MIV-1(3)	0.0038	0.0037	0.65	55.56	0.10	1.7	0.11	0.46	70.96
MIV-2(1)	0.0189	0.0178	7.00	57.10	0.76	4.0	0.36	5.56	79.21
MIV-2(2)	0.0100	0.0093	4.12	57.31	0.42	3.8	0.21	3.33	76.17
MIV-2(3)	0.0090	0.0079	6.98	57.29	0.50	4.4	0.22	6.03	75.95
MIV-3(1)	0.0213	0.0201	7.47	58.31	0.71	3.3	0.41	6.15	80.32
MIV-3(2)	0.0125	0.0118	4.37	58.68	0.48	3.3	0.28	3.48	79.51
MIV-3(3)	0.0081	0.0076	2.93	56.52	0.38	3.3	0.22	2.20	78.32
MIV-4(1)	0.0255	0.0240	9.17	56.85	0.88	3.8	0.44	7.49	78.47
MIV-4(2)	0.0206	0.0194	6.76	58.12	0.78	3.8	0.39	5.40	81.81
MIV-4(3)	0.0167	0.0157	5.78	58.04	0.75	3.8	0.38	4.39	80.57

APPENDIX B

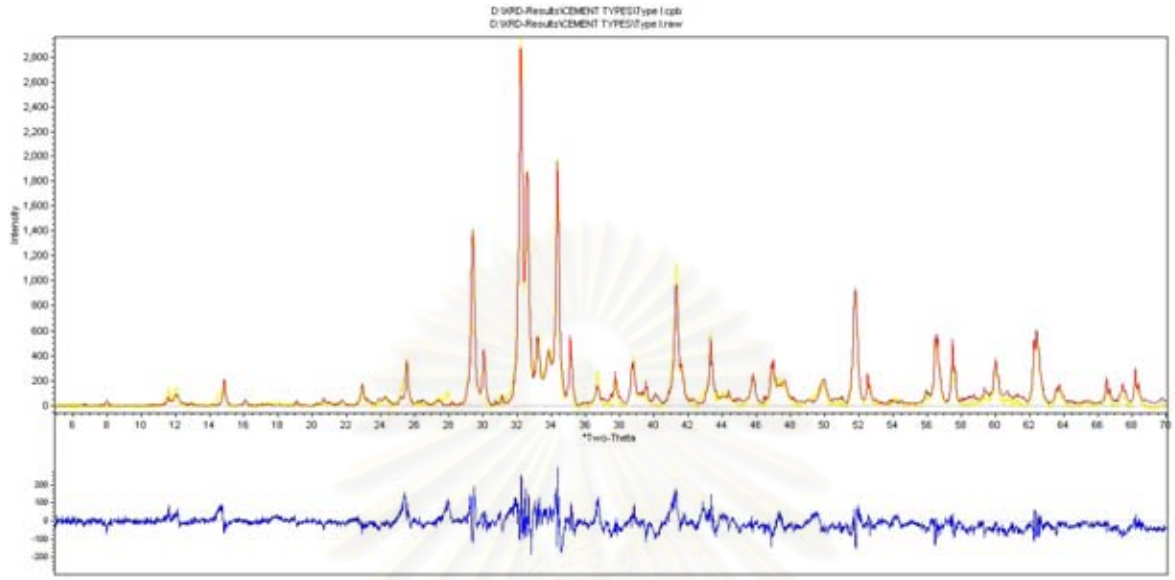

Figure B1. XRD pattern of cement type I

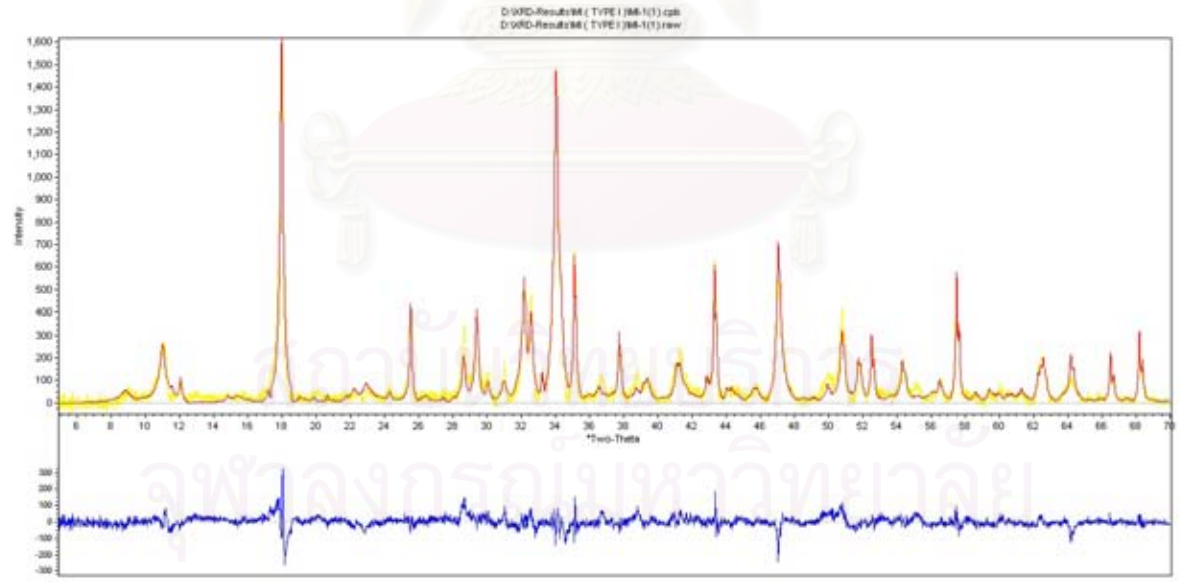

Figure B2. XRD pattern of cement paste made of cement type I and *w/c*=0.3

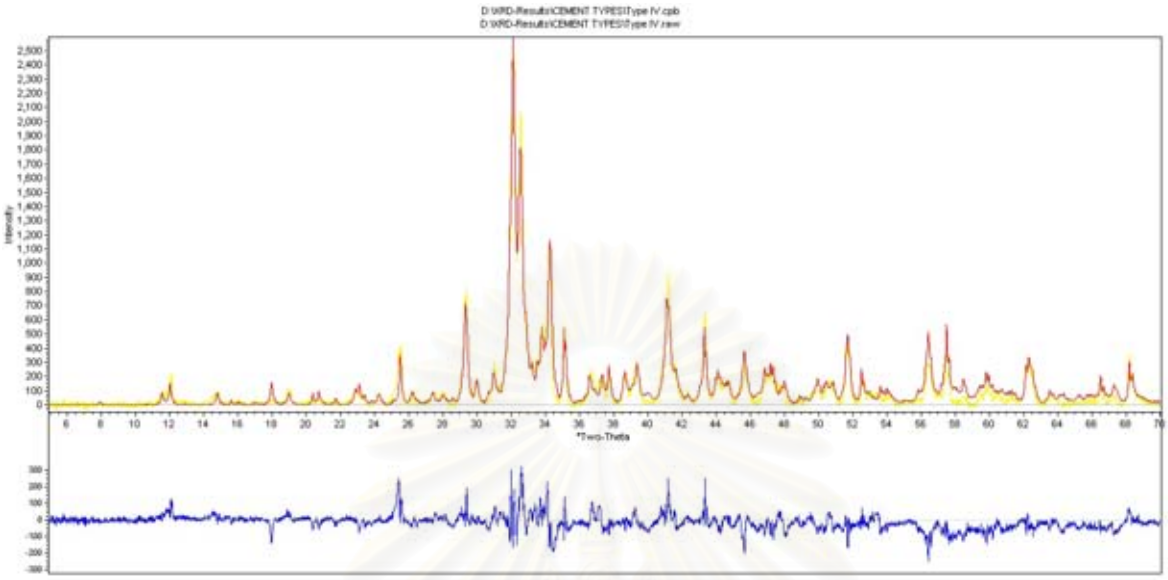

Figure B3. XRD pattern of cement type IV

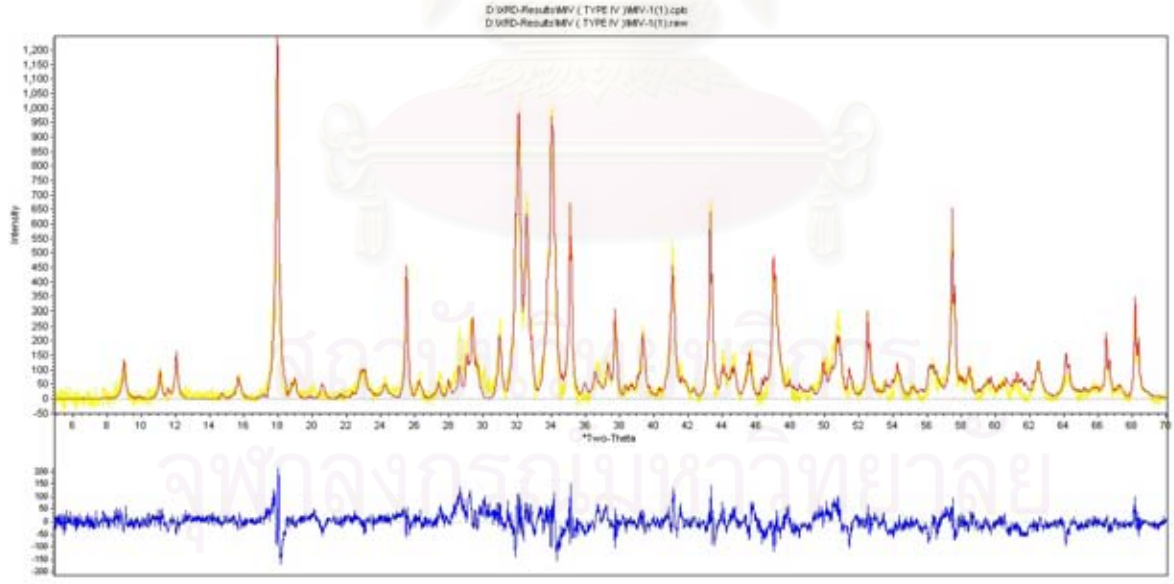

Figure B4. XRD pattern of cement paste made of cement type IV and *w/c*=0.3

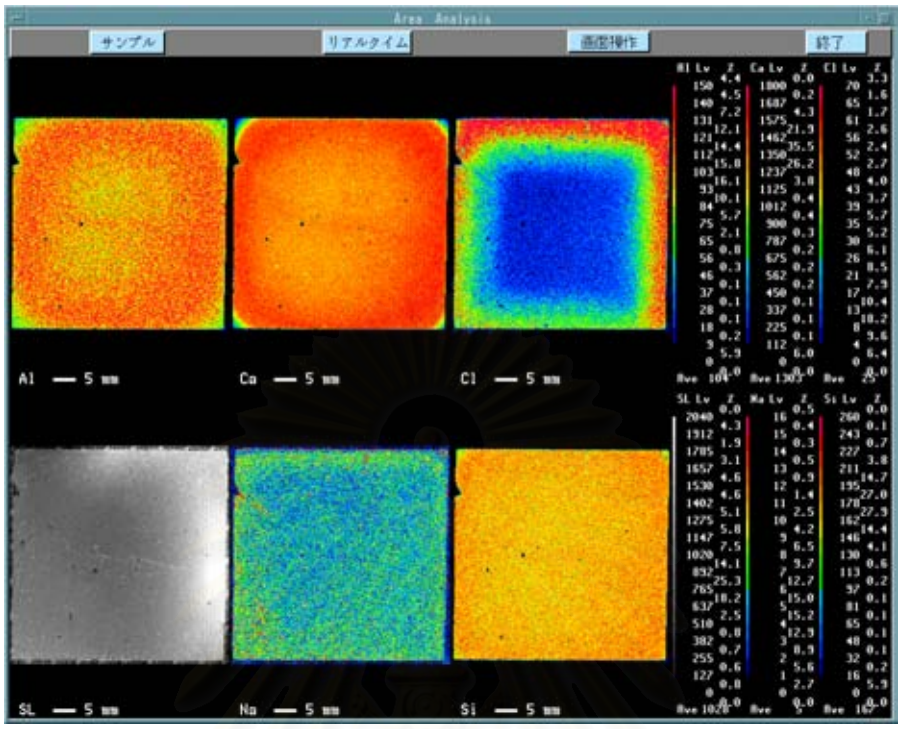

Figure B5. EPMA result of cement paste made of cement type I and *w/c*=0.4

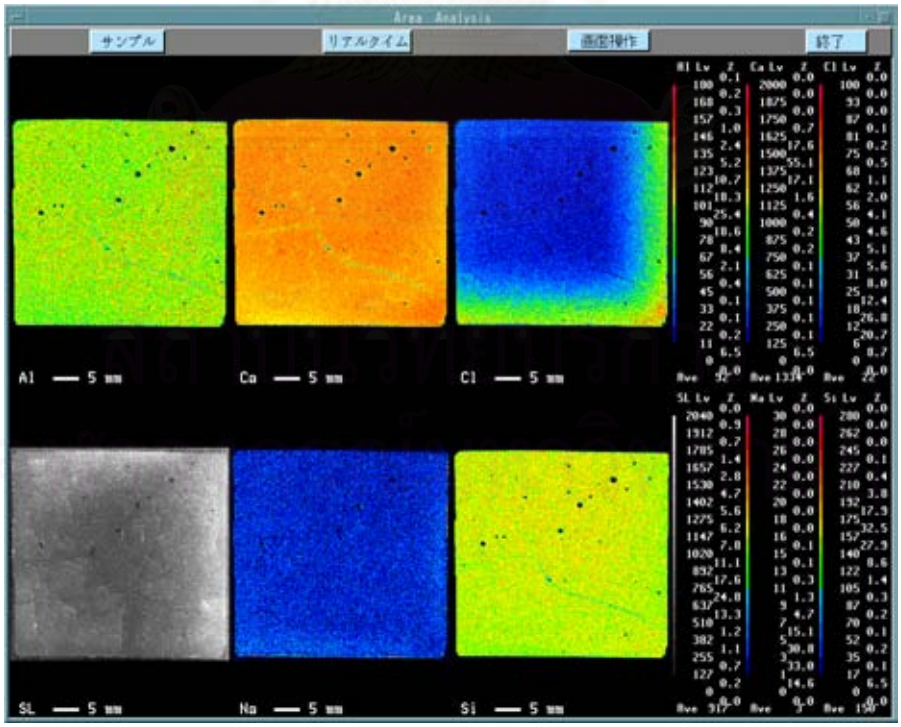

Figure B6. EPMA result of cement paste made of cement type III and *w/c*=0.4

APPENDIX C: Matlab source code for predicting fatigue deformation of concrete beam

```
%-------------------------------------------------------------------------------------------
function fatiguecrack
% This program computes the crack width at the specific cycle number
% Fc is compression strength of concrete (MPa)
% Ft is tension strength of concrete (MPa)
% Pmax is maximum flexural load (N)
% P is applied flexural load (N)
% SR is the flexural load level
% E is the elastic modulus of conrete (GPa)
% SU is the flexural stress (MPa)
% M is the moment due to bending (N.mm)
% B is the width of concrete beam (mm)
% h is the height of concrete beam (mm)
% L is the span of concrete beam (mm)
% Wmax is the maximum crack width at which concrete beam will be fracture(mm)
% x1 and x2 is material parameters depending on Wmax
% W is CMOD at the bottom of beam (mm)
% C is the number of cycle

format short;

Fc=input('The compression strength (MPa):');
Pmax=input('The maximum flexural load (N):');
SR=input('The flexural load level:');
Wmax=input('The initial maximum crack width (mm):');
B=input('width of beam (mm):');
h=input('The height of beam (mm):');
L=input('The span of beam (mm):');
C=input('The number of cycle:');
```

```
P=SR*Pmax;
M=P*L/6;
SU=P*L/(B*h*h);
E=4.7*sqrt(Fc);

if (0<Wmax)&(Wmax<=0.017)
   x1=1;    x2=-33.48;
end
if (0.017<Wmax)&(Wmax<=0.044)
   x1=0.569;    x2=-8.12;
end
if (0.044<Wmax)&(Wmax<=0.081)
   x1=0.321;    x2=-2.49;
end
if (0.081<Wmax)&(Wmax<=0.2)
   x1=0.187;    x2=-0.84;
end

Ft=0.3*(Fc)^(2/3);
F1=Ft*(x1+x2*Wmax);

If C=1
syms x m a b W h B F1 Ft FN E M;

FIx=F1*W*(1-x/(a*h));
FIIx=Ft*(1-(x-a*h)/(b*h-a*h));
FNx=FN*W*(1-x/(a*h));
Mc=simple(int(B*FIx*(h/2-x),0,a*h));
Fc=simple((1/h)*int(FIx,0,a*h));
V1a=0.33-1.42*a+3.87*a^2-2.04*a^3+0.66/(1-a)^2;
V2a=0.8-1.7*a+2.4*a^2+0.66/(1-a)^2;
```

```
V3a=(1.46+3.42*(1-cos(pi*a/2)))/(cos(pi*a/2))^2;

f1=simple(int(FIx,0,a*h)+int(FIIx,a*h,h));
f2=simple(int(B*(h-x)*FIx,0,a*h)+int(B*(h-x)*FIIx,a*h,h))-M;
f3=simple((24*a/(B*h*E*1000))*(M*V1a-Mc*V2a)-4*Fc*a*h*V3a/(E*1000)-W);
f1a=simple(diff(f1,'a'));
f1b=simple(diff(f1,'b'));
f1W=simple(diff(f1,'W'));
f2a=simple(diff(f2,'a'));
f2b=simple(diff(f2,'b'));
f2W=simple(diff(f2,'W'));
f3a=simple(diff(f3,'a'));
f3b=simple(diff(f3,'b'));
f3W=simple(diff(f3,'W'));

a=0.005; b=0.5; W=Wmax;
      for i=1:20
         Z=[f1a f1b;f2a f2b];
         f=[f1;f2];
         Xo=[a;b];
         Xi=Xo-inv(Z)*f;
         ea=abs((Xi(1)-Xo(1))/Xo(1));
         eb=abs((Xi(2)-Xo(2))/Xo(2));
         a=Xi(1); b=Xi(2);
         if (ea<=0.001)&(eb<=0.001), break, end
      end
end

m=Xi(1); a=0.005; b=0.5; W=0.0005; k=0.08+4*Wmax;
for N=2:C
```

```
FN=F1*(1-k*log(N));
syms x m a b W h B F1 Ft FN E M;

FIx=F1*W*(1-x/a*h);
FIIx=Ft*(1-(x-a*h)/(b*h-a*h));
FNx=FN*W*(1-x/a*h);
Mc=simple(int(B*FIx*(h/2-x),m*h,a*h)+int(B*FNx*(h/2-x),0,m*h));
Fc=(1/h)*simple(int(FIx,m*h,a*h)+int(FNx,0,m*h));

V1a=0.33-1.42*a+3.87*a^2-2.04*a^3+0.66/(1-a)^2;
V2a=0.8-1.7*a+2.4*a^2+0.66/(1-a)^2;
V3a=(1.46+3.42*(1-cos(pi*a/2)))/(cos(pi*a/2))^2;

R1=simple(int(FNx,0,m*h)+int(FIx,m*h,a*h)+int(FIIx,a*h,b*h)-int(FIIx,b*h,h));
R2=simple(int(B*(h-x)*FNx,0,m*h)+int(B*(h-x)*FIx,m*h,a*h)+int(B*(h-x)*FIIx,a*h,b*h)-
int(B*(h-x)*FIIx,b*h,h))+M;
R3=simple((24*a/(B*h*E*1e3))*(M*V1a-Mc*V2a)-4*Fc*a*h*V3a/(E*1e3)-W);

R1a=simple(diff(f1,'a'));
R1b=simple(diff(f1,'b'));
R1W=simple(diff(f1,'W'));

R2a=simple(diff(f2,'a'));
R2b=simple(diff(f2,'b'));
R2W=simple(diff(f2,'W'));

R3a=simple(diff(f3,'a'));
R3b=simple(diff(f3,'b'));
R3W=simple(diff(f3,'W'));
   for i=1:100
        Z=[R1a R1b R1W;R2a R2b R2W;R3a R3b R3W];
```

```
        R=[R1;R2;R3];
        Xo=[a;b;W];
        X=Xo-inv(Z)*R;
        ea=abs((X(1)-Xo(1))/Xo(1));
        eb=abs((X(2)-Xo(2))/Xo(2));
        eW=abs((X(3)-Xo(3))/Xo(3));
        a=X(1); b=X(2); W=X(3);
        if (ea<=0.001)&(eb<=0.001)&(eW<=0.001), break, end
    end
    m=X(1); Wmax=X(3);
end
A=[N;X(3)];
fprintf('Normalized Crack length\n')
fprintf('%5d %10.4f\n',X(1))
fprintf('Cycle     Crack width(mm)\n')
fprintf('%5d %10.4f\n',A)

%End of source code
%-------------------------------------------------------------------------------------------
```

APPENDIX D: Matlab source code for predicting humidity diffusion in tidal zone

```
%-----------------------------------------------------------------------------------------------------
function programhumidity
% This program computes the humidity at the specific time and depth
% Weather is tidal environment that has 12h wetting and 12h drying
% The time step dt is 12h
% The depth step dx is 5mm
% Dh is humidity diffusion coefficient
% n is the number of time step
dt=input('The time step (s):');
dx=input('The depth step (m):');
Dh=input('The humidity diffusion coefficient (m2/s):');
n=input('The number of time step:');

dl=Dh*dt/(dx^2)
ho1=0; ho2=0; ho3=0;ho4=0;ho5=0;ho6=0;ho7=0;ho8=0;ho9=0;ho10=0;
ho11=0;ho12=0;ho13=0;ho14=0;ho15=0;ho16=0;ho17=0;ho18=0;ho19=0;ho20=0;

for l=1:n
  if mod(l,2)==0
     h=0; ho=1;
   else
     h=1; ho=0;
   end

   a1=dl*h + dl*ho + 2*(1-dl)*ho1 + dl*ho2;
   a2=dl*ho1 + 2*(1-dl)*ho2 + dl*ho3;
   a3=dl*ho2 + 2*(1-dl)*ho3 + dl*ho4;
   a4=dl*ho3 + 2*(1-dl)*ho4 + dl*ho5;
   a5=dl*ho4 + 2*(1-dl)*ho5 + dl*ho6;
   a6=dl*ho5 + 2*(1-dl)*ho6 + dl*ho7;
   a7=dl*ho6 + 2*(1-dl)*ho7 + dl*ho8;
```

```
a8=dl*ho7 + 2*(1-dl)*ho8 + dl*ho9;
a9=dl*ho8 + 2*(1-dl)*ho9 + dl*ho10;
a10=dl*ho9 + 2*(1-dl)*ho10 + dl*ho11;
a11=dl*ho10 + 2*(1-dl)*ho11 + dl*ho12;
a12=dl*ho11 + 2*(1-dl)*ho12 + dl*ho13;
a13=dl*ho12 + 2*(1-dl)*ho13 + dl*ho14;
a14=dl*ho13 + 2*(1-dl)*ho14 + dl*ho15;
a15=dl*ho14 + 2*(1-dl)*ho15 + dl*ho16;
a16=dl*ho15 + 2*(1-dl)*ho16 + dl*ho17;
a17=dl*ho16 + 2*(1-dl)*ho17 + dl*ho18;
a18=dl*ho17 + 2*(1-dl)*ho18 + dl*ho19;
a19=dl*ho18 + 2*(1-dl)*ho19 + dl*ho20 + dl*(2*dl*ho19 + (1-2*dl)*ho20);

a=[a1;a2;a3;a4;a5;a6;a7;a8;a9;a10;a11;a12;a13;a14;a15;a16;a17;a18;a19];

b1=[2*(1+dl) -dl 0 0 0 0 0 0 0 0 0 0 0 0 0 0 0 0 0];
b2=[-dl 2*(1+dl) -dl 0 0 0 0 0 0 0 0 0 0 0 0 0 0 0 0];
b3=[0 -dl 2*(1+dl) -dl 0 0 0 0 0 0 0 0 0 0 0 0 0 0 0];
b4=[0 0 -dl 2*(1+dl) -dl 0 0 0 0 0 0 0 0 0 0 0 0 0 0];
b5=[0 0 0 -dl 2*(1+dl) -dl 0 0 0 0 0 0 0 0 0 0 0 0 0];
b6=[0 0 0 0 -dl 2*(1+dl) -dl 0 0 0 0 0 0 0 0 0 0 0 0];
b7=[0 0 0 0 0 -dl 2*(1+dl) -dl 0 0 0 0 0 0 0 0 0 0 0];
b8=[0 0 0 0 0 0 -dl 2*(1+dl) -dl 0 0 0 0 0 0 0 0 0 0];
b9=[0 0 0 0 0 0 0 -dl 2*(1+dl) -dl 0 0 0 0 0 0 0 0 0];
b10=[0 0 0 0 0 0 0 0 -dl 2*(1+dl) -dl 0 0 0 0 0 0 0 0];
b11=[0 0 0 0 0 0 0 0 0 -dl 2*(1+dl) -dl 0 0 0 0 0 0 0];
b12=[0 0 0 0 0 0 0 0 0 0 -dl 2*(1+dl) -dl 0 0 0 0 0 0];
b13=[0 0 0 0 0 0 0 0 0 0 0 -dl 2*(1+dl) -dl 0 0 0 0 0];
b14=[0 0 0 0 0 0 0 0 0 0 0 0 -dl 2*(1+dl) -dl 0 0 0 0];
b15=[0 0 0 0 0 0 0 0 0 0 0 0 0 -dl 2*(1+dl) -dl 0 0 0];
b16=[0 0 0 0 0 0 0 0 0 0 0 0 0 0 -dl 2*(1+dl) -dl 0 0];
b17=[0 0 0 0 0 0 0 0 0 0 0 0 0 0 0 -dl 2*(1+dl) -dl 0];
```

```
    b18=[0 0 0 0 0 0 0 0 0 0 0 0 0 0 0 0 0 -dl 2*(1+dl) -dl];
    b19=[0 0 0 0 0 0 0 0 0 0 0 0 0 0 0 0 0 0 -dl 2*(1+dl)];
    bt=[b1;b2;b3;b4;b5;b6;b7;b8;b9;b10;b11;b12;b13;b14;b15;b16;b17;b18;b19];

    h=inv(bt)*a;
    ho1=h(1,1); ho2=h(2,1); ho3=h(3,1);ho4=h(4,1);ho5=h(5,1);ho6=h(6,1);
    ho7=h(7,1);ho8=h(8,1);ho9=h(9,1);ho10=h(10,1);ho11=h(11,1);ho12=h(12,1);
    ho13=h(13,1);ho14=h(14,1);ho15=h(15,1);ho16=h(16,1);ho17=h(17,1);
    ho18=h(18,1);ho19=h(19,1);
    h20=dl*(2*dl*h(19,1) + (1-2*dl)*ho20); ho20=h20;
end
disp('')
disp('Value of humidity :')
disp(h)
disp('Value of humidity at the end node:')
disp(h20)
x=0:5:100;
t=[ho h(1,1) h(2,1) h(3,1) h(4,1) h(5,1) h(6,1) h(7,1) h(8,1) h(9,1) h(10,1) h(11,1) h(12,1)
h(13,1) h(14,1) h(15,1) h(16,1) h(17,1) h(18,1) h(19,1) h20];
plot(x,t)

%End of source code
%-----------------------------------------------------------------------------------------------
```

APPENDIX E: Matlab source code for predicting chloride penetration in tidal zone

```
%-----------------------------------------------------------------------------------------------
function programchloride
% This program computes the chloride content in tidal environment at the specific time and
depth
% Weather is tidal environment that has 12h wetting and 12h drying
% The time step dt is 12h
% The depth step dx is 5mm
% Dh is humidity diffusion coefficient
% Da is the apparent chloride diffusion coefficient at 28 days
% ex is the exposed time, year
% w is evaporable water
% theta is chloride binding capacity
% m is constant to account for time dependent diffusion coefficient

dt=input('The time step (s):');
dx=input('The depth step (m):');
Dh=input('The humidity diffusion coefficient (m2/s):');
Da=input('The apparent chloride diffusion coefficient at 28 days (m2/s):');
w=input('The evaporable water :');
theta=input('The chloride binding capacity:');
ex=input('The number of year to expose to tide:');
m=input('constant to account for time dependent diffusion coefficient:');

dl=Dh*dt/(dx^2)
n=ex*365*2
e=w/(theta*dt)
g=dx^2

clo1=0; clo2=0; clo3=0;clo4=0;clo5=0;clo6=0;clo7=0;clo8=0;clo9=0;clo10=0;
clo11=0;clo12=0;clo13=0;clo14=0;clo15=0;clo16=0;clo17=0;clo18=0;clo19=0;clo20=0;
```

```
po1=0; po2=0; po3=0;po4=0;po5=0;po6=0;po7=0;po8=0;po9=0;po10=0;
po11=0;po12=0;po13=0;po14=0;po15=0;po16=0;po17=0;po18=0;po19=0;po20=0;

for l=1:n
    f=dt*Da*(28/(28+0.5*n))^m;

    if mod(l,2)==0
    h=0; ho=1;cl=0; clo=13;
    else
    h=1; ho=0; cl=13; clo=0;
    end
  c1=dl*h + dl*ho + 2*(1-dl)*po1 + dl*po2;
  c2=dl*po1 + 2*(1-dl)*po2 + dl*po3;
  c3=dl*po2 + 2*(1-dl)*po3 + dl*po4;
  c4=dl*po3 + 2*(1-dl)*po4 + dl*po5;
  c5=dl*po4 + 2*(1-dl)*po5 + dl*po6;
  c6=dl*po5 + 2*(1-dl)*po6 + dl*po7;
  c7=dl*po6 + 2*(1-dl)*po7 + dl*po8;
  c8=dl*po7 + 2*(1-dl)*po8 + dl*po9;
  c9=dl*po8 + 2*(1-dl)*po9 + dl*po10;
  c10=dl*po9 + 2*(1-dl)*po10 + dl*po11;
  c11=dl*po10 + 2*(1-dl)*po11 + dl*po12;
  c12=dl*po11 + 2*(1-dl)*po12 + dl*po13;
  c13=dl*po12 + 2*(1-dl)*po13 + dl*po14;
  c14=dl*po13 + 2*(1-dl)*po14 + dl*po15;
  c15=dl*po14 + 2*(1-dl)*po15 + dl*po16;
  c16=dl*po15 + 2*(1-dl)*po16 + dl*po17;
  c17=dl*po16 + 2*(1-dl)*po17 + dl*po18;
  c18=dl*po17 + 2*(1-dl)*po18 + dl*po19;
  c19=dl*po18 + 2*(1-dl)*po19;
  c=[c1;c2;c3;c4;c5;c6;c7;c8;c9;c10;c11;c12;c13;c14;c15;c16;c17;c18;c19];
```

```
d1=[2*(1+dl) -dl 0 0 0 0 0 0 0 0 0 0 0 0 0 0 0 0];
d2=[-dl 2*(1+dl) -dl 0 0 0 0 0 0 0 0 0 0 0 0 0 0 0];
d3=[0 -dl 2*(1+dl) -dl 0 0 0 0 0 0 0 0 0 0 0 0 0 0];
d4=[0 0 -dl 2*(1+dl) -dl 0 0 0 0 0 0 0 0 0 0 0 0 0];
d5=[0 0 0 -dl 2*(1+dl) -dl 0 0 0 0 0 0 0 0 0 0 0 0];
d6=[0 0 0 0 -dl 2*(1+dl) -dl 0 0 0 0 0 0 0 0 0 0 0];
d7=[0 0 0 0 0 -dl 2*(1+dl) -dl 0 0 0 0 0 0 0 0 0 0];
d8=[0 0 0 0 0 0 -dl 2*(1+dl) -dl 0 0 0 0 0 0 0 0 0];
d9=[0 0 0 0 0 0 0 -dl 2*(1+dl) -dl 0 0 0 0 0 0 0 0];
d10=[0 0 0 0 0 0 0 0 -dl 2*(1+dl) -dl 0 0 0 0 0 0 0];
d11=[0 0 0 0 0 0 0 0 0 -dl 2*(1+dl) -dl 0 0 0 0 0 0];
d12=[0 0 0 0 0 0 0 0 0 0 -dl 2*(1+dl) -dl 0 0 0 0 0];
d13=[0 0 0 0 0 0 0 0 0 0 0 -dl 2*(1+dl) -dl 0 0 0 0];
d14=[0 0 0 0 0 0 0 0 0 0 0 0 -dl 2*(1+dl) -dl 0 0 0];
d15=[0 0 0 0 0 0 0 0 0 0 0 0 0 -dl 2*(1+dl) -dl 0 0];
d16=[0 0 0 0 0 0 0 0 0 0 0 0 0 0 -dl 2*(1+dl) -dl 0];
d17=[0 0 0 0 0 0 0 0 0 0 0 0 0 0 0 -dl 2*(1+dl) -dl];
d18=[0 0 0 0 0 0 0 0 0 0 0 0 0 0 0 0 -dl 2*(1+dl)];
d19=[0 0 0 0 0 0 0 0 0 0 0 0 0 0 0 0 0 -dl 2*(1+dl)];
dt=[d1;d2;d3;d4;d5;d6;d7;d8;d9;d10;d11;d12;d13;d14;d15;d16;d17;d18;d19];

ht=inv(dt)*c;
k1=ht(1,1)-po1; k2=ht(2,1)-po2;k3=ht(3,1)-po3;k4=ht(4,1)-po4;k5=ht(5,1)-po5;
k6=ht(6,1)-po6;k7=ht(7,1)-po7;k8=ht(8,1)-po8;k9=ht(9,1)-po9;k10=ht(10,1)-po10;
k11=ht(11,1)-po11;k12=ht(12,1)-po12;k13=ht(13,1)-po13;k14=ht(14,1)-po14;
k15=ht(15,1)-po15;k16=ht(16,1)-po16;k17=ht(17,1)-po17;k18=ht(18,1)-
po18;k19=ht(19,1)-po19;

cl1=f*cl + f*clo + (-2*f + 2*g + e*k1)*clo1 + f*clo2;
cl2=f*clo1 + (-2*f + 2*g + e*k2)*clo2 + f*clo3;
cl3=f*clo2 + (-2*f + 2*g + e*k3)*clo3 + f*clo4;
cl4=f*clo3 + (-2*f + 2*g + e*k4)*clo4 + f*clo5;
```

```
cl5=f*clo4 + (-2*f + 2*g + e*k5)*clo5 + f*clo6;
cl6=f*clo5 + (-2*f + 2*g + e*k6)*clo6 + f*clo7;
cl7=f*clo6 + (-2*f + 2*g + e*k7)*clo7 + f*clo8;
cl8=f*clo7 + (-2*f + 2*g + e*k8)*clo8 + f*clo9;
cl9=f*clo8 + (-2*f + 2*g + e*k9)*clo9 + f*clo10;
cl10=f*clo9 + (-2*f + 2*g + e*k10)*clo10 + f*clo11;
cl11=f*clo10 + (-2*f + 2*g + e*k11)*clo11 + f*clo12;
cl12=f*clo11 + (-2*f + 2*g + e*k12)*clo12 + f*clo13;
cl13=f*clo12 + (-2*f + 2*g + e*k13)*clo13 + f*clo14;
cl14=f*clo13 + (-2*f + 2*g + e*k14)*clo14 + f*clo15;
cl15=f*clo14 + (-2*f + 2*g + e*k15)*clo15 + f*clo16;
cl16=f*clo15 + (-2*f + 2*g + e*k16)*clo16 + f*clo17;
cl17=f*clo16 + (-2*f + 2*g + e*k17)*clo17 + f*clo18;
cl18=f*clo17 + (-2*f + 2*g + e*k18)*clo18 + f*clo19;
cl19=f*clo18 + (-2*f + 2*g + e*k19)*clo19;
c=[cl1;cl2;cl3;cl4;cl5;cl6;cl7;cl8;cl9;cl10;cl11;cl12;cl13;cl14;cl15;cl16;cl17;cl18;cl19];

a1=[2*(g+f) -f 0 0 0 0 0 0 0 0 0 0 0 0 0 0 0 0];
a2=[-f 2*(g+f) -f 0 0 0 0 0 0 0 0 0 0 0 0 0 0 0];
a3=[0 -f 2*(g+f) -f 0 0 0 0 0 0 0 0 0 0 0 0 0 0];
a4=[0 0 -f 2*(g+f) -f 0 0 0 0 0 0 0 0 0 0 0 0 0];
a5=[0 0 0 -f 2*(g+f) -f 0 0 0 0 0 0 0 0 0 0 0 0];
a6=[0 0 0 0 -f 2*(g+f) -f 0 0 0 0 0 0 0 0 0 0 0];
a7=[0 0 0 0 0 -f 2*(g+f) -f 0 0 0 0 0 0 0 0 0 0];
a8=[0 0 0 0 0 0 -f 2*(g+f) -f 0 0 0 0 0 0 0 0 0];
a9=[0 0 0 0 0 0 0 -f 2*(g+f) -f 0 0 0 0 0 0 0 0];
a10=[0 0 0 0 0 0 0 0 -f 2*(g+f) -f 0 0 0 0 0 0 0];
a11=[0 0 0 0 0 0 0 0 0 -f 2*(g+f) -f 0 0 0 0 0 0];
a12=[0 0 0 0 0 0 0 0 0 0 -f 2*(g+f) -f 0 0 0 0 0];
a13=[0 0 0 0 0 0 0 0 0 0 0 -f 2*(g+f) -f 0 0 0 0];
a14=[0 0 0 0 0 0 0 0 0 0 0 0 -f 2*(g+f) -f 0 0 0];
a15=[0 0 0 0 0 0 0 0 0 0 0 0 0 -f 2*(g+f) -f 0 0];
```

```
   a16=[0 0 0 0 0 0 0 0 0 0 0 0 0 0 -f 2*(g+f) -f 0 0];
   a17=[0 0 0 0 0 0 0 0 0 0 0 0 0 0 0 -f 2*(g+f) -f 0];
   a18=[0 0 0 0 0 0 0 0 0 0 0 0 0 0 0 0 -f 2*(g+f) -f];
   a19=[0 0 0 0 0 0 0 0 0 0 0 0 0 0 0 0 0 -f 2*(g+f)];
   a=[a1;a2;a3;a4;a5;a6;a7;a8;a9;a10;a11;a12;a13;a14;a15;a16;a17;a18;a19];

   clo=inv(a)*c;

   po1=ht(1,1); po2=ht(2,1); po3=ht(3,1);po4=ht(4,1);po5=ht(5,1);po6=ht(6,1);
   po7=ht(7,1);po8=ht(8,1);po9=ht(9,1);po10=ht(10,1);po11=ht(11,1);po12=ht(12,1);
   po13=ht(13,1);po14=ht(14,1);po15=ht(15,1);po16=ht(16,1);po17=ht(17,1);
   po18=ht(18,1);po19=ht(19,1);

   clo1=clo(1,1); clo2=clo(2,1); clo3=clo(3,1);clo4=clo(4,1);clo5=clo(5,1);clo6=clo(6,1);

clo7=clo(7,1);clo8=clo(8,1);clo9=clo(9,1);clo10=clo(10,1);clo11=clo(11,1);clo12=clo(12,1);
   clo13=clo(13,1);clo14=clo(14,1);clo15=clo(15,1);clo16=clo(16,1);clo17=clo(17,1);
   clo18=clo(18,1);clo19=clo(19,1);
 end
 disp('')
 disp('Value of chloride content (kg/m3) :')
 disp(clo)

 x=5:5:95;
t=[clo(1,1) clo(2,1) clo(3,1) clo(4,1) clo(5,1) clo(6,1) clo(7,1) clo(8,1) clo(9,1) clo(10,1)
clo(11,1) clo(12,1) clo(13,1) clo(14,1) clo(15,1) clo(16,1) clo(17,1) clo(18,1) clo(19,1)];
plot(x,t)
z=[x;t];
fprintf('x(mm)     clo(kg/m3)\n');
fprintf('%5d %10.4f\n',z);
%End of source code
%-------------------------------------------------------------------------------------------
```

BIOGRAPHY

Mr. Mien Van Tran was born in Quang Ninh, Viet Nam in 1979. He received his Bachelor's degree in 2002 and Master's degree in 2005 in Civil Engineering from HoChiMinh City University of Technology (HCMUT), Viet Nam. He has been an academic staff of Faculty of Civil Engineering, HCMUT, Viet Nam since 2002. He has been granted the scholarship by AUN/SEED-Net to study PhD degree in the field of Structural Engineering, Department of Civil Engineering, Chulalongkorn University, Thailand since 2005. His interests are High performance concrete, Durability of concrete in aggressive media.